Title

On the uses of hyperspectral data analysis and watershed analytical methods to evaluate the extent of riparian vegetation and habitat in the Navarro River, California

Authors

Viers, Joshua H.
Ramirez, Carlos
Quinn, James F.

Publication Date

2003-01-23

A Report to the California Department of Forestry and Fire Protection and the United States Department of Agriculture – Forest Service Region 5 Remote Sensing Laboratory

On the uses of Hyperspectral Data Analysis and Watershed Analytical Methods to evaluate the extent of Riparian Vegetation and Habitat in the Navarro River, California

by

Joshua H. Viers, Ph.D.
Information Center for the Environment
Department of Environmental Science and Policy
& John Muir Institute of the Environment
University of California, Davis

Carlos M. Ramirez
Information Center for the Environment
Center for Spatial Technologies and Remote Sensing
University of California, Davis

and

Professor James F. Quinn
Information Center for the Environment
Department of Environmental Science and Policy
University of California, Davis

Outline of Contents

Executive Summary

The primary goal of this project was to test the feasibility of using high-spatial resolution, Airborne Visible/Infrared Imaging Spectrometer (AVIRIS) data to identify and assess riparian vegetation over an area with complex topography and land use. In particular, our goals were to use ecological field data to 1) provide *a priori* expectations of vegetation classifications, 2) serve as verification for spectral classification, and 3) to form a basis from which to nest the classification results within ongoing ecological research. The second aspect of this research was the use of watershed analytical methods to develop a classification of stream segments based on their macro-scale geomorphic properties. In particular, we used terrain-based algorithms to cluster stream segments to describe their geomorphic confinement. Lastly, to benefit longer-term and more broad scale vegetation mapping efforts throughout the region, we compared two vegetation data, the AVIRIS Riparian classification and CALVEG 2000, to determine which, if any, conclusions could be drawn from the examination.

The following entities contributed to this study in the form of project funding and material support: North Coast Regional Water Quality Control Board, California Department of Forestry and Fire Protection, USDA-Forest Service, , California Department of Transportation, Center for Spatial Technologies and Remote Sensing, NASA — Jet Propulsion Laboratory, John Muir Institute of the Environment, and the Information Center for the Environment at the University of California, Davis.

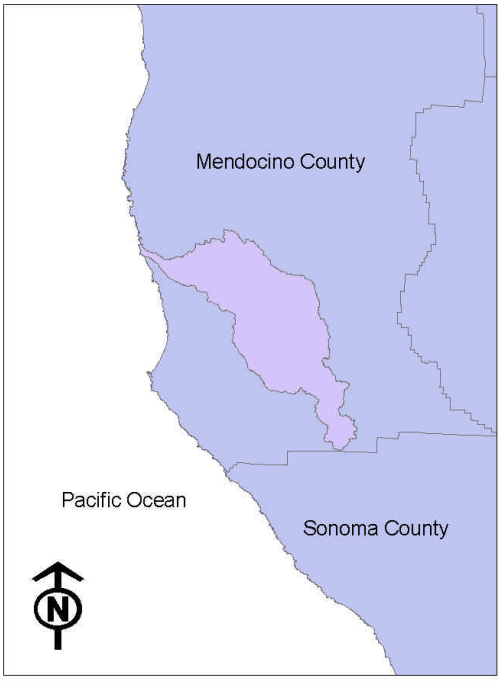

The Navarro watershed is a coastal watershed located in southern Mendocino County, California and approximately 820 km^2 in area. A combination of redwood and mixed conifer forests, mixed hardwoods, annual grasslands, and agricultural areas provides an array of land uses from which to analyze interactions with aquatic and riparian habitats. The watershed is the focal point of many ongoing, multidisciplinary investigations concerning anthropogenic disturbance of watershed processes, such as logging, road building, and land conversion to vineyards and other agriculture, and resulting ecological responses. These studies have focused on the role that land use activities play in perturbing aquatic habitat and key populations of threatened anadromous salmonids. Riparian vegetation is a critical habitat parameter in that it regulates many of the ecosystem components necessary for salmon reproduction, rearing, and migration through its effect on stream shading, contribution of large woody debris, and allochthonous inputs to the stream system. The Navarro River system provides habitat for two Evolutionarily Significant Units of salmon fisheries in the state of California. Sustainability of these fisheries, and others throughout the state, will be facilitated by the

conservation and restoration of riparian forests, which not only provide shade to the streams, but also contribute Large Woody Debris (LWD). LWD is a vital component contributing to the success of salmonid survival by providing habitat and facilitating the development of pools during the winter months.

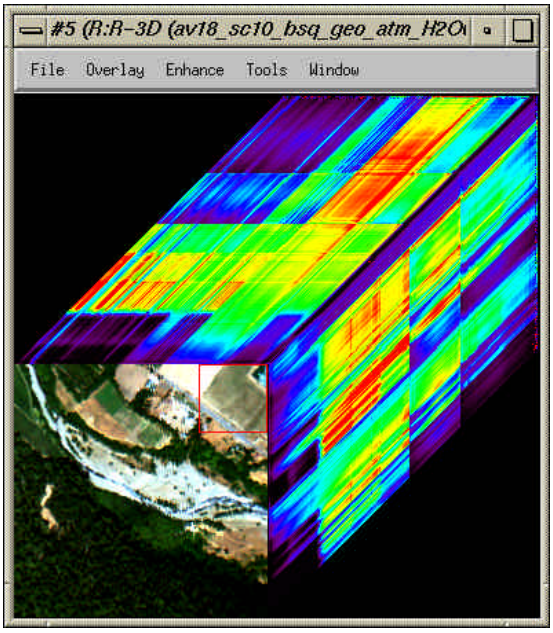

This project used high-spatial resolution, hyperspectral data from the NASA-JPL AVIRIS 2000 campaign to distinguish and classify vegetation cover within a riparian zone. For this aspect of the study, a single source of hyperspectral information was used. The AVIRIS instrument is unique in that it has 224 contiguous, spectral channels with a 10-nanometer sampling interval across the spectral wavelength region of 374 to 2500 nanometers. In contrast, the Enhanced Landsat Thematic Mapper Plus (ETM+) covers the same spectral region but uses only six broad channels and one thermal channel. Of the 26 total flightlines, we selected Flightline 18 as the focal area of this research because it contains the Anderson Valley and is representative of the Navarro River watershed and other coastal watersheds in the region. Most notably, it includes areas under viticultural, timber, and pastoral management. The watershed includes several dominant types of vegetation and it also has an extant riparian corridor throughout most of its spatial domain.

Preprocessing of the flightlines included orthorectifying the images to account for the highly variable topography present in most flightlines and atmospheric correction to account for strong water absorption features, aerosols and other atmospheric constituents. The riparian vegetation classification procedure used a combination of DEM-derived "riparian zone" masks, along with a vegetation mask derived by thresholding the Tasseled Cap transformation, to restrict the analysis to pixels within the riparian zone. Flightline 18 was transformed using the Minimum Noise Fraction (MNF) method, a type of Principal Components Analysis. We restricted the number of analysis bands to the top twenty MNF residuals, which captured a majority of the variance from the original spectral reflectance data. This downselection process decreased the computational time needed for the classification procedures and still provided a robust data set from which to base our analyses.

Three broad vegetation classes were identified from the field data using minimum criteria for TWINSPAN (Two-Way Indicator Species Analysis) classification. Two classes are typically considered upland vegetation; however, they are well represented in the riparian zone (Class A & B). These two classes have three species that are ubiquitous and representative: California bay laurel (*Umbellularia californica*), Douglas-fir (*Pseudotsuga menziesii*), and tanoak (*Lithocarpus densiflorus*). These two classes are separated by two diagnostic species: coast redwood (*Sequoia sempervirens*), and big-leaf maple (*Acer macrophyllum*); representing wetter and drier climes respectively. The riparian class (Class C) is represented by a heterogeneous mixture of species; however, arroyo willow (*Salix*

lasiolepis), Himalayan blackberry (*Rubus discolor*), and white alder (*Alnus rhombifolia*) emerged as diagnostic species.

The results of the K-Means unsupervised classification of the Minimum Noise Fraction transformed flightline 18 showed an overall accuracy of 71.77% and a Kappa Coefficient of 0.58 when using post-classification verification field plots. Class A (*Sequoia*) had a Producer's / User's Accuracy of 66.7% / 86.5%. Class B (*Umbellularia*) had a Producer's / User's Accuracy of 71.1% / 63.4%. Class C (*Salix*) had a Producer's / User's Accuracy of 78.9% / 72.3%. A Spectral Angle Mapper (SAM) classification was performed on the same data array to spectrally isolate species specific pixels identified from field data as indicator species diagnostic of the riparian vegetation class.

For the supervised SAM classification, California bay laurel (*Umbellularia californica*) was the only indicator species to not represent more than 50% of its associated Class pixels; it represented only 28.84% of Class B. Without additional fieldwork, it is difficult to determine if the SAM classification performed poorly for bay laurel or if the incorporation of other diagnostic species, such as big leaf maple (*Acer macrophyllum*), would be more appropriate for this class. Class B is considered a "mixed hardwood" community and, as such, would naturally have a great number of possible species in its class. The other indicator species represented the majority of pixels within its associated K-Means class. Coastal redwood (*Sequoia sp.*) performed the best at 70.72% of its SAM pixels in Class A. Furthermore, it is also apparent that traditional riparian vegetation, as represented by willow (*Salix spp.*) for example, are true to their ecological form in terms of being generally interspersed within other vegetation communities; this is evidenced by each of the three K-Means riparian classes having more than 20% of its pixels classified as arroyo willow (*S. lasiolepis*) by SAM. Arroyo willow represented 53.43% of Class C. In the case of true riparian vegetation, additional diagnostic species will need to be incorporated into future SAM classification efforts if the identification of species will be used as a surrogate for classifying vegetation communities. The overall accuracy of this comparison was 97.82%. These results indicate that the cross-comparison of individual species to classes was accurate in both field and spectral settings.

The second aspect of this research was the use of watershed analytical methods to develop a classification of stream segments based on their macro-scale geomorphic properties and to determine if there is any correlation with observed vegetation types. We used terrain-based algorithms to cluster stream segments based on their geomorphic confinement. This is an automated procedure to classify streams as "Source", "Transport", or "Response" categories, each defined in terms of net sediment movement. We used three primary variables to drive a K-Means clustering of segments: stream gradient, upstream accumulative area, and cross-valley gradient. These results were then used to examine the distribution of riparian vegetation within AVIRIS Flightline 18 by confinement cluster. Our examination of Flightline 18 showed that Transport reaches are largely composed of Riparian with moderate Conifer and low Hardwood. Response reaches are moderate compositions of all three Conifer, Hardwood, and Riparian classes. The dominance of Riparian vegetation in Transport reaches is as expected given the dynamic nature of these reaches and the responsiveness of Riparian vegetation.

The third phase of the study was to compare the results of the AVIRIS classification exercise to other data products. Specifically, we examined the vegetation composition for Flightline 18 depicted by the CALVEG2000 data set produced by the California Department of Forestry and Fire Protection. CALVEG2000 now has classified vegetation into 191 vegetation types for much of California, including all portions of the Navarro River watershed, and was created by an exhaustive system of data acquisition, calibration, classification, and verification. The underlying basis for these data is a combination of satellite imagery (ETM+), reconnaissance (ground and air), and processing techniques. A cross-comparison of CALVEG and the FL 18 classification is confounded by the different spectral and spatial resolution of the their respective instruments. The high-spatial resolution of AVIRIS was better for discriminating riparian vegetation. This was most striking for narrow corridors of riparian vegetation interspersed within barren (gravel and cobble river beds), annual grasslands, and agriculture. Conceivably, comparable classification accuracy would be possible with a high spatial resolution multispectral sensor, such as IKONOS, but this has yet to be validated with multispectral simulations from the AVIRIS data set.

Finally, we offer a brief analysis of the level of effort required for similar research and the continuation of this research. The incorporation of different data, produced at various spatial and spectral resolutions, would be an advantageous undertaking. Many of the newer technologies provide both the spatial and spectral resolution necessary to discriminate resources limited in distribution at increasingly reduced costs. However, the computing and personnel capabilities necessary to undertake research efforts over large spatial areas using the methods outlined here is enormous. Multiple software packages were used in generating the data: ArcGIS v. 8.1; ERDAS Imagine v. 8.5; ENVI v. 3.5; IDL v. 5.5, PARGE v. 1.3; ATCOR4 v. 2.0, and PC ORD v. 4.14. Not only is it costly to acquire the imagery, but purchasing software and licensing adds a considerable amount to the overall cost of the project. Data production for research into the uses of hyperspectral data and watershed analysis methodologies was challenging. It required focused effort on behalf of the researchers, a substantial monetary investment by collaborators, and flexibility to follow important discoveries as they arose. The volume of data became an obstacle at some steps of the processing because of the time it took to transfer the data and the amount of disc space required to house them. At over 400GB, the imagery had to be spread across four different servers.

One of the caveats of using hyperspectral imagery is the sheer volume of a full image cube. A typical flightline in this data set averages 1.5 Gigabytes, while the transformed image cube can be almost twice the size of the original image. Additionally, a Minimum Noise Fraction Transformation can take several hours on a desktop with only slightly better performance on a mutli-processor supercomputer. Finding homogenous training sites for supervised classification purposes can be difficult and labor intensive in such a varied landscape. In this study, field crews had worked in the area areas for several years, simplifying the selection of appropriate training and verification sites. Theoretically, a higher resolution DEM or surface model would have improved our calibration efforts by accounting for the height of the conifers, in particular the redwoods.

In conclusion, the high-spectral and spatial resolution of AVIRIS makes it useful for mapping riparian vegetation, however, it comes at the price of large images (1.5GB+), high acquisition costs, labor intensive preprocessing and increased computational time.

Overview and Synopsis

The research presented in the following report represents the results of several ongoing projects to develop next generation methods for the identification, cataloging, and monitoring of watershed resources. This report, in particular, examines two primary methodologies used in the identification and cataloging of resources within selected portions of the Navarro River watershed. The report also examines two data in a comparison of vegetation typing within a selected portion of the Navarro River watershed. Collectively, this research supports a broad program of developing remote methodologies of watershed analysis and its application to the conservation and restoration of anadromous salmonids and their freshwater habitats.

The first methodology used in this research is the use of high-spatial resolution, hyperspectral data to distinguish and classify vegetation cover within a riparian zone. For this particular aspect of the study, a single source of hyperspectral information – Airborne Visible Infrared Imaging Spectrometer data – was used for one acquired flightline of the NASA-JPL AVIRIS 2000 campaign. We selected Flightline 18 as the focal area of this research because it is typical of the Anderson Valley, in particular, and of the Navarro River watershed, in general. Most notably, it includes areas under viticultural, timbering, and pastoral enterprises; it also includes several types of vegetation and it has an extant riparian corridor throughout most of its spatial domain.

We employed a hybrid methodology to delineate both riparian extent and vegetation within that extent. The riparian extent is essentially terrain-based analysis, in which a digital elevation model is used to calculate a maximum Euclidean distance from streams and an envelope of least-cost accumulation over valley side slope. The discrimination of vegetation within the riparian envelope was handled by bisecting a Greenness data plane, developed from a Tasseled Cap transformation of the AVIRIS hyperspectral data, to limit further analyses to vegetation pixels solely. Using an unsupervised K-Means classification on Minimum Noise Fraction transformed hyperspectral data, we classified pixels within the riparian-vegetation spatial array. Additionally, we employed a Spectral Angle Mapper routine to identify individual species on a pixel probability basis. Overall results of each routine were generally favorable when compared to field verification data; a comparison of both the K-Means cover type classes to Spectral Angle Mapper species classes showed positive outcomes and confirmed *a priori* expectations.

The second aspect of this research was the use of watershed analytical methods to develop a classification of stream segments based on their macro-scale geomorphic properties. In particular, we used terrain-based algorithms to cluster stream segments based on their geomorphic confinement. In essence, this is an automated procedure to classify streams as Source, Transport, or Response categories in relation to sediment movement, as described by authors Montgomery and Buffington (1997). We used three primary variables to drive a K-Means clustering of segments: stream gradient, upstream accumulative area, and cross-valley gradient. A robust classification of stream segments resulted from this new method; these results were then used to examine the distribution of riparian vegetation within AVIRIS Flightline 18 by confinement cluster. Our examination of Flightline 18 showed that much of

the Source stream reaches are predominated by hardwoods with Response reaches showing a greater homogeneity in vegetation cover within the riparian zone.

To benefit longer-term and more broad scale vegetation mapping efforts throughout the region, we compared two vegetation data, the AVIRIS Riparian classification and the CALVEG 2000 digital spatial data, to determine which, if any, conclusions could be drawn from the examination. These two data are vastly different in several respects; notably, they are different in their scale of resolution, their methods of generation and classification, and their intended uses. Subsequently, the results of their comparison are mixed. Furthermore, we examined specific vegetation typing of CALVEG 2000, selected for identified species of importance, in comparison to the AVIRIS Riparian classification. For these data comparisons, we show both statistical and visual evaluations of their comparability; acknowledging the aforementioned caveats of this directed research, the results of these comparisons suggest that the identification and cataloging of riparian vegetation communities requires both a fine scale of analysis and a robust method of discrimination within heterogeneous stands of vegetation.

Lastly, we offer a brief analysis of the level of effort required for similar research and the continuation of this research. The incorporation of different data, produced at various spatial and spectral resolutions, would be an advantageous course of direction. Many of the newer technologies are providing both the spatial and spectral resolution necessary to discriminate resources limited in distribution at increasingly reduced costs. However, the infrastructure, both in terms of computing and personnel capabilities, necessary to undertake research efforts over large spatial areas using the methods outlined here is considerably prodigious. These insights are coupled with a brief overview of selected scientific papers related to hyperspectral data analysis and other noteworthy topics. This body of work, as presented, constitutes a fulfillment of portions of an agreement between the Information Center for the Environment and the California Department of Forestry and Fire Protection.

Indeed, much of the research presented is original work pursued by Joshua H. Viers in support of his doctoral studies at the University of California, Davis, and, as such, it may not reflect the views, philosophies, or policy positions of the University, the California Resources Agency, or the United States Department of Agriculture.

Introduction and Background

The Information Center for the Environment and the John Muir Institute of the Environment, at the University of California, Davis, have been assisting state and federal agencies, as well as international governments and non-governmental organizations, with resource management decision-making through environmental information brokerage and research. These activities are global; however, intensive studies have largely focused on the state of California and California's watersheds and coastal resources in particular. From the inception of the California Rivers Assessment (Viers et al. 1998), our research has refined the methods in which resource inventories and monitoring are carried out by regulatory agencies. This is particularly true in the case of the federal Clean Water Act and, most importantly, the provisions from Section 303(d) that articulate the development of total maximum daily loads (TMDLs) for impaired waterbodies. These TMDLs are currently being applied to non-point source pollutants in large, rural watersheds throughout northern California (see *Pacific Coast Federation of Fishermen's Associations, et al. v. Marcus,* No. 95-4474 MHP, March 11, 1997).

The listing of the Navarro River watershed in southern Mendocino County, California, for the impairments of temperature and sediment, has prompted a number of agencies to collaborate with the University of California, Davis, in the development of surrogate measures of "loads" for non-point source pollutants, such as shade as a surrogate for water temperature. The development of next-generation methods for the cataloging and inventorying of resources of interest is another such example. Riparian habitats are now at the forefront of managerial interest for a number of reasons, but most particularly because they are one of the few ecosystem components that humans have the ability to manage effectively — as evidenced by the many riparian restoration activities now taking place throughout the western United States. Also, and perhaps more importantly, many waterbody impairments in northern California's coastal watersheds are borne out of their decreasing ability to support anadromous salmonid fisheries. It is the relationship between land use, aquatic and riparian habitat, and the decline of anadromous salmonids that warrants investigation and is the focus of our research. In essence, environmental policy is being driven by declines in salmonid populations; however, watershed processes are the primary drivers of salmonid population health and aquatic habitability. Thus, a significant effort is underway across state and federal governmental agencies to develop watershed assessment methods that are scientifically sound and, due to timeliness and cost considerations, pervasive in manner. As such, remote methods of habitat assessment are required to fill existing knowledge and data gaps to forestall future salmonid population declines and potential extinction.

The Navarro River watershed is located in southern Mendocino County, California, USA. This watershed, 820 km^2 in size, drains into the Pacific Ocean and provides a unique opportunity to investigate a closed hydrologic system (Figure 1). A mixture of redwood and mixed conifer forests, oak woodlands, open grasslands, and agricultural areas provides an array of land uses from which to analyze interactions with aquatic and riparian habitats. The Navarro River watershed supports a resource-based economy; timbering, grazing, and limited cropping are the primary land use activities in the watershed. However, recent changes in the California economy have resulted in increased viticultural activities and an increase in the local human population (ca. 3500) within this watershed. These combined

factors have resulted in pervasive land use change in the last 150 years, from which researchers have sought to inventory, catalogue, and provide a synopsis of the ecological state of the watershed.

Thus, the Navarro River watershed is the focal point of many ongoing, multidisciplinary investigations concerning anthropogenic disturbance of watershed processes, such as logging, road building, and land conversion to vineyards and other agriculture, and resulting ecological responses. Namely, these studies have focused on the role that land use activities play in perturbing anadromous salmonid populations and habitat. Riparian vegetation is a key habitat parameter in that it regulates many of the ecosystem components necessary for salmon reproduction, rearing, and migration through its effect on stream shading, contribution of large woody debris, and allochthonous inputs to the stream system — none of which can be assessed comprehensively from ground studies due both to the size of the area and limited access to private lands. Ultimately, however, it is the population decline of several Evolutionarily Significant Units of anadromous salmonids that serves to anchor activities within the watershed.

The decline and subsequent listings, as part of the federal Endangered Species Act, of both coho salmon and steelhead throughout their native range in California, and therefore the Navarro River, is not without precedent. Indeed, population declines of native fishes have been well documented for decades (see Nehlsen et al. 1991 and Moyle and Williams 1990 for examples). Reasons for these declines are many, but they have been best qualified for anadromous salmonids and, thus, provide only a subset of the many issues related to declining populations of aquatic vertebrates in California. Specifically, Nehlson et al. (1991), Brown et al. (1994), and Yoshiyama et al. (1998) discuss the reasons contributing to the decline of anadromous salmonids, both natural and anthropogenic. The anthropogenic factors are many, but primarily reflect unsustainable economies of natural resource exploitation: over-fishing and habitat destruction. Habitat destruction comes in many forms; migration route blocking and spawning area inundation by dams; spawning area sedimentation by road-building and timber harvest practices; increased water temperatures due to reduced canopy cover and sedimentation by timber harvesting and riparian grazing; and the reduction in coarse woody debris used for juvenile cover due to timber removal. The natural factors contributing to the population decline of anadromous salmonids are oceanic conditions, such as abnormally warm sea surface temperatures during El Niño events, and sporadic precipitation, such as droughts. These natural factors, as Brown et al. (1994) point out, are catastrophic events that salmon have experienced throughout their evolutionary existence. Therefore, it is the concerted and or cumulative effect of these many factors that are responsible for the decline in salmonid populations. Furthermore, it is the anthropogenic stress on the aquatic systems that make salmonids and other aquatic and riparian dependent organisms more susceptible to perturbations by natural disturbance regimes.

The factors associated with disturbance, natural or otherwise, are often dynamic in both space and time. The ability to quantify changes in landscape use and configuration, and their relationship to changes in habitat structure, is key to understanding spatio-temporal dynamics within a watershed. As Naiman et al. (1992) acknowledge, watershed processes at a macro scale regulate fluvial features and riparian vegetation at lesser scales; this regulation has reinforced the need to include spatial and temporal dynamics when considering aquatic ecosystem structure and function at a meso- or micro scale. Therefore,

conservation measures that focus on patterns and processes provide an opportunity to act effectively at many spatial scales and ensure long-term viability (Ligon et al. 1999). Thus the detection and quantification of land use patterns, even if macroscopic, is paramount to elucidating the potential impacts on and recovery of habitats and their associated biota (Montgomery and Buffington 1993).

Instream limiting factors to anadromous salmonids, such as stream temperature, are often a function of riparian cover and can be characterized by the riparian vegetation composition and structure. Riparian habitats are one of the most ecologically productive systems in temperate biomes, owing to the land-water interface and the diversity of physical factors affecting their formation and distribution (Naiman et al. 1992). Riparian vegetation largely affects fish populations by providing canopy cover induced shade (reducing water temperature), contributing organic matter directly to the stream, and forming coarse woody debris (Naiman et al. 1992, Murphy 1995). Coarse woody debris is important for salmonid spawning because it increases the trapping of substrate in gravel poor streams and scours silt in sediment filled streams, while also providing heterogeneous stream morphology in the form of pools, channels, and backwaters (Naiman et al. 1992, Murphy 1995).

Due to its biological importance and susceptibility to disturbance, riparian habitats are the cornerstone of most aquatic conservation and restoration scenarios. As such, our research has focused on next generation methods for the detection and delineation of riparian habitat in California's north, coastal watersheds. Currently, many policy questions regarding riparian forests and associated channel conditions are based on limited, coarse-scale spatial data. This research investigates the use of fine-scale, high spectral resolution data to identify and map vegetation in different geomorphic reaches within the riparian zone. In essence, it is an attempt to bridge contemporary macroscopic assessments to meso-level entities by assessing riparian vegetation within a cataloging framework of geomorphic reaches.

Understanding and accounting for geomorphic characteristics of streams is critical to any conservation or restoration scenario for stream segments, especially those that provide habitats for anadromous salmonids. This critical nature is largely marked by the capacity of a stream to move sediment through the fluvial system, sediments whose quality and quantity help define in-stream habitat. Obviously, there are several components that drive the geomorphic properties of streams; however, most scientific analyses have focused on sediment budgets and sediment delivery to streams, transport capacity of streams, and the retention of sediment within the system. Additional research has investigated the role of stream structure, whether it is the presence of coarse woody debris or bedrock constrictions, in trapping fine sediments, creating plunge pools, or stratifying substrates; all of which is under the pretense of understanding and accounting for geomorphic characteristics of streams. Most foci for conservation and restoration activities take the view, albeit a macroscopic one, that most issues in habitat loss stem from pervasive habitat changes that can only be remedied at the formation, or geomorphic channel type, level. However, actual implementation of conservation or restoration activities for salmonids is restricted to site-specific instances, such as migration barrier removal or anchoring inputs of coarse woody debris.

Therefore it is the ability to scale from site to segment to watershed, whether it is within the confines of riparian habitat or in-stream habitat or some other sphere of interest, which has restricted meaningful watershed assessment and analysis. In our research, we focus on the development of methods that provide spatial scaling and the ability to account for processes and implementation at a variety of scales. This report examines the use of AVIRIS imagery to map and characterize riparian vegetation, evaluate riparian vegetation along different geomorphic reaches and explore the similarities and differences between the AVIRIS riparian classification and CALVEG 2000.

Part 1. Hyperspectral Data Analysis

Part 1.1. Hyperspectral Data Analysis Background

In July of 2000, the Information Center for the Environment (ICE) and Center for Spatial Technologies and Remote Sensing (CSTARS) collaborated with National Aeronautics and Space Administration - Jet Propulsion Laboratory (NASA – JPL) to obtain Airborne Visible/InfraRed Imaging Spectrometer (AVIRIS) data of the Navarro River watershed. AVIRIS records data over 224 contiguous, spectral channels with a ~10-nanometer sampling interval across the spectral wavelength region of 374 to 2500 nanometers (VNIR to SWIR). The data received at ICE consisted of the uncorrected, calibrated radiance images. The geo-ortherectification of each flightlines was accomplished with the Parametric Geocoding (PARGE) program (Schläpfer 2000). Atmospheric correction was performed to remove the influence of atmospheric water vapor and aerosols using ATCOR4 (Richter 2000). For a more detailed explanation of the preprocessing sequence for the AVIRIS data see Viers *et al*. (2002). Using this large area, high spatial resolution collection of AVIRIS data for the Navarro River watershed, a classification of riparian vegetation was initiated using a combination of traditional ecological assessment techniques and hyperspectral data analysis.

The primary goal of this project was to test the suitability of hyperspectral analytical techniques to identify and assess riparian vegetation over an area with complex topography and land use. In particular, our goals were to use ecological field data to 1) provide *a priori* expectations of vegetation classifications, 2) serve as verification for spectral classification, and 3) to serve as a basis from which to nest the classification results within ongoing, national efforts of cataloging vegetation.

A series of traditional vegetation classification methods were employed on field data to determine the expected species composition of vegetation communities within the riparian zone. The traditional methods of vegetation classification from field collections are based on clustering algorithms and factor analyses, in this case TWINSPAN (Hill 1979), and these methods were used to establish an expected distribution of species for the watershed. Subsequently, we spatially delineated a riparian zone by using topographic features generated from a digital elevation model of the watershed; this topographic mask serves to limit spectral feature extraction of possible riparian vegetation to locations near waterways. The process results in a hierarchical framework with expected species distributions that represent field conditions; this framework was then integrated with hyperspectral feature

extraction methods, such as endmember selection and spectral classification, to discriminate different vegetation communities within the riparian zone.

Efforts to bridge vegetation community ecology and spectral technologies are not new; however, the use of hyperspectral data analysis to elucidate both specific constituents of vegetation communities and intra-community differences is a dynamic, adaptive science (Roberts et al. 1998). Techniques of both vegetation ecologists and spectrometrists are directed toward pattern detection. Vegetation ecologists typically do not test *a priori* hypotheses – studies are far more often observational or descriptive, with a focus on inductive, multivariate methodologies. Similarly, spectrometry relies on the multi-, or hyper-, variate differences among materials to effectively discriminate and identify classes of objects. In this research, we engage in methods to identify physical relationships that are evident in both ecological and spectral space. Namely, riparian plant species were identified and categorized into communities on the ground. AVIRIS data were used to both classify vegetation communities within the riparian zone and to identify diagnostic species spectrally. The results of our study indicate that the composition of species within vegetation communities is reflected in both variable spaces: ecological and spectral.

Part 1.2. Hyperspectral Data Analysis Methods

The following software packages were necessary for the procedures detailed below: Environmental Systems Research Institute Inc. ArcInfo v. 8.1 (Redlands, CA); ERDAS Imagine v. 8.5 (Leica Geosystems -- Atlanta, GA); Research Systems Incorporated ENVI v. 3.5 (Boulder, CO); Research Systems Incorporated IDL v. 5.5, PARGE v. 1.3 (Schläpfer ReSe – Switzerland) and ATCOR4 v. 2.0 (Schläpfer ReSe – Switzerland), and PC ORD v 4.14 (MjM Software Design – Gleneden Beach, OR).

In all, NASA flew 26 of the 29 proposed flightlines over a period of three days in late July of 2000. For this preliminary hybrid classification analysis, we have chosen one representative flightline from the collection to process: AVIRIS Flightline 18 (Figure 1).

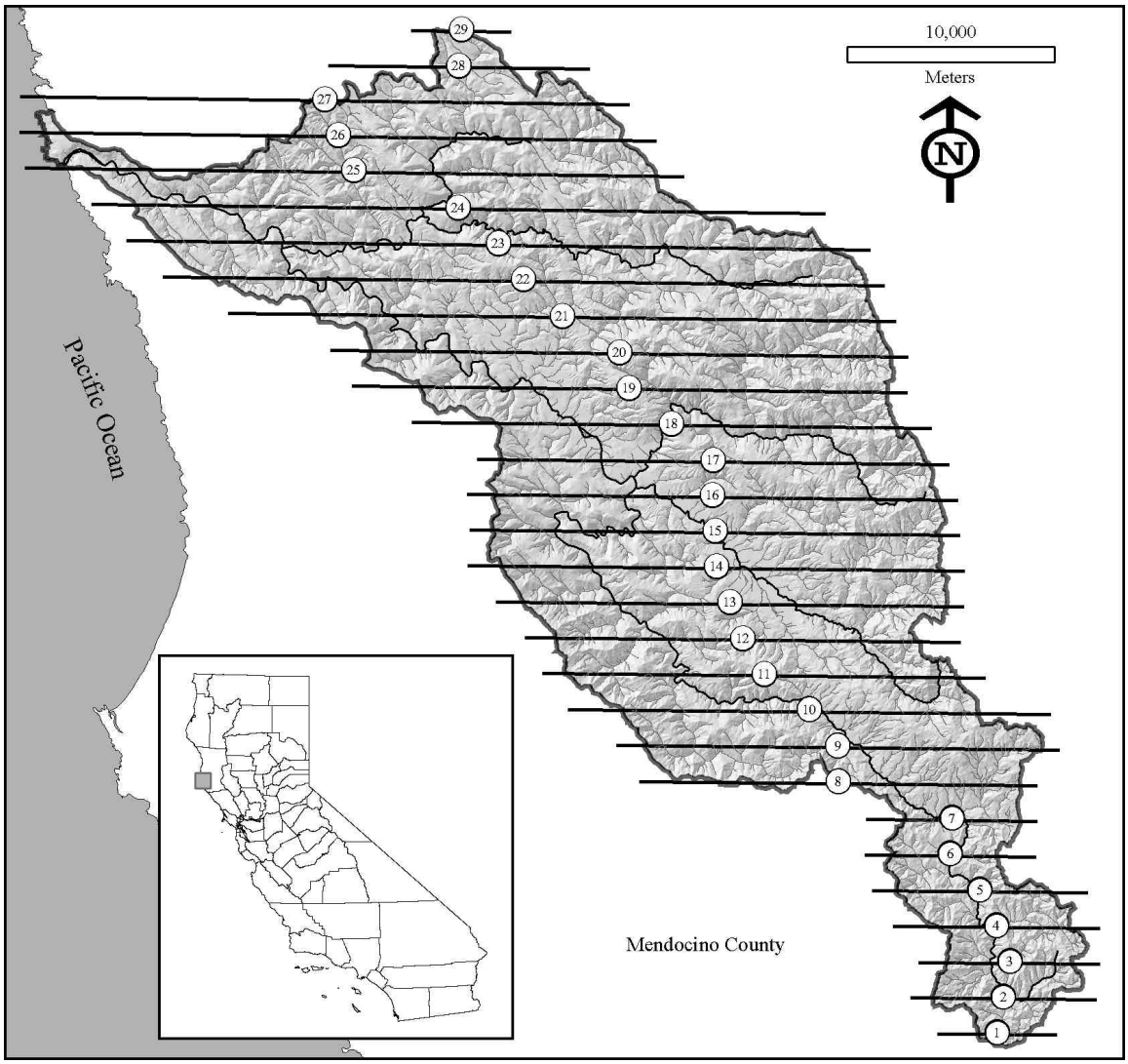

Figure 1. Map of the Navarro River Watershed with the proposed AVIRIS flightlines and primary hydrographic features. All but flightlines 1-3 were flown in July 2000. Flightline 18 is the focus of this study. Inset Map shows position of watershed in Mendocino County, California.

NASA – JPL supplied the Navarro River AVIRIS data in radiometrically corrected format on 8mm tape. Tape contents were uncompressed to a common file space on a sixteen-processor SGI Origin 2000 supercomputer; each flightline totals approximately 1.5 – 2.5 Gigabytes. To geometrically correct flightline data, a terrain correction software package, Parametric Geocoding (PARGE) (Schläpfer 2000), was used. PARGE integrates the inertial navigation unit readings, flight GPS positions, and ground control points (GCPs) to correct for pitch, roll, heading, and yaw. This procedure also incorporates a Digital Elevation Model to adjust for topographic effects. Prior to initiating PARGE, each frame was mosaicked in ENVI to create a seamless flightline. AVIRIS data were converted from BIP to BSQ in ENVI. GCPs were collected by using a combination of ENVI and Imagine tool sets and Digital Orthophoto Quarter Quadrangles as a visual anchor. GCPs were systematically eliminated based on their X and Y coordinate offsets until the GCP Residual (RMSE) was less than 5.0 m. A 10m USGS Digital Elevation Model of the watershed was resampled to 5m cell resolution using bilinear

interpolation and converted in ArcInfo from a grid to a DEM in USGS format (ESRI 2001). The USGS format DEM was imported into ENVI to be used with PARGE, along with the GCPs.

The final AVIRIS data were resampled to 5m from the native 3.3m - 4.2m spatial resolution. The geo-corrected results from PARGE were incorporated into ATCOR4, an atmospheric correction software package (Richter 2000). ATCOR4 corrects for sun angle, atmospheric moisture and particulates, topography, off-nadir viewing angles, and shadows. Once the flightlines were geometrically and atmospherically corrected, "noisy" bands were eliminated. Bands were visually inspected and dropped from the analysis if their respective response signatures for a known material deviated from the expected response. The following bands were chosen as acceptable for further analysis: 2-104, 116-152, 168-220 (384.46nm - 1324.15nm, 1443.79nm - 1802.45nm, 1950.66nm - 2469.24nm respectively) and resulted in a final spectral product.

The process for isolating riparian vegetation relies on a hybrid methodology, which incorporates an intersection of two masks, an ecological field data classification, a field-integrated spectral classification, an ecological field data indicator species analysis, and a final spectral comparison of indicator species within classes (see Figure 2 for Process Flow Diagram). The dual masking procedure is part terrain analysis and part spectral transformation. The spectral masking involved the transformation of the spectral array into three data planes using the Tasseled Cap transformation (Jackson 1983, Richards and Jia 1999). A processing script was developed in Interactive Data Language (IDL) to extract data planes via the Tasseled Cap procedure for soil brightness, vegetation greenness, and water saturation (Jackson 1983, Richards and Jia 1999). The IDL script uses Regions of Interest (ROIs) as inputs for each data plane and the spectral downselected bands are used in the input array. To develop a series of ROIs, FL 18 was transformed using Boardman and Kruse's (1994) Minimum Noise Fraction (MNF) routine to collapse the input data array into the twenty dimensions with the highest eigenvalues. ROIs were defined in part by pixels encoded by the Pure Pixel Index (1000 iterations) (Boardman et al 1995) on the MNF transformed arrays. ROIs, in this case, were selected to represent soil brightness, vegetation greenness, and water saturation to seed the Tasseled Cap transformation. Flightline 18 was examined for the distribution of values from the three-band transform array and each plane was bisected to separate materials based on its modal distribution. Vegetation was determined to have a "greenness" array value greater than the least first standard deviation from the mean.

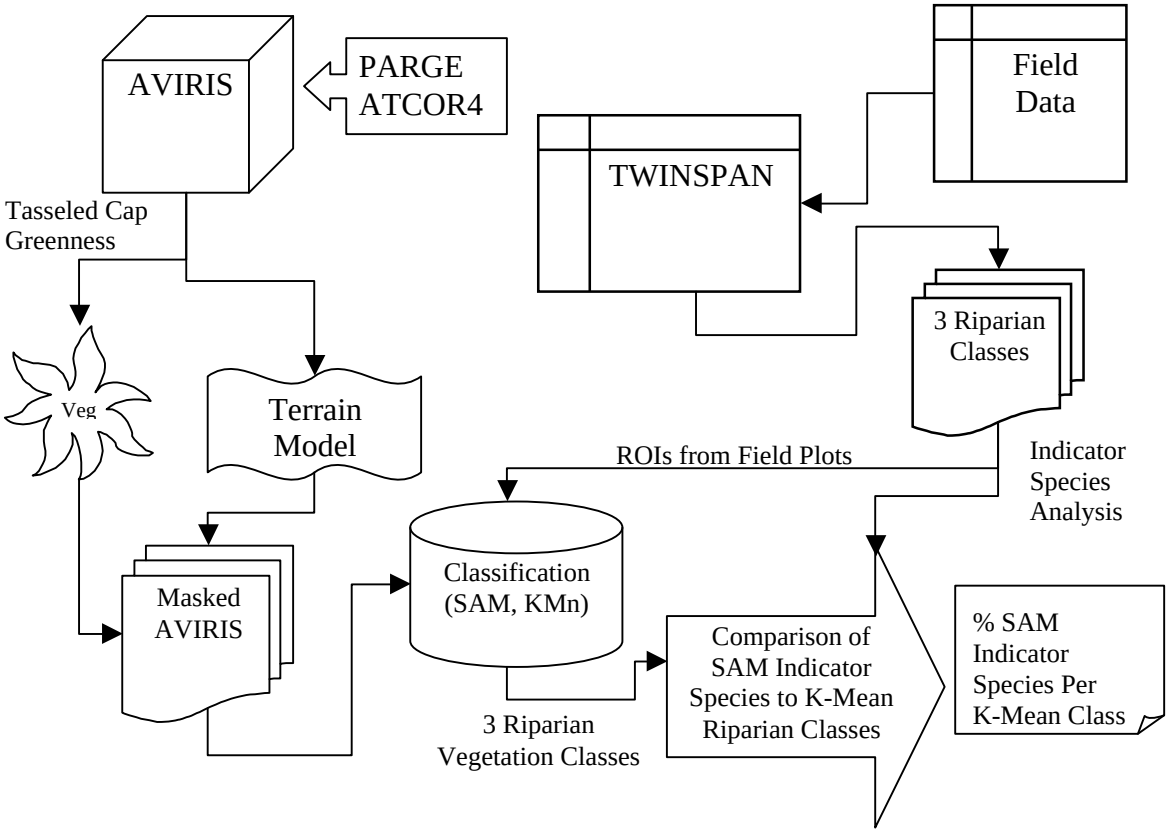

Figure 2. Processing flow diagram for the hybrid methodology to discriminate riparian vegetation.

To reduce spectral variability and errant classification of riparian vegetation in upland vegetation communities, the vegetation pixels were further segmented with a Riparian Extent Mask. The Riparian Extent data grid was created as a combination of two inputs. The first input is a Euclidean distance from streams data grid that was natural log transformed and rescaled from 1-100. A break point of 37.4 was chosen; it represents one standard deviation less than the mean. The second input represents the least cost path away from streams where Degree Slope is the cost. The results were natural log transformed and rescaled 1-100. A break point of 76.6 was chosen; it represents one standard deviation less than the mean. The Riparian Extent Mask represents the intersection of these two grids. This Riparian Extent Mask was then used to limit the influence of upslope vegetation on the spectral classification of the AVIRIS data and the Tasseled Cap Greenness plane was used as a mask to restrict the spectral classification to vegetation solely.

The hyperspectral classification incorporated the results of ecological data analysis of fieldwork conducted in the summer of 2000. The initial riparian fieldwork consisted of 6 - 10m x 10m quadrats randomly placed along each study reach at sixteen study sites throughout the watershed (Figure 3). Study sites were stratified to represent major tributaries in the watershed and position in the watershed, in terms of upstream accumulative drainage area. This stratification also recognizes differences in elevation, geologic substrates, and distance to the Pacific Ocean – a primary climatic determinant. We identified all woody species, estimated percent cover of each woody species, measured all stems greater than 10cm at diameter breast height, measured tree heights with a LaserTech Impulse 2000 Rangefinder, and located quadrat boundaries with a Trimble ProXRS Differential Global Positioning System (DGPS). Additional field verification plots and

individual species locations were geographically located with DGPS as well; these sites were located throughout Flightline 18.

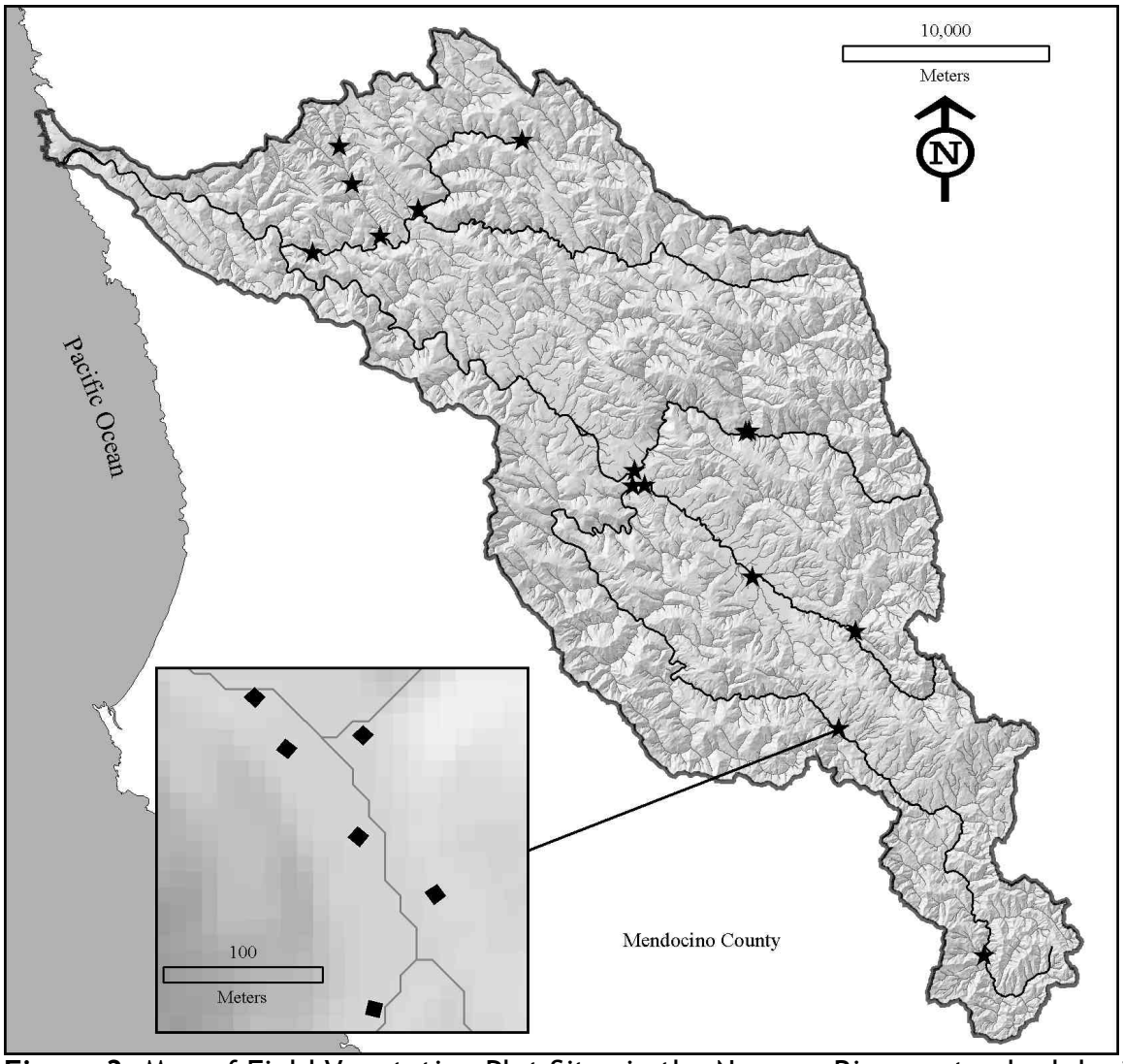

Figure 3. Map of Field Vegetation Plot Sites in the Navarro River watershed depicts a stratification based on major tributaries and watershed position. Study plots are 10m x 10m and are in clusters of six plots per site, as shown in the inset map.

The species cover data were analyzed using Two-Way Indicator Species Analysis (Hill 1979, McCune and Mefford 1999). TWINSPAN can be described as dichotomized ordination analysis, in that an iterative character weighting is used to separate species affinities based on the incorporation of *pseudo-species* to represent differences in abundance for each observed species (van Tongeren 1995). Similarly, sample sites are dichotomized and, ultimately, added to a species-by-site matrix. The result of this ordination is a fidelity matrix with an approximate positive diagonal, from upper-left to lower-right, which can be used to characterize un-sampled sites (van Tongeren 1995); in this exercise, it is used as an *a priori* guide to vegetation communities within the riparian zone and resulted in three broad classes (Appendix I). Lastly, in terms of the ecological field data analysis, an Indicator

Species Analysis was performed using the three Riparian Vegetation classes derived from TWINSPAN (Dufrene and Legendre 1997). Indicator Species Analysis is a method that combines information on the concentration of species abundance for a particular group and the faithfulness of occurrence of a species in that group, as a function of frequency (McCune and Mefford 1999). It produces indicator values for each species in each group, reflecting abundance and frequency, and this score is tested for statistical significance using a Monte Carlo technique (McCune and Mefford 1999).

Two classification methods were performed on the AVIRIS data to accomplish two separate, but related, objectives: 1) an unsupervised classification to establish vegetation communities within the riparian extent; and 2) a supervised classification of Indicator Species reference spectra to establish distributions of plant species indicative of vegetation communities. The purpose of this two-staged approach is to determine if hyperspectral data analysis can be used to identify patterns of species indicative of vegetation communities observed in the field; essentially, this two-stage method tries to establish whether vegetation communities observed in the field, in terms of composition and constancy, are reflected in the spectral characteristics of AVIRIS. A Spectral Angle Mapper (SAM) supervised classification was performed in ENVI using ROIs defined by the field quadrat boundaries and ancillary field identifications. The SAM classification (Kruse et al 1993) was seeded to represent Indicator Species from the TWINSPAN classification using ROI endmembers for coast redwood, California bay laurel, and arroyo willow with a 0.1 radian deviance threshold from the reference spectra for classification. For each diagnostic species, a series of ROIs were identified, mean and standard deviation spectra were collected, and spectral libraries created to be used in the SAM classification. Additionally, a K-Means unsupervised classification was implemented on the twenty-band MNF in ENVI to classify vegetation communities within the riparian extent (Figure 4.1). A total of four classes were chosen to represent vegetation within the riparian extent (Figure 4.2); three classes are described in field plot results, and one class represents cultivated crops. The K-Means classification was performed with five hundred iterations and a 2% class deviance. Field plots and individual species' locations were geographically located with a Trimble ProXRS GPS unit, differentially corrected, and brought into ENVI as vector data for verification. These verification vectors are shown in Figure 4.3 with white outlines.

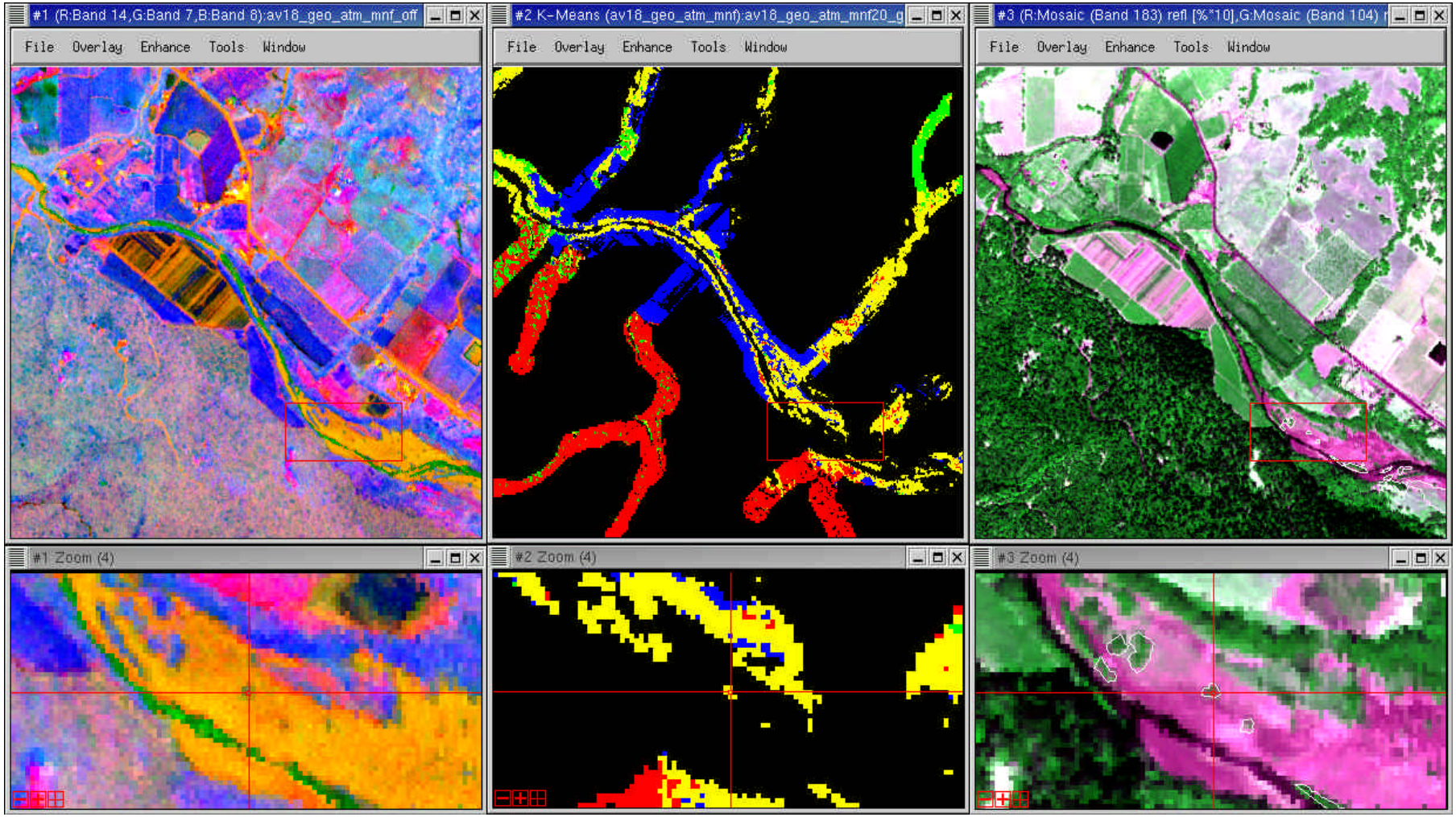

Figure 4.1. Navarro River AVIRIS Image Minimum Noise Fraction Transform (Planes 14, 7, 8)
Figure 4.2. Navarro River AVIRIS Riparian Vegetation Classification (Class A in Red, Class B in Green, Class C in Yellow, and Cultivated Crops in Blue);
Figure 4.3. Navarro River AVIRIS Image of Hendy Woods State Park (Bands 183, 104, 195) with GPS Verification Overlay (White Polygons) targeting Class C pixels.

Part 1.3. Hyperspectral Data Analysis Results

Using minimum criteria for TWINSPAN classification of field data, three broad classes of vegetation emerged. Two classes are typically considered upland vegetation; however, they are well represented in the riparian zone (Class A & B). These two classes have three species that are ubiquitous and representative: California bay laurel (*Umbellularia californica*), Douglas-fir (*Pseudotsuga menziesii*), and tanoak (*Lithocarpus densiflorus*). These two classes are separated by two diagnostic species: coast redwood (*Sequoia sempervirens*), and big-leaf maple (*Acer macrophyllum*); representing wetter and drier climes respectively. Other species that are marginally diagnostic are Pacific madrone (*Arbutus menziesii*) for wetter environments and coast live oak (*Quercus agrifolia*) for drier environments. The riparian class (Class C) is represented by a heterogeneous mixture of species; however, arroyo willow (*Salix lasiolepis*), Himalayan blackberry (*Rubus discolor*), and white alder (*Alnus rhombifolia*) emerged as diagnostic species. Although Himalayan blackberry only occurs in a small percentage of the sampled quadrats, it is dominate where present and is reflected by the high indicator value. Other indicator species in this riparian class are: California blackberry (*Rubus vitifolius*), Pacific dogwood (*Cornus nuttallii*), and white willow (*Salix alba*). Furthermore, many of these species have significant Indicator Values in determining riparian class as determined by Indicator Species Analysis (Table 1), which determines a species Indicator Value as a function of abundance and frequency (Dufrene and Legendre 1997). For Class A, redwood had the highest Indicator Value. For Class B, California bay laurel was the best indicator species. Arroyo willow had the highest Indicator Value for Class C.

The results of the K-Means classification of the MNF transformed flightline 18 showed an overall accuracy of 71.77% and a Kappa Coefficient of 0.58 when using post-classification verification field plots. Class A (*Sequoia*) had a Producer's / User's Accuracy of 66.7% / 86.5%. Class B (*Umbellularia*) had a Producer's / User's Accuracy of 71.1% / 63.4%. Class C (*Salix*) had a Producer's / User's Accuracy of 78.9% / 72.3%. The results of the Spectral Angle Mapper classification for the three class diagnostic species (Table 1, in **bold**), determined from Indicator Species Analysis (results in Table 2), describe the relationship between vegetation community class, as defined by K-Means, and spectral libraries developed from field observation ROIs. The comparison of the SAM Indicator Species classification to the K-Means Community classification had overall accuracy 97.82% of and a Kappa Coefficient of 0.7471. These results are further detailed in Table 1.

Class	Indicator Species	No. SAM Pixels	No. Class Pixels	Pct. Indication by SAM
A	***Sequoia sempervirens***	**46551**	**65822**	**70.72**
B	*Sequoia sempervirens*	17745	46766	37.94
C	*Sequoia sempervirens*	4849	38890	12.47
A	*Umbellularia californica*	531	65822	0.81
B	***Umbellularia californica***	**13486**	**46766**	**28.84**
C	*Umbellularia californica*	1801	38890	4.63
A	*Salix lasiolepis*	15589	65822	23.68
B	*Salix lasiolepis*	13892	46766	29.71

C	*Salix lasiolepis*	20777	38890	53.43

Table 1. Results of Spectral Angle Mapper Classification on Discriminated Riparian Vegetation using field mean and standard deviation spectra for selected Indicator Species defined by K-Means Classification.

Part 1.4. Hyperspectral Data Analysis Discussion

Riparian vegetation communities identified in the field were identified spectrally via a restricted K-Means classification on MNF transformed AVIRIS data. The results of this classification, with an overall accuracy of 71.77%, suggest that the three vegetation classes within the riparian extent largely represent field observations (Figure 4.3) and the association with the field plots, classified by TWINSPAN to cluster communities of plant species, was generally correct. Thus, each spectral class had a representative surrogate field class that was verified via cluster analysis of field data plots. Additionally, and perhaps more significantly, SAM classification of AVIRIS data for selected species shows similar patterns of species associations observed in the field. In particular, Indicator Species Analysis, a method using species' observed abundance and frequency in relation to developed classes or communities, produced three diagnostic species for the three observed riparian communities. Spectral libraries of these diagnostic species were used in the SAM classification, which in turn were compared to the K-Means classified riparian communities. The overall accuracy of this comparison was 97.82%. Ultimately, these results indicate that the cross-comparison of individual species to classes was accurate in both field and spectral settings.

Comparatively, California bay laurel (*Umbellularia californica*) was the only Indicator Species to not represent more than 50% of its associated Class pixels; it represented only 28.84% of Class B. Without additional fieldwork, it is difficult to determine if the SAM performed poorly for bay laurel or if the incorporation of other diagnostic species, such as big leaf maple (*Acer macrophyllum*), would be more appropriate for this class. Class B must also be considered a "mixed hardwood" community and, as such, would naturally have a great number of possible species in its class. Regardless, each Indicator Species had the predominate percent of its pixels within its associated K-Means class. Coastal redwood (*Sequoia sp.*) performed the best at 70.72% of its SAM pixels in Class A. Furthermore, it is also apparent that traditional riparian vegetation, as represented by willow (*Salix spp.*) for example, are true to their ecological form in terms of being generally interspersed within other vegetation communities; this is evidenced by each of the three K-Means riparian classes having more than 20% of its pixels classified as arroyo willow (*S. lasiolepis*) by SAM. Arroyo willow represented 53.43% of Class C. In the case of true riparian vegetation, additional diagnostic species will need to be incorporated into future SAM classification efforts if the identification of species will be used as a surrogate for classifying vegetation communities.

These results are for a limited portion of the watershed and could change with the incorporation of other flightlines and other field plots. Some considerations for addressing possible error include: 1) the mixed composition of vegetation communities are difficult to separate spectrally by species; 2) the "ribbon" forest nature of riparian vegetation can be overwhelmed by upland species; and 3) canopy structure, especially with 80-100m tall

coastal redwood trees, can obscure other vegetation features. The preliminary results of this effort indicate that hybrid methods of feature extraction work best in this varied landscape of topography, climate, and vegetation communities. Additional research will be focused on assessing other discriminatory methods for feature extraction within the riparian zone and other feature types. However, assessing the distribution and composition of riparian vegetation at a watershed scale is essential to protecting salmonid habitat and guiding restoration efforts. The methods outlined here, as they are improved, will aid land use managers in their ability to inventory, restore, and monitor riparian ecosystems. This is particularly true for north, coastal California watersheds where recent policy determinations under the federal Clean Water Act and Endangered Species Act require regulatory agencies to assess ecosystem integrity in a comprehensive and timely manner.

Table 2. Indicator Species Analysis Results

	Taxon Name	Common Name	Class	Indicator Value	p*
1	*Salix lasiolepis*	arroyo willow	C	53.7	0.001
2	*Acer macrophyllum*	big-leaf maple	B	30.7	0.015
3	*Umbellularia californica*	California bay	B	68.1	0.001
4	*Quercus kelloggii*	California black oak	B	13.2	0.069
5	*Rubus ursinus*	California blackberry	C	20.8	0.121
6	*Aesculus californica*	California buckeye	B	2.4	1
7	*Rhamnus californica*	California coffeeberry	A	10.8	0.109
8	*Corylus cornuta var. californica*	California hazelnut	A	11.9	0.225
9	*Torreya californica*	California nutmeg	B	7.1	0.481
10	*Vitis californica*	California wild grape	B	7.3	0.415
11	*Quercus chrysolepis*	canyon live oak	B	10.5	0.159
12	*Quercus agrifolia*	coast live oak	B	17	0.069
13	*Sequoia sempervirens*	coast redwood	A	83.4	0.001
14	*Ceanothus incanus*	coast whitethorn	B	7.9	0.189
15	*Salix hookeriana*	coastal willow	C	6.6	0.327
16	*Arctostaphylos manzanita*	Common manzanita	B	2.6	1
17	*Baccharis pilularis*	coyote brush	C	14.3	0.023
18	*Pseudotsuga menziesii var. menziesii*	Douglas-fir	A	45.4	0.005
19	*Abies grandis*	grand fir	A	10.7	0.143
20	*Rubus discolor*	Himalayan blackberry	C	70.4	0.001
21	*Arbutus menziesii*	Madrone	A	9	0.587
22	*Fraxinus latifolia*	Oregon ash	B	3.4	0.762
23	*Cornus nuttallii*	Pacific dogwood	C	15.4	0.021

24	*Taxus brevifolia*	Pacific yew	B	5.1	0.579
25	*Toxicodendron diversilobum*	poison oak	B	13.8	0.119
26	*Alnus rubra*	red alder	B	4.7	0.662
27	*Salix laevigata*	red willow	C	7.7	0.139
28	*Rubus spectabilis*	salmon berry	B	5.3	0.498
29	*Salix sessilifolia*	sandbar willow	B	2.6	1
30	*Salix sitchensis*	Sitka willow	C	7.7	0.15
31	*Lithocarpus densiflorus*	Tanoak	A	63.2	0.001
32	*Heteromeles arbutifolia*	Toyon	C	5.1	0.447
33	*Quercus lobata*	valley oak	B	10.5	0.103
34	*Myrica californica*	wax-myrtle	A	5.4	0.311
35	*Rhododendron occidentale*	western azalea	A	15.4	0.038
36	*Plantanus racemosa*	western sycamore	C	7.7	0.135
37	*Alnus rhombifolia*	white alder	C	51	0.001
38	*Salix alba*	white willow	C	23.1	0.006

* proportion of randomized trials with indicator value equal to or exceeding the observed indicator value (Dufrene and Legendre 1997).

P = (1 + number of runs >= observed)/(1 + number of randomized runs)

Part 2. Techniques for Geomorphic Stream Typing

Part 2.1. Geomorphic Typing Background

The approach detailed here, in the context of the hyperspectral data analysis and the delineation of riparian vegetation within the Navarro River watershed, is the development of a landscape scale approach to classify streams by their geomorphic type. This geomorphic typing is then used to determine which types of streams are associated with which types of riparian vegetation. Discussed in detail below, we use the classified AVIRIS data for Flightline 18 to comparatively examine the vegetation composition of geomorphically different stream segments.

Previous efforts have been made in Oregon and Washington to map source, transport and response reaches, however, they have been strongly qualitative and have relied on visual interpretation of elevation contours. To classify stream segments based on geomorphic properties, three primary variables were used to cluster stream segments with other segments with similar properties. These variables are upstream accumulative area, stream gradient, and latitudinal profile gradient. Much of the background for the determination of stream segment geomorphic type can be found in Montgomery and Buffington (1997), but is also qualitatively expressed by other authors (e.g., Rosgen 1994); Montgomery and Buffington (1997) argue that stream channel morphology and response are a direct outcome of the interaction between sediment supply, transport capacity, and vegetation. As stream morphology regulates, to a great degree, the availability of salmonid habitat in the form of spawning gravels, rearing pools, and migration corridors, its identification and description is important for all aspects of management. Montgomery and Buffington (1997) continue to classify stream segment networks as either source, transport, or response reaches, based on the variables listed above. The primary variable in their matrix is valley confinement or latitudinal profile gradient – the rapidity for which side slope increases away from the stream channel. Although the more strict definition of channel confinement is the ratio of channel width to valley width, a generally accepted assessment of confinement considers the steepness of valley walls (Montgomery and Buffington 1993)

Established techniques in watershed based GIS computing were used to delineate stream segments and to calculate variables of interest for each segment (e.g., upstream accumulative area) (Tarboten 1991, Viers et al. 1999); to define riparian extent of stream segments (Viers et al. 2002); and to segregate stream segments based on their geomorphic homogeneity (Viers et al. 2002). In the end, we believe these methods can be used to help resource managers determine areas for riparian habitat conservation and restoration.

Part 2.2. Geomorphic Typing Methods

The vehicle for this research is the use of terrain-based analysis within a geographic information system (GIS). All GIS work was performed in ArcGIS 8.1 (ESRI – Redlands, CA) using many modules, but the raster-based GRID module was

predominately used. All statistical computations were carried out in JMP5.0 (SAS Institute Inc. – Cary, NC).

In this portion of the study, we used several GRID algorithms on a Digital Elevation Model (10m) produced by the United States Geological Survey to generate a stream segment network and assign upstream accumulative area and stream gradient to each segment. Stream gradient was calculated by using a zonal mean of masked streams cells converted to percent slope in which each stream segment was considered a separate zone. Furthermore, we used the FOCALRANGE algorithm at 20m intervals (30m – 190m) in a circular pattern to determine the mean majority elevation range for each stream segment. This analytical product, in essence, determines the confinement of each stream segment by iteratively expanding away from the stream center to define the parameters of side-slope: rise, majority elevation range, and run, radius of focal circle, where intervals are collectively averaged for each stream segment. A K-Means clustering algorithm was used in JMP5.0 to develop a sense of the distribution of valley confinement within the watershed by examining linear and quadratic regressions between elevation range and distance from stream channel. Furthermore, accumulative area and stream gradient, each natural log transformed, were combined with the mean majority elevation range and used to develop three final clusters of stream segments by using the K-Means clustering algorithm in JMP5.0.

The second phase of the geomorphic typing analysis was to determine the distribution of riparian vegetation classes among the geomorphic types. The riparian classes were outcomes of the previous hyperspectral data analysis procedure in which the Riparian Extent, a combination of distance from stream and cross-sectional slope, was used to limit the spatial extent of the AVIRIS vegetation pixels being classified; thus, the procedure limited the amount of "noise" from upland vegetation communities. The Riparian Extent was also used in determining the spatial area used to calculate the percent of a stream segment attributed to riparian vegetation communities. The AVIRIS riparian vegetation classes were examined as a function of geomorphic class: source, transport, and response. This stream segment clustering procedure elucidates patterns of riparian vegetation within the context of a geomorphic framework. In the end, classified vegetation pixels within the riparian extent were examined as a percent vegetation type by geomorphic confinement type.

Part 2.3. Geomorphic Typing Results

The analysis of vegetation classes within the geomorphic confinement clusters was restricted to Flightline 18 solely. The geomorphic confinement analysis as whole, however, was computed for the entire Navarro River watershed. The distributions of stream segment mean majority elevation range, as a function of distance from stream, were normal; moments for each unit are presented in Table 3 and overall distribution is presented in Figure 5.1. Distributions of stream gradient and upstream accumulative area were not normally distributed and thus natural log transformed for further analysis; their distributions are presented in Figures 5.2 and 5.3, respectively. K-Means clustering of stream segments was for three groups, to

represent source, transport, and response reaches (Montgomery and Buffington 1997), and resulted in a robust classification from nineteen iterations (Table 4) and an intuitive map of stream segments (Figure 6).

Distance from Stream (m)	30	50	70	90	110	130	150	170	190
Mean Majority Elevation Range (m)	13.54	26.29	37.42	49.91	61.17	72.48	83.14	92.87	102.50
Std Dev	7.71	12.67	16.43	20.36	23.65	27.09	30.16	33.00	35.92
Upper 95% Mean	13.70	26.56	37.77	50.35	61.68	73.06	83.78	93.57	103.27
lower 95% Mean	13.37	26.02	37.07	49.47	60.66	71.90	82.49	92.16	101.74

Table 3. Distribution of Side Slope (Cross-Valley) Elevation Range Values for the Navarro River watershed.

Cluster Summary

Step	Criterion
19	0

Cluster	Count	Max Dist	Prior Dist
1	1413	3.21272433	3.90536163
2	2885	2.57270968	3.71814347
3	3477	3.43994531	3.66760957

Cluster Means

Cluster	Natural Log Percent Stream Gradient	Natural Log Maximum Accumulative Area (100m^2)	Averaged Mean Majority Side Slope
1	0.47343201	13.2755961	37.1641435
2	1.30922018	9.02096074	41.3697642
3	2.3703203	8.15335163	70.3444611

Cluster Standard Deviations

Cluster	Natural Log Percent Stream Gradient	Natural Log Maximum Accumulative Area (100m^2)	Averaged Mean Majority Side Slope
1	0.43282151	1.50191044	15.9575819
2	0.50079762	1.23640695	14.5450165
3	0.39305451	1.0848862	13.1580471

Table 4. K-Means Clustering Output for Stream Confinement Criteria in Montgomery and Buffington (1997). Confinement Clusters 1-3 represent Response, Transport, and Source Reaches, respectively.

Figure 5.1. Averaged Mean Majority Side Slope Gradient by Stream Segment

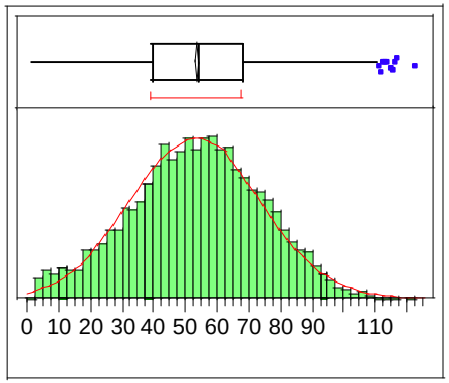

Normal(53.563,20.7884)

Moments

Mean	53.563009
Std Dev	20.788431
Std Err Mean	0.2357608
upper 95% Mean	54.025164
lower 95% Mean	53.100855
N	7775

Figure 5.2. Natural Log Transformed Stream Segment Mean Gradient

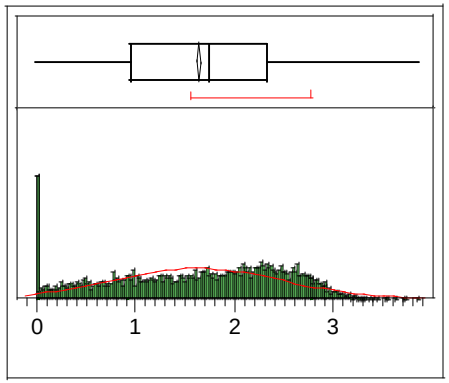

Normal(1.63185,0.85005)

Moments

Mean	1.6318538
Std Dev	0.8500536
Std Err Mean	0.0096404
upper 95% Mean	1.6507516
lower 95% Mean	1.612956
N	7775

Figure 5.3. Natural Log Transformed Maximum Upstream Accumulative Area by Stream Segment

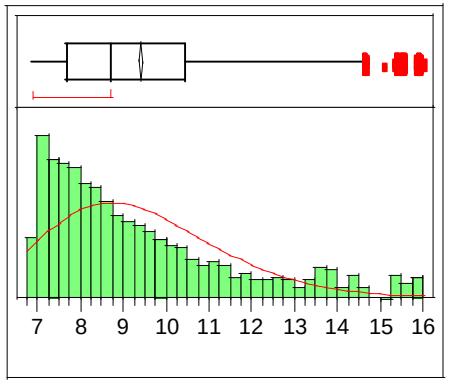

LogNormal(2.21633,0.21784)

Moments

Mean	9.4061855
Std Dev	2.2319385
Std Err Mean	0.0253123
upper 95% Mean	9.4558045
lower 95% Mean	9.3565666
N	7775

Figure 6. Close-Up Map of Confinement Clusters for the Navarro River Watershed, Single Cell Area equals 100m^2.

Confinement Cluster Category	Linear Model	Linear Model Fit (r^2)	Polynomial Model with Zeroed Intercept
Response	-6.757248 + 0.4568701 Distance	0.571865	0 + 0.4174833 Distance - 0.0005512 (Distance-110)^2
Transport	-3.180633 + 0.4566623 Distance	0.619368	0 + 0.4435071 Distance - 0.0005305 (Distance-110)^2
Source	2.3917929 + 0.6803434 Distance	0.808389	0 + 0.7076774 Distance - 0.0004791 (Distance-110)^2

Table 5. Fitted model comparison for Confinement Clusters.

Table 5 shows fitted models, linear and polynomial, for the three Confinement Cluster categories and a stylized graph of the polynomial fitted models for each category is shown in Figure 7. An analysis of side slope gradient by Confinement Cluster resulted in expected distributions; linear regressions of elevation range against distance from stream are presented with quantile density contours in Figures 8-10.

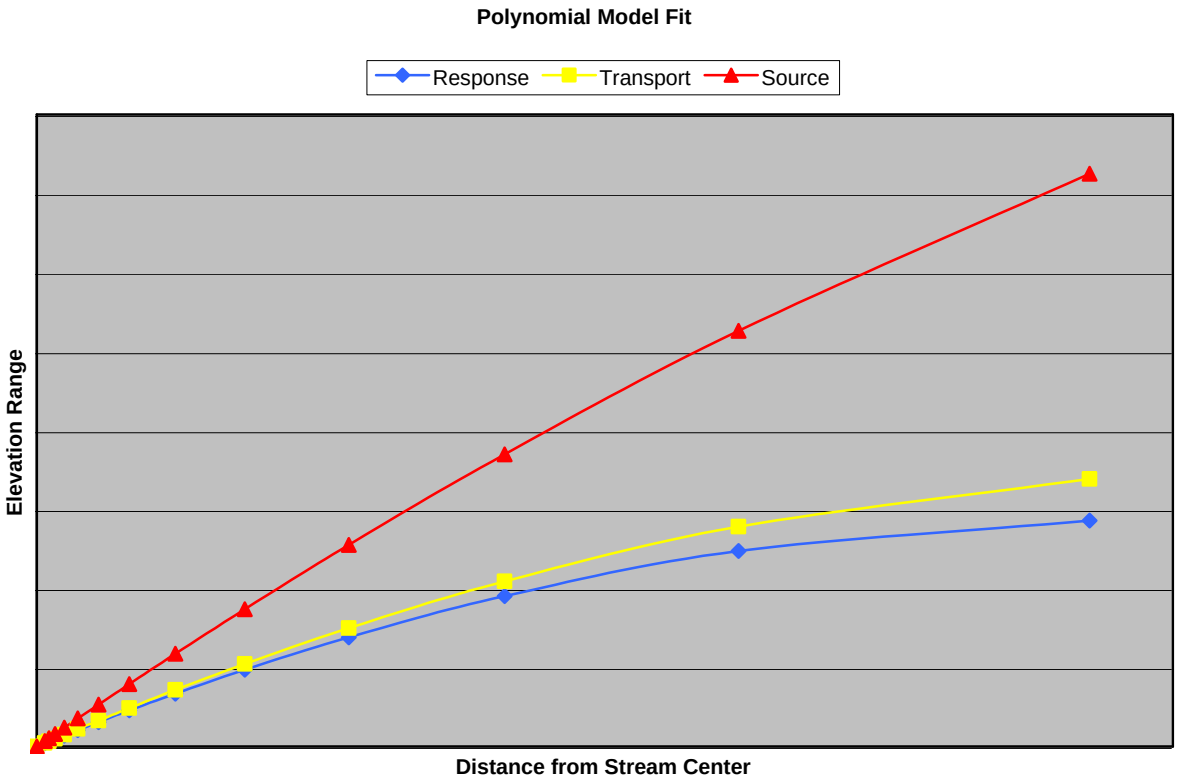

Figure 7. Stylized graph of polynomial fitted models for Response, Transport, and Source stream segments from Confinement Cluster regressions of Elevation Range against Distance from Stream Center.

Figure 8 shows the distribution of stream segments clustered as Response reaches. The linear regression of elevation range against distance from stream center is significant (F Ratio = 16983.55; Prob. > F = 0.0000); the moderate beta parameter (0. 4568701 Distance), negative intercept, and lower polynomial coefficients suggest that these are wide-bodied streams with moderate and variable (r^2 = 0.571831) cross-valley gradients. The lack of geomorphic confinement is somewhat similar to that of the Transport Reach cluster; however, the Response Reaches are also characterized by higher upstream accumulative areas and by stream gradients near one percent. Similarly, Figure 9 diagrams model fits of elevation range against distance from stream center, but for Transport Reaches. Again, the linear regression is significant (F Ratio = 42247.29; Prob. > F = 0.000) with a moderate beta coefficient (0.4566623 Distance) and a negative intercept; however, this stream segment cluster is characterized by slightly less variability (r^2 = 0.619354) and a steeper polynomial fitted cross-valley gradient than the Response Reach cluster. Figure 10 diagrams the Source Reach stream segment cluster; it has a much higher beta coefficient (0.6803434 Distance), thus steeper cross-valley gradient, and better fitting of the linear regression of elevation range against distance from stream center (r^2 = 0.808382; F Ratio = 132013.4; Prob. > F = 0.000). In summary, examinations of the K-Means clustering of stream segments in relation to elevation range and distance from stream center resulted in two similar fitted models (Transport and Response Reaches) and one very different model (Source Reach). The differences between Transport and Response Reaches are in the two other clustering

parameters, upstream accumulative area and stream gradient, which are in accordance with observations of Montgomery and Buffington (1993).

We also examined the distribution of classified AVIRIS Riparian Vegetation for the three Confinement Clusters to determine which, if any, relationships exist. The results of this analysis show that vegetation classes are distributed differently in each confinement cluster. Only pixels containing forested classes were considered in this analysis, thus each stream segment was characterized by a total of 100% classified pixels parceled among the three AVIRIS classes. Each forested class was evaluated as a percent of each stream segment; stream segments were subsequently treated to a one-way analysis of variance to determine if variability differences among confinement clusters were greater than variability within clusters. The results for all treatments are statistically significant, including tests using non-parametric assumptions. Comparisons of all pairs were also considered using the Tukey-Kramer HSD (honestly significant difference) method, which is conservative under non-parametric assumptions (Zar 1999).

The results of comparing AVIRIS Riparian Vegetation classes a function of Confinement Clusters are presented in Figures 11-13. Each forest class is presented separately, with Figure 11 providing results for the Conifer class. Transport reaches had a mean of 56% Conifer, as opposed to Source and Response reaches with 43% and 26%, respectively. This distributional difference is significant (F Ratio = 16.8483; Prob. > F < 0.0001; DF = 331) for the single factor ANOVA; non-parametric tests (Prob. > Chi^2 < 0.0001) and group comparisons (a = 0.05) are also significant. The separation of Source and Response reaches is most pronounced, with Transport reaches more closely resembling the distribution of Conifer in Source reaches. Figure 12 presents a comparative analysis for the distribution of true Riparian vegetation within Confinement Clusters. The percent of classified stream segment AVIRIS pixels considered Riparian were lowest in Source reaches (24%), highest in Transport reaches (50%), and intermediate in Response reaches (39%). A single factor ANOVA was statistically significant (F Ratio = 15.1525; Prob. > F < 0.0001; DF = 306), as were all non-parametric tests (Prob. > Chi^2 = 0.0002) and group comparisons (a = 0.05). Response and Transport reaches were more closely allied than the Source reaches in Riparian vegetation composition. Lastly, Figure 13 presents the examination of the AVIRIS Hardwood class distribution within Confinement Clusters. Source and Response reach clusters showed high percent distributions with 76% and 61% Hardwood, respectively. Transport reaches were markedly lower at 47% Hardwood. Again, tests of confinement were statistically significant for single factor ANOVA (F Ratio = 23.4285; Prob. > F < 0.0001; DF = 478), non-parametric Chi^2 approximations (Prob. > Chi^2 < 0.0001), and all group comparisons using Tukey-Kramer HSD (a = 0.05).

Confinement Cluster: Response Reach
Bivariate Fit of Elevation Range By Distance

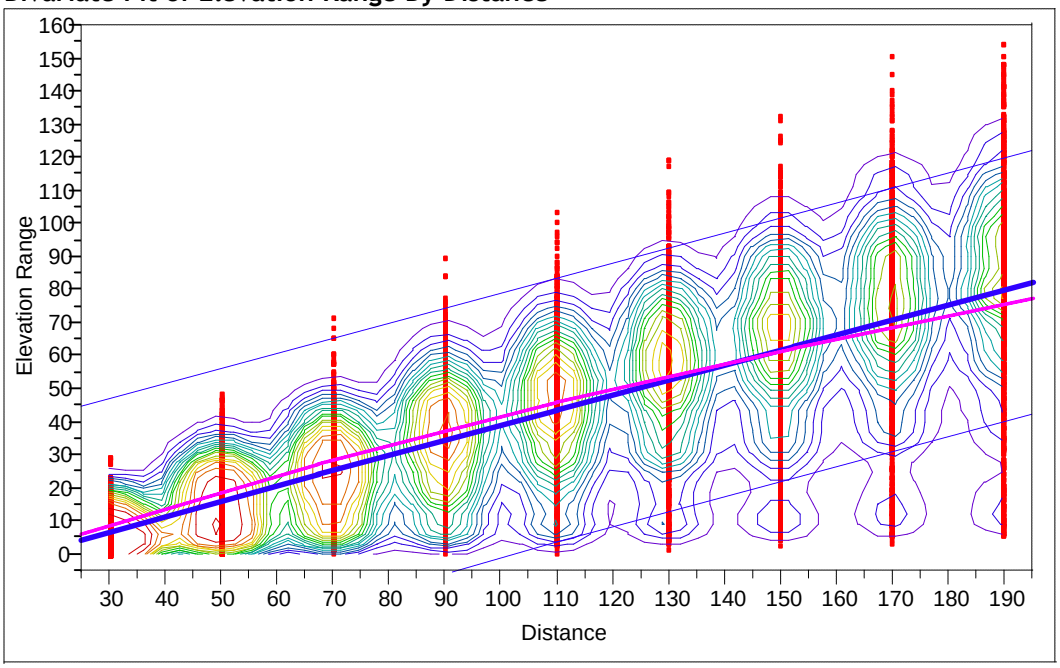

.1 .2 .3 .4 .5 .6 .7 .8 .9 Quantile Density Contours
Linear Fit
Polynomial Fit Degree=2

Linear Fit Elevation Range = -6.757248 + 0.4568701 Distance

Summary of Fit

Rsquare	0.571865
RSquare Adj	0.571831
Root Mean Square Error	20.41528
Mean of Response	43.49847
Observations (or Sum Wgts)	12717

Source	DF	Sum of Squares	Mean Square	F Ratio
Model	1	7078463	7078463	16983.55
Error	12715	5299403	417	Prob > F
C. Total	12716	12377865		0.0000

Parameter Estimates

Term	Estimate	Std Error	t Ratio	Prob>|t|
Intercept	-6.757248	0.42601	-15.86	<.0001
Distance	0.4568701	0.003506	130.32	0.0000

Polynomial Fit Degree=2

Elevation Range = 0 + 0.4174833 Distance - 0.0005512 (Distance-110)^2

Parameter Estimates

Term		Estimate	Std Error	t Ratio	Prob>|t|
Intercept	Zeroed	0	0	.	.
Distance		0.4174833	0.002048	203.86	0.0000
(Distance-110)^2		-0.000551	0.00007	-7.86	<.0001

Figure 8. Linear and Polynomial Fit of Elevation Range as a Function of Distance from Stream for Confinement Cluster: Response Reach.

Confinement Cluster: Transport Reach
Bivariate Fit of Elevation Range By Distance

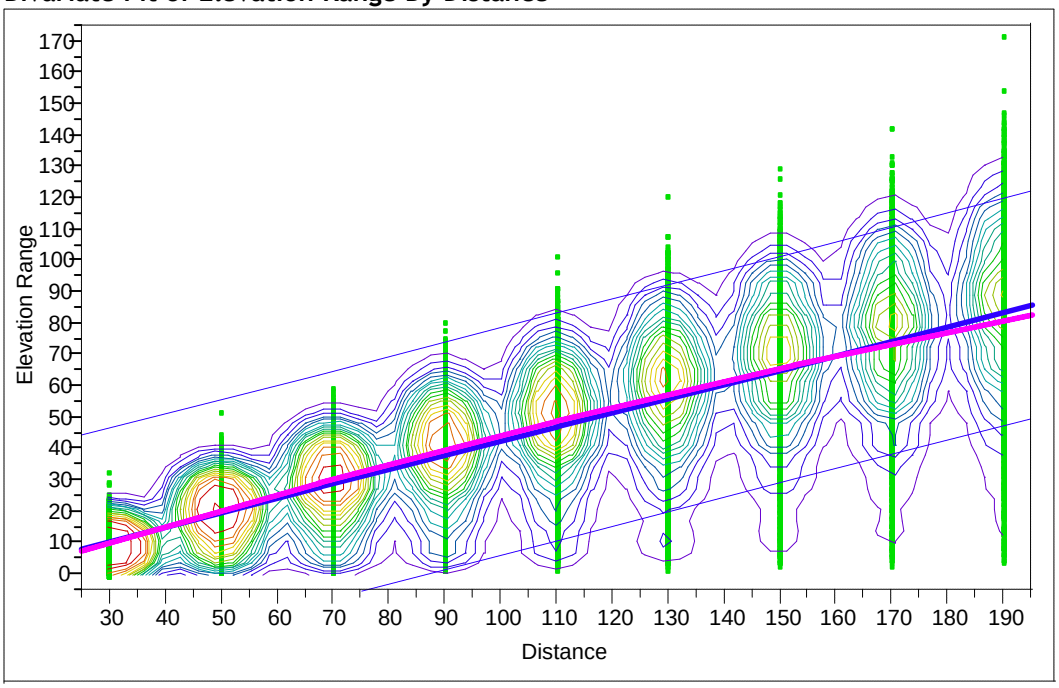

.1 .2 .3 .4 .5 .6 .7 .8 .9 Quantile Density Contours
Linear Fit
Polynomial Fit Degree=2

Linear Fit Elevation Range = -3.180633 + 0.4566623 Distance

Summary of Fit

Rsquare	0.619368
RSquare Adj	0.619354
Root Mean Square Error	18.48733
Mean of Response	47.05222
Observations (or Sum Wgts)	25965

Source	DF	Sum of Squares	Mean Square	F Ratio
Model	1	14439343	14439343	42247.29
Error	25963	8873674	341.78153	Prob > F
C. Total	25964	23313017		0.0000

Parameter Estimates

Term	Estimate	Std Error	t Ratio	Prob>|t|
Intercept	-3.180633	0.269983	-11.78	<.0001
Distance	0.4566623	0.002222	205.54	0.0000

Polynomial Fit Degree=2

Elevation Range = 0 + 0.4435071 Distance - 0.0005305 (Distance-110)^2

Parameter Estimates

Term		Estimate	Std Error	t Ratio	Prob>|t|
Intercept	Zeroed	0	0	.	.
Distance		0.4435071	0.001288	344.29	0.0000
(Distance-110)^2		-0.00053	0.000044	-12.02	<.0001

Figure 9. Linear and Polynomial Fit of Elevation Range as a Function of Distance from Stream for Confinement Cluster: Transport Reach.

Confinement Cluster: Source Reach
Bivariate Fit of Elevation Range By Distance

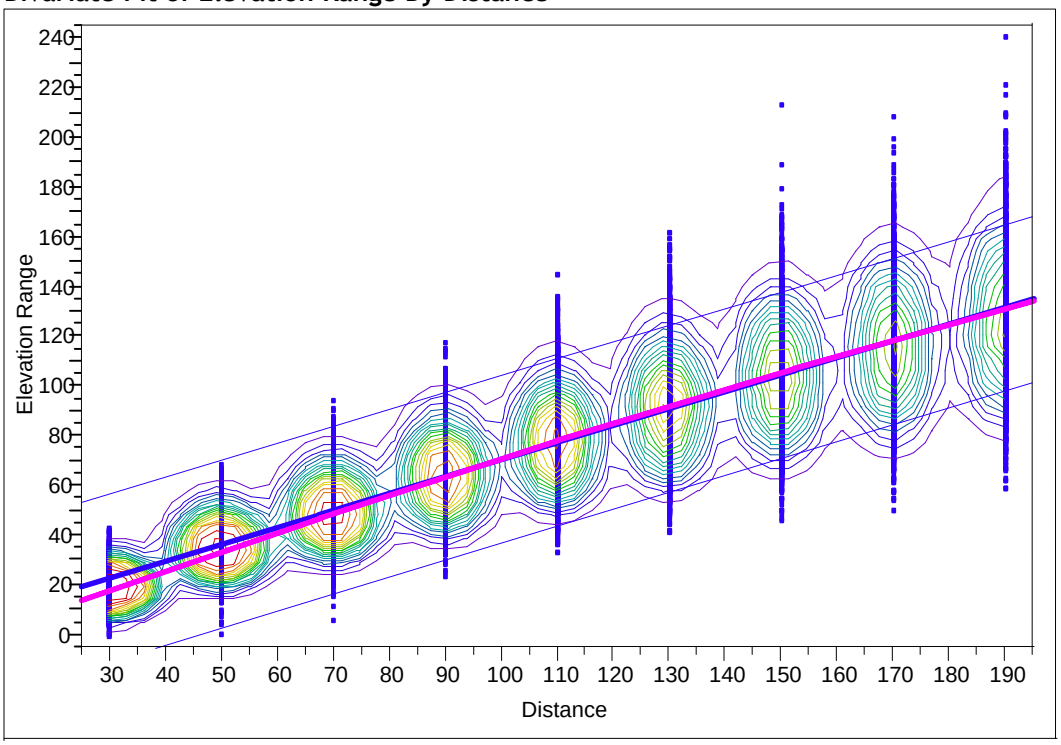

.1 .2 .3 .4 .5 .6 .7 .8 .9 Quantile Density Contours
Linear Fit
Polynomial Fit Degree=2

Linear Fit Elevation Range = 2.3917929 + 0.6803434 Distance

Summary of Fit

Rsquare	0.808389
RSquare Adj	0.808382
Root Mean Square Error	17.10516
Mean of Response	77.22957
Observations (or Sum Wgts)	31293

Source	DF	Sum of Squares	Mean Square	F Ratio
Model	1	38625343	38625343	132013.4
Error	31291	9155322	292.58643	Prob > F
C. Total	31292	47780665		0.0000

Parameter Estimates

Term	Estimate	Std Error	t Ratio	Prob>|t|
Intercept	2.3917929	0.227541	10.51	<.0001
Distance	0.6803434	0.001872	363.34	0.0000

Polynomial Fit Degree=2

Elevation Range = 0 + 0.7076774 Distance - 0.0004791 (Distance-110)^2

Parameter Estimates

Term		Estimate	Std Error	t Ratio	Prob>|t|
Intercept	Zeroed	0	0	.	.
Distance		0.7076774	0.001085	652.33	0.0000
(Distance-110)^2		-0.000479	0.000037	-12.89	<.0001

Figure 10. Linear and Polynomial Fit of Elevation Range as a Function of Distance from Stream for Confinement Cluster: Source Reach.

Oneway Analysis of Percent Conifer By Confinement

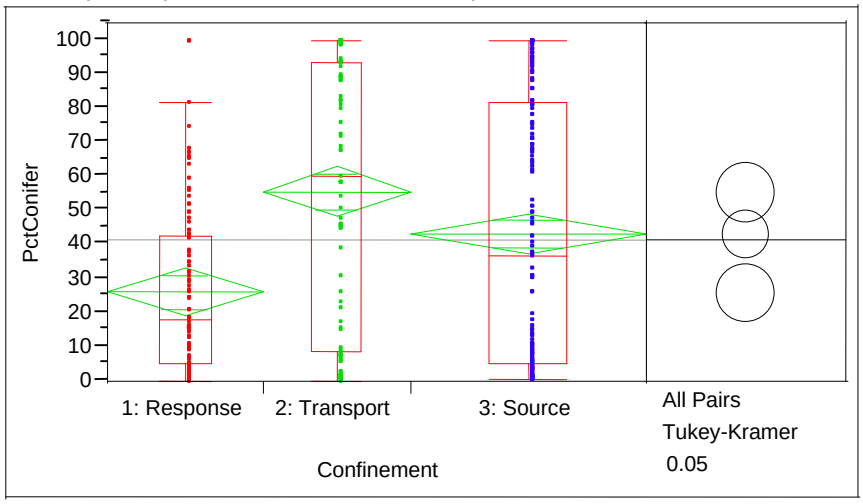

Oneway Anova
Summary of Fit

Rsquare	0.092906
Adj Rsquare	0.087392
Root Mean Square Error	34.99306
Mean of Response	41.87338
Observations (or Sum Wgts)	332

Analysis of Variance

Source	DF	Sum of Squares	Mean Square	F Ratio	Prob > F
Confinement	2	41262.00	20631.0	16.8483	<.0001
Error	329	402865.17	1224.5		
C. Total	331	444127.18			

Means for Oneway Anova

Level	Number	Mean	Std Error	Lower 95%	Upper 95%
1: Response	96	26.3334	3.5715	19.308	33.359
2: Transport	91	55.8362	3.6683	48.620	63.052
3: Source	145	43.3990	2.9060	37.682	49.116

Std Error uses a pooled estimate of error variance

Wilcoxon / Kruskal-Wallis Tests (Rank Sums)

Level	Count	Score Sum	Score Mean	(Mean-Mean0)/Std0
1: Response	96	12880.5	134.172	-3.915
2: Transport	91	17999.5	197.797	3.652
3: Source	145	24398	168.262	0.294

1-way Test, ChiSquare Approximation

ChiSquare	DF	Prob>ChiSq
20.6323	2	<.0001

Means Comparisons

Dif=Mean[i]-Mean[j]	2: Transport	3: Source	1: Response
2: Transport	0.000	12.437	29.503
3: Source	-12.437	0.000	17.066
1: Response	-29.503	-17.066	0.000

Alpha=0.05 Comparisons for all pairs using Tukey-Kramer HSD

q*	Alpha
2.35437	0.05

Abs(Dif)-LSD	2: Transport	3: Source	1: Response
2: Transport	-12.214	1.419	17.449
3: Source	1.419	-9.676	6.225
1: Response	17.449	6.225	-11.891

Figure 11. Analysis of AVIRIS Conifer Vegetation as Percent of Classified Pixels for Confinement Clusters.

Oneway Analysis of Percent Riparian By Confinement

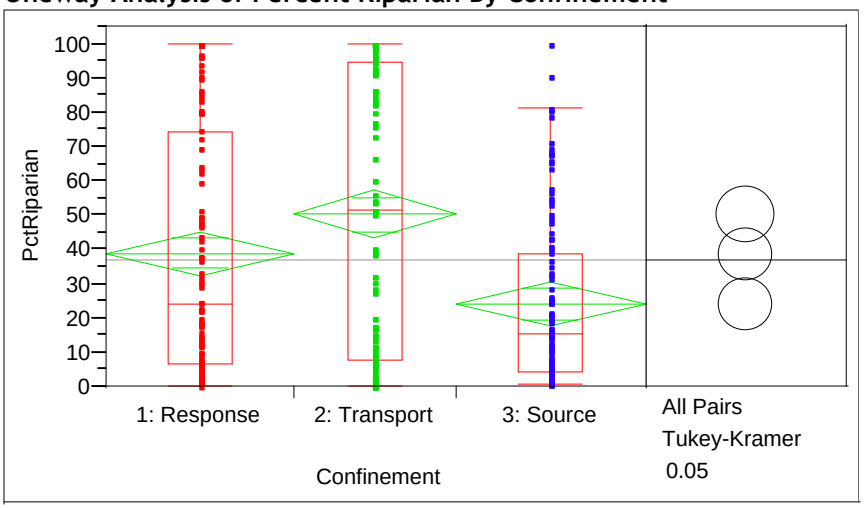

Oneway Anova
Summary of Fit

Rsquare	0.090651
Adj Rsquare	0.084668
Root Mean Square Error	33.74809
Mean of Response	37.14095
Observations (or Sum Wgts)	307

Analysis of Variance

Source	DF	Sum of Squares	Mean Square	F Ratio	Prob > F
Confinement	2	34515.45	17257.7	15.1525	<.0001
Error	304	346235.87	1138.9		
C. Total	306	380751.32			

Means for Oneway Anova

Level	Number	Mean	Std Error	Lower 95%	Upper 95%
1: Response	108	38.9598	3.2474	32.570	45.350
2: Transport	91	50.3862	3.5378	43.425	57.348
3: Source	108	24.1618	3.2474	17.772	30.552

Std Error uses a pooled estimate of error variance

Wilcoxon / Kruskal-Wallis Tests (Rank Sums)

Level	Count	Score Sum	Score Mean	(Mean-Mean0)/Std0
1: Response	108	17287	160.065	0.881
2: Transport	91	16236	178.418	3.128
3: Source	108	13755	127.361	-3.874

1-way Test, ChiSquare Approximation

ChiSquare	DF	Prob>ChiSq
17.1254	2	0.0002

Means Comparisons

Dif=Mean[i]-Mean[j]	2: Transport	1: Response	3: Source
2: Transport	0.000	11.426	26.224
1: Response	-11.426	0.000	14.798
3: Source	-26.224	-14.798	0.000

Alpha=0.05 Comparisons for all pairs using Tukey-Kramer HSD

q*	Alpha
2.35533	0.05

Abs(Dif)-LSD	2: Transport	1: Response	3: Source
2: Transport	-11.784	0.116	14.914
1: Response	0.116	-10.817	3.981
3: Source	14.914	3.981	-10.817

Figure 12. Analysis of AVIRIS Riparian Vegetation as Percent of Classified Pixels for Confinement Clusters.

Oneway Analysis of Percent Hardwood By Confinement

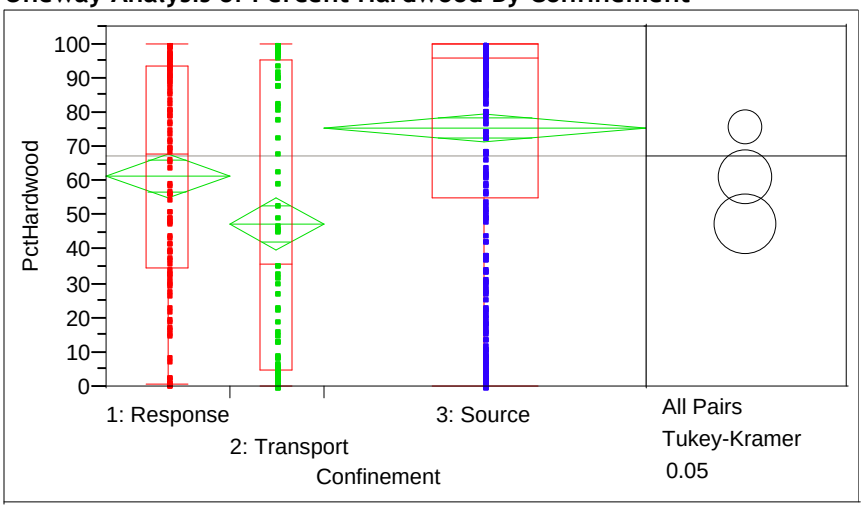

Oneway Anova
Summary of Fit

Rsquare	0.089617
Adj Rsquare	0.085792
Root Mean Square Error	34.93665
Mean of Response	67.42331
Observations (or Sum Wgts)	479

Analysis of Variance

Source	DF	Sum of Squares	Mean Square	F Ratio	Prob > F
Confinement	2	57192.34	28596.2	23.4285	<.0001
Error	476	580991.21	1220.6		
C. Total	478	638183.56			

Means for Oneway Anova

Level	Number	Mean	Std Error	Lower 95%	Upper 95%
1: Response	110	61.4939	3.3311	54.948	68.039
2: Transport	85	47.4561	3.7894	40.010	54.902
3: Source	284	75.6960	2.0731	71.622	79.770

Std Error uses a pooled estimate of error variance

Wilcoxon / Kruskal-Wallis Tests (Rank Sums)

Level	Count	Score Sum	Score Mean	(Mean-Mean0)/Std0
1: Response	110	21784.5	198.041	-3.671
2: Transport	85	14391.5	169.312	-5.261
3: Source	284	78784	277.408	7.235

1-way Test, ChiSquare Approximation

ChiSquare	DF	Prob>ChiSq
54.4670	2	<.0001

Means Comparisons

Dif=Mean[i]-Mean[j]	3: Source	1: Response	2: Transport
3: Source	0.000	14.202	28.240
1: Response	-14.202	0.000	14.038
2: Transport	-28.240	-14.038	0.000

Alpha=0.05 Comparisons for all pairs using Tukey-Kramer HSD

q*	Alpha
2.35107	0.05

Abs(Dif)-LSD	3: Source	1: Response	2: Transport
3: Source	-6.893	4.978	18.085
1: Response	4.978	-11.076	2.176
2: Transport	18.085	2.176	-12.599

Figure 13. Analysis of AVIRIS Hardwood Vegetation as Percent of Classified Pixels for Confinement Clusters.

Part 2.4. Geomorphic Typing Discussion

Notably, the geomorphic classification promoted by Montgomery and Buffington (1997) is used by resource managers to assign regulatory status for various activities, such as timber harvesting, stream restoration, and critical habitat for fisheries. Here we use a surrogate approximation of their geomorphic classification in developing Confinement Clusters, in which we examine the distribution of riparian vegetation cover types – determined by an unsupervised classification of AVIRIS hyperspectral data – as a function of geomorphic confinement.

An analysis of the Confinement Clusters developed from the K-Means classification had intuitive results. For example, the role of stream gradient and upstream accumulative areas is pronounced, as evidenced by Figure 5 in which segments downstream with little gradient are classified differently than segments upstream with high relief. However, side slope gradient, and thus measures of confinement, is also critical to assigning a categorical cluster response, thus we implemented an innovative spatial analysis technique to incorporate this important variable. An additional intuitive result from this analysis is that segments with high side slope gradient are clustered with the same Source confinement clusters and those with less side slope gradient are Response reaches. The remainder or intermediate segments are also clustered. It is worth noting that the separation of Transport and Response reaches is predicated on upstream accumulative area, which in turn is a prime predictor of flow and channel volume, and stream gradient, which regulates transport capacity.

Examinations of riparian vegetation, determined from classified AVIRIS hyperspectral data, as a function of Confinement Clusters discussed above, yielded compelling findings. Source reaches are dominated by Hardwood, with moderate Conifer and low Riparian class distributions. Transport reaches are largely composed of Riparian with moderate Conifer and low Hardwood. Response reaches are moderate compositions of all three Conifer, Hardwood, and Riparian classes. Visual examinations of the distributions of Conifer and Hardwood suggest that non-considered factors such as aspect have a non-random effect on the distribution of these vegetation types; therefore, the elevated percentage values for Hardwood and Conifer in Source reaches is tenable. Moreover, the dynamic fluvial nature of Transport reaches, including both deposition and erosion, is reflected by the elevated proportion of true Riparian vegetation, a vegetation type that is often more tolerant and responsive to dynamic growing conditions. The consideration of Response reach composition is one that is perhaps more difficult to explain; these stream segments are heterogeneous in many respects, thus a heterogeneous vegetation composition is just reflective of the environmental conditions. However, it must be noted that the vegetation distributions presented here reflect current conditions, undoubtedly altered by land use practices; therefore, additional causal conclusions should not be drawn from these observations.

Part 3. Comparison of Vegetation Data

Part 3.1. Vegetation Data Comparison Background

The final phase of the research presented here is to compare the results of the AVIRIS classification exercise to other data products. Specifically, we examined the vegetation composition for Flightline 18 depicted by the CALVEG2000 data set produced by the

California Department of Forestry and Fire Protection and the United States Department of Agriculture - Forest Service. CALVEG2000 data are comprehensive in both spatial domain and attribution for much of California, including all portions of the Navarro River watershed, and was created by an exhaustive system of data acquisition, calibration, classification, and verification. The underlying basis for these data is a combination of satellite imagery (Landsat 7 Thematic Mapper Plus), reconnaissance (ground and air), and processing technique.

Although CALVEG 2000 covers all of the Navarro River watershed, AVIRIS Flightline 18 is spread across two data tiles: 11 & 12 (see http://frap.ca.gov/ for metadata). These two data tiles straddle the counties of Humboldt, Trinity, Mendocino, Lake, and Sonoma; the Navarro River watershed is wholly within Mendocino County (Figure 14).

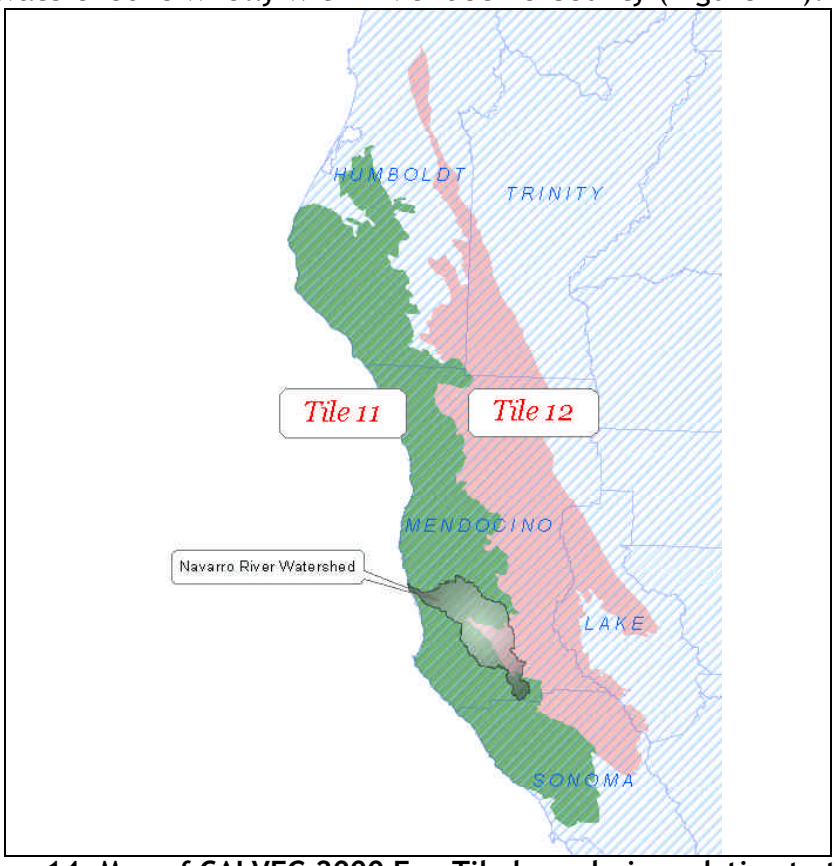

Figure 14. Map of CALVEG 2000 Eco-Tile boundaries relative to the Navarro River watershed and counties of north, coastal California.

It is this difference in base data resolution, aggregated 5m pixels versus 1 hectare minimum mapping unit; area of coverage or extent; and intended use that requires further mention. The straddling of data products for Flightline 18, and the Navarro River watershed, and general differences required an investigation as to the composition of attributes for the two tiles. This additional analysis was necessary because any inferences drawn from the comparison of these two very different data should be couched within the understanding of their respective limitations. As such, the attribute composition was compared at two levels: tile and watershed, for the vegetation type attribute. The results of this investigation are presented here as to not interfere with the direct comparison of the two data themselves, CALVEG2000 and AVIRIS Riparian Vegetation Classification, presented later, at the watershed

and flightline level. It should be noted that while CALVEG2000 uses a stand-based approach and the AVIRIS classification uses a pixel-based approach but that both methods are based on "mixed" pixels; the usefulness of comparing these different methods is subject to interpretation.

Table 6 shows the relative contributions of vegetation types, considered to be riparian in nature, to data tiles 11 & 12. Because each tile represents different environmental conditions, whether they climatic or otherwise, the distributions of vegetation types are not uniform across both tiles. Table 7 shows all vegetation types within the Navarro River watershed for the combined tiles 11 & 12 of CALVEG2000 and notes which types are also considered riparian in Table 6. Of the twelve vegetation types considered riparian, only two are represented in the Navarro River watershed in the combination of tiles. The two riparian types common at both levels are Coyote Brush and Red Alder and they constitute less than 0.25% of the watershed as depicted in CALVEG2000.

CALVEG Data Tile	Number of Polygons	CALVEG Vegetation Type Code	CALVEG Vegetation Type Description	Total Area in Tile (ha)	Percent Riparian Type in Tile
11	278	CK	Coyote Brush	3305.07	32.29
11	2	HJ	Wet Grass/Herbs	83.52	0.82
11	2	HT	Tule-Cattail	43.47	0.42
11	9	QE	White Alder	40.14	0.39
11	23	QM	Bigleaf Maple	51.57	0.50
11	81	QO	Willow	225.45	2.20
11	1521	QR	Red Alder	4202.10	41.05
11	821	QY	Willow-Alder	2207.70	21.57
11	30	QZ	Eucalyptus	77.04	0.75
12	4	CK	Coyote Brush	5.22	0.20
12	10	HJ	Wet Grass/Herbs	44.37	1.73
12	3	QE	White Alder	5.58	0.22
12	219	QF	Fremont Cottonwood	585.54	22.77
12	10	QI	California Buckeye	19.08	0.74
12	517	QL	Valley Oak	1538.19	59.81
12	2	QM	Bigleaf Maple	6.21	0.24
12	32	QO	Willow	118.26	4.60
12	2	QR	Red Alder	7.29	0.28
12	118	QY	Willow-Alder	242.10	9.41

Table 6. Distribution of CALVEG Vegetation Types within Data Tiles considered "riparian" in nature and their respective contributions in area and by percent.

Number of Polygons	CALVEG Vegetation Type Code	Vegetation Type Description	Area (ha)	Percent Area	Average Polygon Area (ha)	* Riparian
28	AG	General Agriculture	1520.77	1.86	54.3133	FALSE
2	AN	Mendocino Manzanita	7.81	0.01	3.908	FALSE
29	BA	General Barren	82.45	0.10	2.8432	FALSE
45	CA	Chamise	219.27	0.27	4.8728	FALSE
5	CK	Coyote Brush	114.22	0.14	22.8445	TRUE
80	CQ	Northern Mixed Shrub	1319.42	1.62	16.4929	FALSE
33	CS	Scrub Oak	220.99	0.27	6.6969	FALSE
2994	DF	Pacific Douglas-fir	8719.31	10.68	2.9123	FALSE
45	GF	Grand Fir	96.15	0.12	2.1367	FALSE
725	HG	Dry Grass/Herbs	12343.31	15.12	17.0253	FALSE
9	MM	Monterey Cypress	31.89	0.04	3.5443	FALSE
27	MU	Ultramafic Mixed Conifer	69.43	0.09	2.5715	FALSE
3192	NX	Non-productive Mixed Hardwood	10161.32	12.44	3.1834	FALSE
4	PM	Bishop Pine	7.21	0.01	1.8046	FALSE
154	QB	California Bay	406.32	0.50	2.6385	FALSE
115	QC	Canyon Live Oak	257.95	0.32	2.2431	FALSE
11	QD	Blue Oak	22.83	0.03	2.076	FALSE
744	QG	Oregon White Oak	2149.19	2.63	2.8887	FALSE
244	QK	California Black Oak	681.09	0.83	2.7914	FALSE
31	QR	Red Alder	74.73	0.09	2.4108	TRUE
1418	QT	Tanoak	3854.72	4.72	2.7184	FALSE
323	QW	Interior Live Oak	839.47	1.03	2.599	FALSE
10944	RD	Redwood-Douglas-Fir	37914.71	46.44	3.4644	FALSE
26	RW	Redwood	89.57	0.11	3.4453	FALSE
58	SC	Blueblossom Ceanothus	215.74	0.26	3.7197	FALSE
10	SD	Manzanita Chaparral	29.74	0.04	2.975	FALSE
3	UB	General Urban	85.61	0.10	28.5382	FALSE
30	WA	General Water	115.57	0.14	3.8526	FALSE

Table 7. Distribution of Vegetation Types within Navarro River watershed by CALVEG2000. *Riparian field indicates if vegetation type was used in selection of "riparian" type polygons used in comparative analysis.

Although it appears that the Navarro River watershed is atypical in its distribution of vegetation types, compared to both data tiles in CALVEG2000, at least in terms of riparian vegetation, much of this discrepancy reflects the aforementioned challenges in scale; in this case from regional approximations to watershed parcel. Comparability of two disparate data in restricted space, as presented below, must be viewed with the same limitations and challenges of scale.

Part 3.2. Vegetation Data Comparison Methods

We employed the following methods to explore the comparability of the classified AVIRIS riparian spatial data for Flightline 18 to the CALVEG2000 spatial data. All data comparisons are restricted to the classified AVIRIS pixels within the Riparian Extent discussed above and do not include upland areas. Flightline 18 classified riparian data was converted to Arc/Info GRID format using the same 5 m raster resolution as the ENVI-based image and maintaining its UTM Zone 10 projection and analysis window. Although there are specific protocols for the development of CALVEG2000, in practicality, its use of the lifeform at the VEGTYPE level is implied. Furthermore, the value attribute table of the converted AVIRIS data uses the following codes to develop a numeric equivalent of the AVIRIS Classes described above:

0 – Null [these data were later converted to 'No Data' or –9999 in GRID]
1 – Conifer [*Sequoia sp.* predominate & known as Class A from above]
2 – Agriculture
3 – Riparian [*Salix spp.* predominate & known as Class C from above]
4 – Hardwood [*Umbellarium sp. et Quercus spp.* predominate & known as Class B from above]

These data were converted in the following matter to match the analytical properties of AVIRIS Flightline 18. CALVEG Tiles 11 and 12 (Figure 14) were clipped to the boundary of the Navarro River watershed. Clipped coverages were edited to include a new attribute [CODE] used to convert the character field of [COVERTYPE] to numeric, using an Arc Macro Language (AML) crosswalk in ESRI ArcEdit (Table 8.)

CALVEG Cover Type Code	Cover Type Description	Assigned Numeric Code
CON	Conifer	1
SHB	Shrub	2
HDW	Hardwood	3
HEB	Herbaceous	4
WAT	General Water	5
MIX	Mixed Forest	6
AGR	General Agriculture	7
URB	General Urban	8
NNA	Ornamental Vegetation	8
BAR	Barren	9

Table 8. Cross-walk of CALVEG Cover Types to Numeric Code.

Clipped coverages were dissolved on the numeric code and converted to raster format in GRID using the 5 meter resolution and spatial analysis window set for Flightline18. The field [CODE] attribute was converted to the field [VALUE] attribute in this process, as per normal rasterization routines in GRID. Furthermore, these two, separate raster grids were combined to form one seamless set of CALVEG cover type values for Flightline 18. Pair wise combinations of values were extracted for each cell, using the SAMPLE request in GRID, to develop tabular data of each cell-by-cell record. Lastly, each raster input was resampled to

the following cell dimensions: 10m, 30m, 90m, and analyzed to determine if data resolution altered their comparability.

Data were analyzed in JMP5.0 for statistical relationships and examined in ArcMap for visual spatial agreement. Statistical tests were limited to Contingency Analysis comparisons of the categorical values outlined above and a diagnostic Correspondence Analysis of the same.

Part 3.3. Vegetation Data Comparison Results

The cell-by-cell comparison of AVIRIS FL18 and CALVEG2000 cover types resulted in very little correspondence in direct evaluation. This lack of agreement, of course, is not unexpected; however, it is valuable to examine the categorical comparisons to gain insight to each set of classified information. Namely, the differences in spatial resolution, classification methods, and ultimate uses limit functional comparisons; that being said, certain patterns do emerge from their nominal comparison. The following Figure 15 of Contingency Analysis shows the general comparison of data in which association are significantly different from random pairings; however, the contingency model only accounts for 17% of the variation in the data comparison ($P > Chi^2 = 0.0000$, $r^2 = 0.1734$).

Table 9 shows that Agriculture was the best agreement category between the two data; indeed, this cover type represents approximately 5.2% of each data set and correspond roughly 49% of the time. The AVIRIS Agriculture class is comparable to the CALVEG cover types in additional ways. For example, the Water cover type occurs in the AVIRIS Agriculture class 10.58%; given the proximity of water storage ponds to agricultural enterprises and the potential overestimation of water bearing pixels in a coarse-level image classification routine, this cross contamination is not unexpected. Also, the 14.92% of Herbaceous cover within the AVIRIS Agriculture class is not unexpected; this is particularly relevant considering the conversion of annual grasslands to vineyards in the Anderson Valley in particular and north, coastal California in general.

The difficulty of comparing the two data is most evident when examining the three general forest cover types: Conifer, Hardwood, and Mixed Forest. The specificity of the AVIRIS classes of Conifer and Hardwood make incorporation of mixed conifer and hardwood forest equivocal; in fact, the ubiquity of the Mixed Forest cover type throughout the AVIRIS classes, representing the majority of CALVEG cover types at 34.67% of the elements analyzed, makes meaningful analyses difficult. An example of this is its similar distribution in both the AVIRIS Conifer and the AVIRIS Hardwood classes at 46.07% and 40.97% respectively; these Mixed Forest pixels represent a contribution of 39.93% to AVIRIS Conifer and 55.58% to AVIRIS Hardwood, showing a slight tendency toward a higher hardwood component. An alternate but unexplored method of comparison would be to use field level data in independent analyses and compare the results. Due to time constraints no such analyses were performed.

Figure 15. Contingency Analysis of AVIRIS Cover Type By EVeg Cover Type Mosaic Plot. This plot emphasizes the cross contamination between cover types

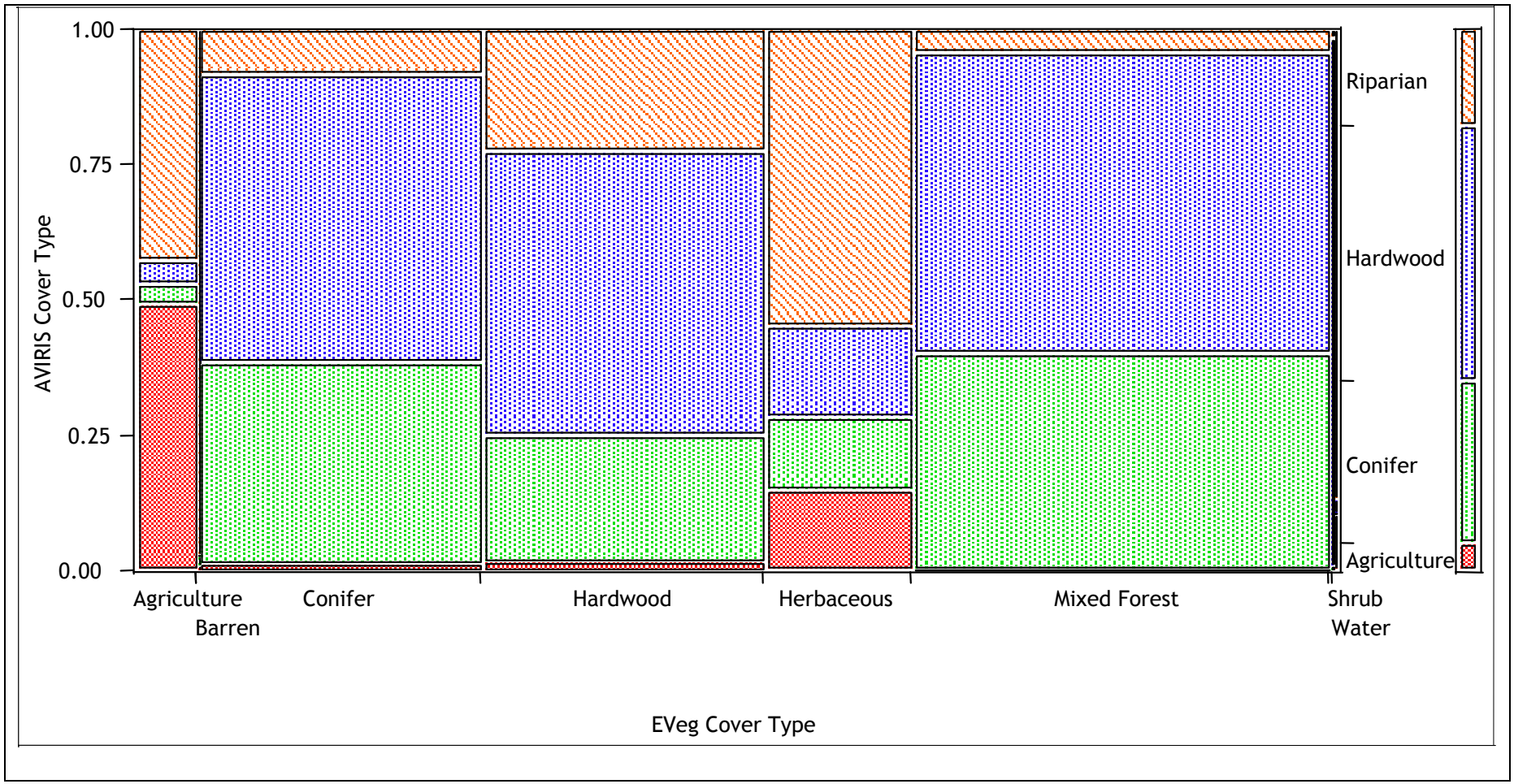

Table 9.
Analysis of AVIRIS Cover Type By CALVEG Cover Type Contingency Table
(CALVEG Cover Type **in Bold** By AVIRIS Cover Type *in Italics*)

Count Total % Col % Row % Cell Chi^2	*Agriculture*	*Conifer*	*Hardwood*	*Riparian*	
Agriculture	5601 2.56 49.31 49.47 42829.9	398 0.18 0.60 3.51 2652.25	498 0.23 0.48 4.40 4375.07	4826 2.20 12.41 42.62 3945.97	11323 5.17
Barren	1 0.00 0.01 0.68 5.7517	3 0.00 0.00 2.04 38.3659	0 0.00 0.00 0.00 69.1248	143 0.07 0.37 97.28 523.802	147 0.07
Conifer	691 0.32 6.08 1.33 1485.86	19239 8.78 29.23 37.07 853.388	27711 12.65 26.90 53.40 448.028	4257 1.94 10.95 8.20 2665.16	51898 23.69
Hardwood	764 0.35 6.73 1.48 1362.29	12150 5.55 18.46 23.57 717.79	27149 12.39 26.35 52.68 350.118	11477 5.24 29.51 22.27 592.728	51540 23.52
Herbaceous	4068 1.86 35.82 14.92 4984.18	3699 1.69 5.62 13.56 2464.42	4612 2.10 4.48 16.91 5257.69	14890 6.80 38.29 54.60 20866.1	27269 12.45
Mixed Forest	222 0.10 1.95 0.29 3506.06	30327 13.84 46.07 39.93 2470.39	42213 19.27 40.97 55.58 1181.33	3194 1.46 8.21 4.21 7850.9	75956 34.67
Shrub	0 0.00 0.00 0.00 44.6341	6 0.00 0.01 0.70 246.803	842 0.38 0.82 97.79 471.947	13 0.01 0.03 1.51 127.934	861 0.39
Water	11 0.01 0.10 10.58 5.8347	0 0.00 0.00 0.00 31.2440	3 0.00 0.00 2.88 43.0887	90 0.04 0.23 86.54 277.245	104 0.05
	11358 5.18	65822 30.04	103028 47.02	38890 17.75	219098

The cross contamination between forest cover data types is even more evident when strictly examining the common conifer and hardwood elements. The AVIRIS classes show Conifer at 30.04% and Hardwood at 47.02% of the classified image. This same spatial domain shows a more equal distribution of cover types within CALVEG; conifers and hardwoods are both ~24% of the data domain each. When examining the coincidence of cover types within the conifer and hardwood domain, the differences in data are more striking. For example, only 21% of the spatial domain is represented by pixels where both AVIRIS and CALVEG are in agreement for both conifers (8.78%) and hardwoods (12.39%). While although 52.68% of the CALVEG Hardwood pixels agree with the AVIRIS Hardwood class, a similar percentage (53.40%) of CALVEG Conifer pixels are crossed with the AVIRIS Hardwood class. Variability in agreement is obviously confounded by the aforementioned issues in data resolution, method of generation, and intent of use; however, in the realm of forested land cover, there is less agreement than for other cover types.

There is no equivalent cover type in CALVEG to match the AVIRIS Riparian cover type (Class C); therefore, it is not a prime candidate for comparative examination. What the Riparian cover type is useful for, however, is the examination of the distribution of CALVEG cover types within the Riparian class (Table 9). This examination is a diagnostic approach to determining general patterns of coarse vegetation data within a fine scale spatial framework. Riparian areas are of interest for the many aforementioned reasons and coarse vegetation data do not adequately represent riparian habitats; therefore, this diagnostic approach examines the distribution of coarse vegetation cover types within this restricted area of interest. In essence, observed patterns from this comparison will help diagnose patterns of vegetation distribution for other spatial locations.

The following CALVEG cover types fall within the AVIRIS Riparian class by percent of each cover type category: Agriculture 42.62%, Barren 97.28%, Conifer 8.20%, Hardwood 22.27%, Herbaceous 54.60%, Mixed Forest 4.21%, Shrub 1.51%, and Water 86.54%. These documented distributions of CALVEG data are notable for the following reasons:

1) Most agriculture in the Anderson Valley is restricted to the alluvial bottomlands (Viers, personal observation) adjacent to riparian vegetation, thus 92% of the CALVEG Agriculture cover type is captured in either the AVIRIS Agriculture or AVIRIS Riparian class (49.47% and 42.62% respectively).
2) The Barren cover type in CALVEG is predominately (97.28%) in the AVIRIS Riparian class, which upon visual examination appears to be largely exposed substrate from streams; thus, the existing riparian vegetation, often in narrow corridors, could be considered to be obscured at coarser scales of analysis, such as 30m.
3) Similarly, 86.54% of the CALVEG Water cover type was in the AVIRIS Riparian class and consists largely of water diversions and water storage ponds constructed in ephemeral drainages. The proximity of this cover type to riparian vegetation is not without expectation.
4) The Herbaceous cover type in CALVEG, 54.60% of which is in the AVIRIS Riparian class, is strongly associated with cleared lands used for animal grazing; as such, many of the small, ribbon-like riparian stands identified in the AVIRIS classification would be indiscernible at coarser scales when surrounded by annual grasslands.
5) Forested cover types in CALVEG, in this case Hardwood, Conifer, and Mixed Forest, are each represented in the AVIRIS Riparian class. The Conifer and Mixed Forest cover

types, contributing 8.20% and 4.21% respectively, represent far less than the Hardwood cover type at 22.27% of its cells falling within riparian vegetation.

6) Lastly, the Shrub cover type in CALVEG has only 1.51% of its contribution within the AVIRIS Riparian class; the mesic site requirements for riparian vegetation preclude association with most shrubs and thus this minor cross association is predictable.

Three additional comparisons were completed at varying resolutions to help discern which, if any, qualities of the two data sources are comparable as a function of decreasing resolution – or increasing coarseness. Each data set was resampled at 10m, 30m, and 90m cell size resolutions and compared on a cell-by-cell basis, as performed previously. Results of these contingency analysis comparisons are similar to the results reported for the initial 5m examination (Figure 16). Notably, the coefficient of determination for each coarser comparison is ~0.14, as compared to the 5m comparison in which $r^2 = 0.17$, and thus the overall comparative analysis does not improve. Although each test is statistically significant in terms of both Likelihood Ratio and Pearson Chi^2 tests, the model Chi^2 values decrease as data become coarser (Figures 17-19). Moreover, correspondence analysis shows three resonant factors across all levels of resolution (Figures 20-23). One, the agricultural class in both the AVIRIS Riparian classification and the CALVEG classification routinely correspond to each other positively. Two, the forested land uses, as defined by Mixed Forest, Coniferous, and Shrub in the CALVEG classification and Coniferous and Hardwood in the AVIRIS Riparian classification, all correspond tightly with each other at each level of comparison. The CALVEG Hardwood class can be considered a non-corresponding factor to all of the AVIRIS classes, as it sits at near right angles to all considered classes except agriculture. Lastly, the Barren, Water, and Herbaceous CALVEG classes correspond with the true riparian class from the AVIRIS Riparian classification. This last factor condenses with increasing data coarseness as the Barren and Water classes essentially drop from the analysis and the AVIRIS Riparian class corresponds to the CALVEG Herbaceous class at the coarsest resolution.

Figure 16. 5m Data Comparison Contingency Test

Source	DF	-LogLike	RSquare (U)
Model	21	44703.40	0.1734
Error	219074	213035.78	
C. Total	219095	257739.18	
N	219098		

Test	ChiSquare	Prob>ChiSq
Likelihood Ratio	89406.8	0.0000
Pearson	112745.3	0.0000

Figure 17. 10m Data Comparison Contingency Test

Source	DF	-LogLike	RSquare (U)
Model	21	11191.163	0.1370
Error	54672	70498.452	
C. Total	54693	81689.615	
N	54700		

Test	ChiSquare	Prob>ChiSq

Test	ChiSquare	Prob>ChiSq
Likelihood Ratio	22382.33	0.0000
Pearson	28223.64	0.0000

Figure 18. 30m Data Comparison Contingency Test

Source	DF	-LogLike	RSquare (U)
Model	21	1253.4665	0.1386
Error	6012	7787.0983	
C. Total	6033	9040.5648	
N	6040		

Test	ChiSquare	Prob>ChiSq
Likelihood Ratio	2506.933	0.0000
Pearson	3114.246	0.0000

Figure 19. 90m Data Comparison Contingency Test

Source	DF	-LogLike	RSquare (U)
Model	15	130.13545	0.1330
Error	635	848.24146	
C. Total	650	978.37691	
N	655		

Test	ChiSquare	Prob>ChiSq
Likelihood Ratio	260.271	<.0001
Pearson	331.430	<.0001

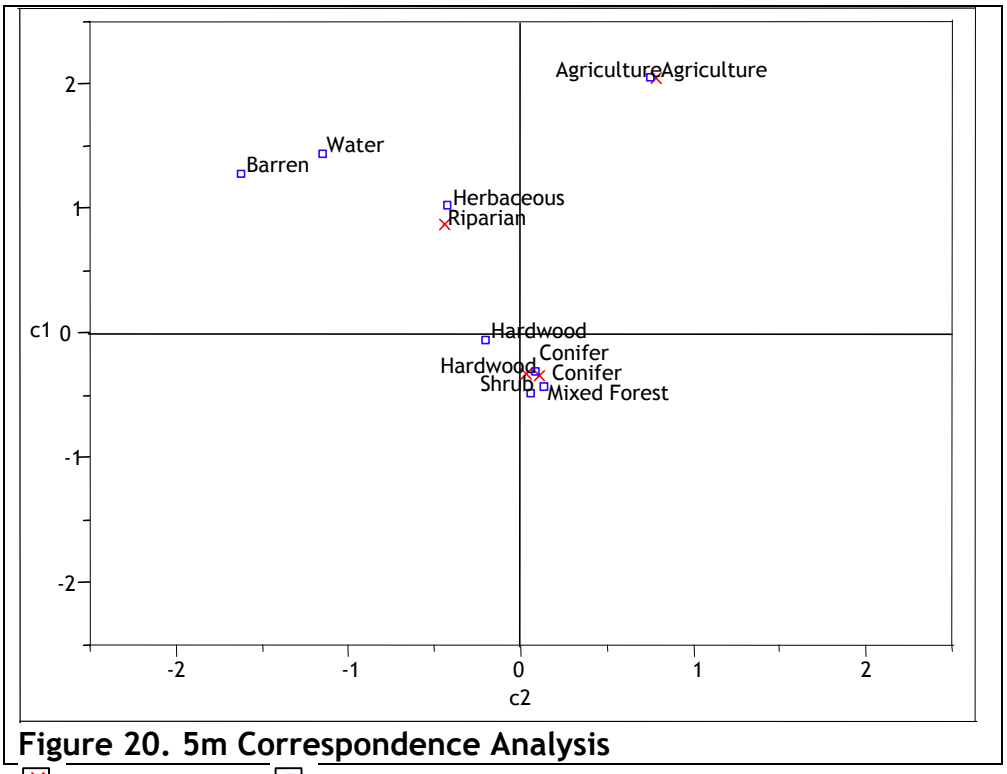

Figure 20. 5m Correspondence Analysis

AVIRIS Cover Type CALVEG Cover Type

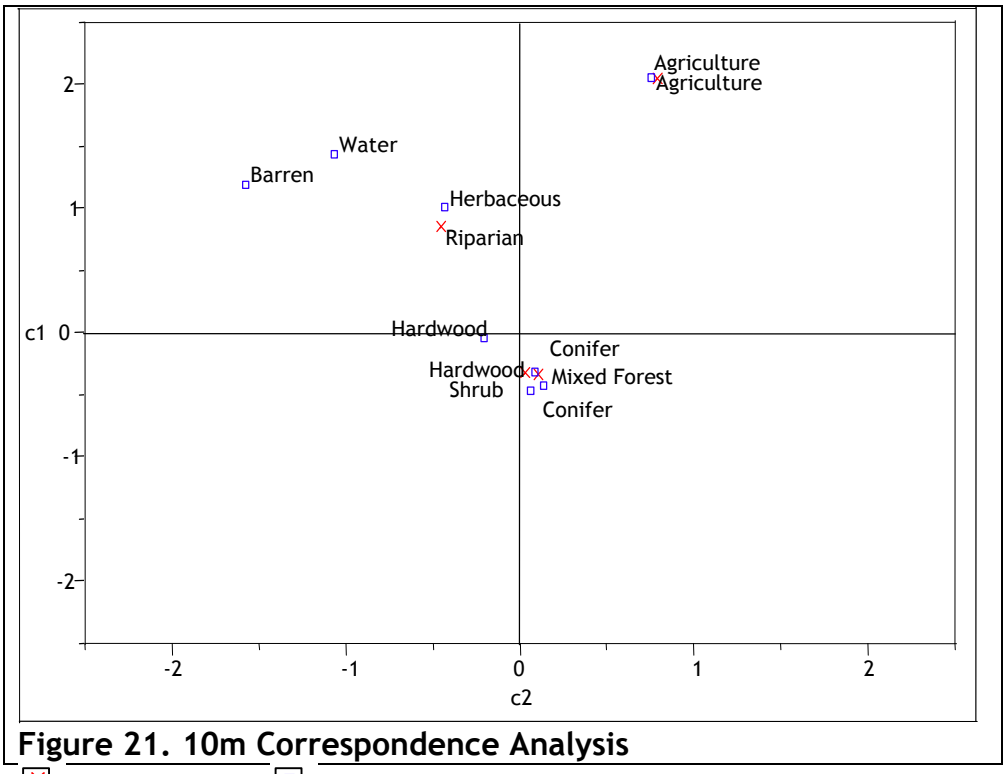

Figure 21. 10m Correspondence Analysis

AVIRIS Cover Type CALVEG Cover Type

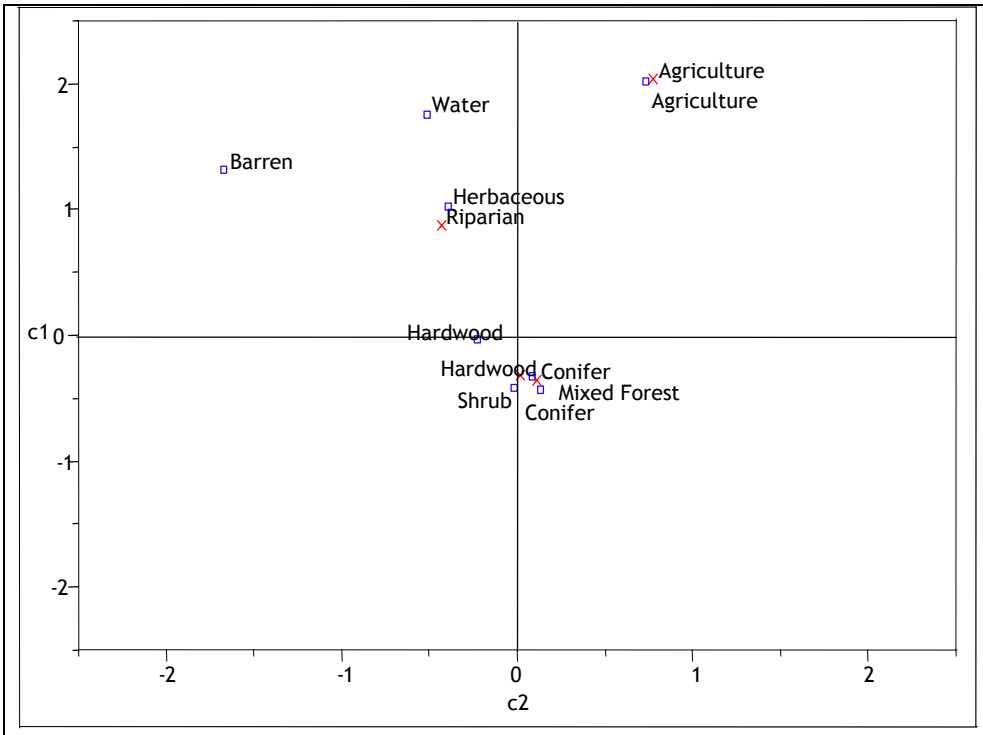

Figure 22. 30m Correspondence Analysis

AVIRIS Cover Type CALVEG Cover Type

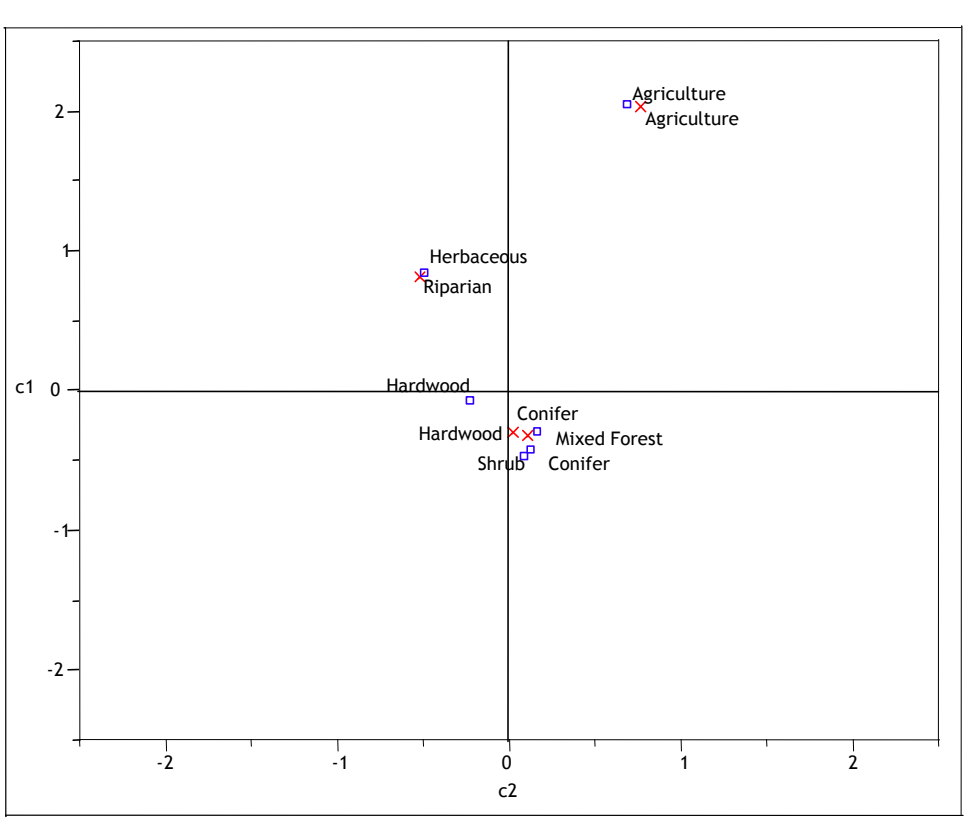

Figure 23. 90m Correspondence Analysis

AVIRIS Cover Type CALVEG Cover Type

When examining the frequency distribution of CALVEG cover types within the AVIRIS Riparian class, it is notable that there are significant differences between the observed CALVEG frequencies within the AVIRIS Riparian Extent of Flightline 18 (Figure 24) and the general frequency of CALVEG cover types within the spatial domain of all pixels in Flightline 18 (Figure 25; $P > Chi^2 = 0.0000$). Thus, one can reject the hypothesis that observations of CALVEG cover types within the Flightline 18 Riparian Extent are random distributions; in essence, the observed increased probability of incidence for Agriculture, Herbaceous, and Water and the observed decreased probability of incidence for Conifer and Mixed Forest cover types within the Riparian Extent are non-random. This relationship also holds when the observed probability distributions of cover types within the Riparian Extent of Flightline 18 are tested against the general distribution of CALVEG cover types for the Navarro River watershed as a whole (Figure 26; $P > Chi^2 = 0.0000$).

Frequencies

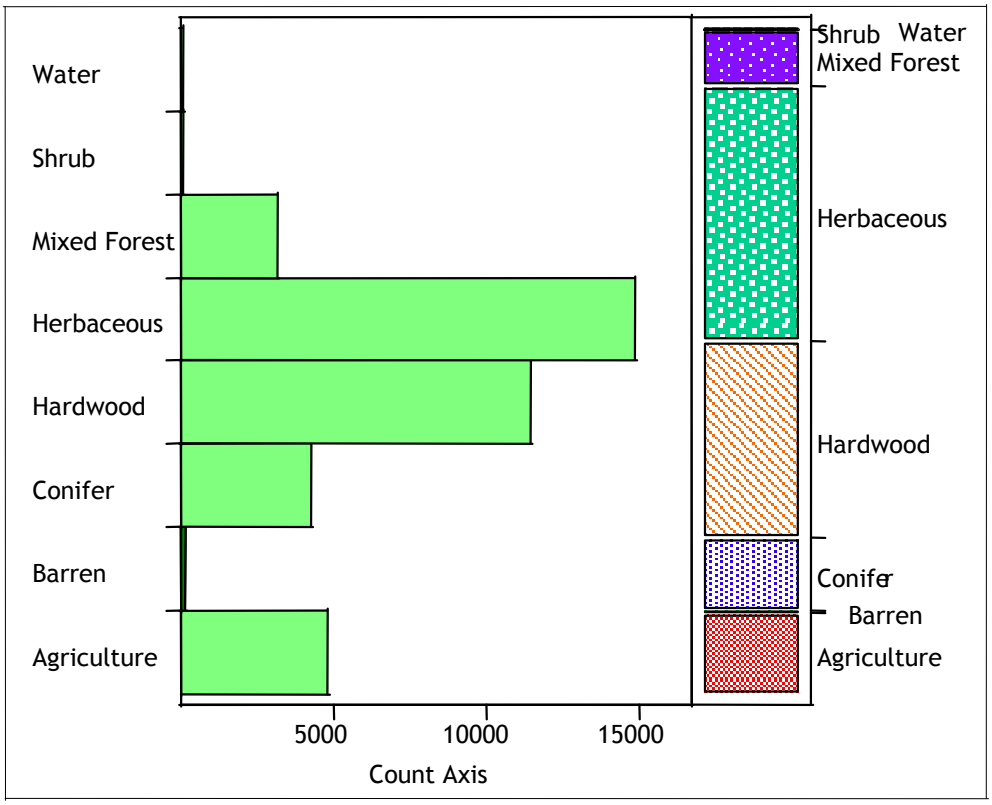

Level	Count	Prob
Agriculture	4826	0.12409
Barren	143	0.00368
Conifer	4257	0.10946
Hardwood	11477	0.29511
Herbaceous	14890	0.38287
Mixed Forest	3194	0.08213
Shrub	13	0.00033
Water	90	0.00231
Total	38890	1.00000

Figure 24. Distribution of CALVEG Cover Types within Riparian Extent of AVIRIS Flightline 18.

Test Probabilities

Level	Estim Prob	Hypoth Prob
Agriculture	0.12409	0.03152
Barren	0.00368	0.00139
Conifer	0.10946	0.15330
Hardwood	0.29511	0.22202
Herbaceous	0.38287	0.19406
Mixed Forest	0.08213	0.36013
Shrub	0.00033	0.03598
Water	0.00231	0.00160

Test	ChiSquare	DF	Prob>Chisq
Likelihood Ratio	27908.82	7	0.0000
Pearson	29017.84	7	0.0000

Figure 25. Testing of Distribution of CALVEG Cover Types within Riparian Extent to CALVEG Cover Types within AVIRIS Flightline 18.

Test Probabilities

Level	Estim Prob	Hypoth Prob
Agriculture	0.12409	0.01862
Barren	0.00368	0.00100
Conifer	0.10946	0.18869
Hardwood	0.29511	0.22613
Herbaceous	0.38287	0.15135
Mixed Forest	0.08213	0.38669
Shrub	0.00033	0.02613
Water	0.00231	0.00140

Test	ChiSquare	DF	Prob>Chisq
Likelihood Ratio	37875.53	7	0.0000
Pearson	49743.31	7	0.0000

Figure 26. Testing of Distribution of CALVEG Cover Types within Riparian Extent to CALVEG Cover Types within Navarro River Watershed.

The last phase of the comparison of AVIRIS Riparian Vegetation classes and the CALVEG data is a visual one. Namely, a series of images are contained in Appendix II. Narrative descriptions of the images are contained in Table 10 below and indexed to the Figures in Appendix II. These images show a selected set of locations in Flightline 18, which serve as a diagnostic approach to examining the similarities and differences between the two data sources. Furthermore, Appendix II also contains sample images showing both the Riparian Extent and Confinement Clusters to provide a better context as to their spatial coverage. In all, the many factors limiting comparability mentioned above are also evident in the visual examination. Where there is good agreement, it is largely in homogenous areas of vegetation. The scale and methodology for the regional approach taken by CALVEG2000 precludes its inclusion of small, intermittent vegetation stands, especially the true riparian vegetation.

Table 10. Table of Images in Appendix II with Notations.

Image	Description
Figure II-1	The spatial extent of Flightline 18 is shown over portions of the Navarro River watershed. The Riparian Extent is the non-black portion of Flightline 18.
Figure II-2	CALVEG2000 Cover Types are shown clipped to the spatial extent of the intersection of Flightline 18 and the Navarro River watershed.
Figure II-3	Three Focal Areas are shown over CALVEG and DOQQs for Flightline 18. The Focal Areas will serve for more in-depth comparative investigations.
Figure II-4	Indian Creek Focal Area showing DOQQ and streams.
Figure II-5	Indian Creek Focal Area showing CALVEG Cover Types. A DOQQ is the backdrop.
Figure II-6	Indian Creek Focal Area showing the AVIRIS Riparian Vegetation classes within the Riparian Extent.
Figure II-7	Indian Creek Focal Area showing Confinement Cluster stream segments restricted to Riparian Extent.
Figure II-8	Indian Creek Focal Area showing two Insets (A & B) that are used for detailed visual comaparisons.
Figure II-9	Inset A of Indian Creek Focal Area showing CALVEG.
Figure II-10	Inset A of Indian Creek Focal Area showing AVIRIS Riparian Vegetation classes.
Figure II-11	Inset A of Indian Creek Focal Area showing both data overlaid. Target points indicate mutual agreement. In this example, the headwater areas of 1st order streams with true riparian from AVIRIS are masked by the coarser CALVEG.
Figure II-12	Inset B of Indian Creek Focal Area showing CALVEG.
Figure II-13	Inset B of Indian Creek Focal Area showing AVIRIS Riparian Vegetation classes.
Figure II-14	Inset B of Indian Creek Focal Area showing both data overlaid. Target points indicate mutual agreement. In this example, the headwater areas of 1st order streams with conifer agree in both AVIRIS and CALVEG. Additionally, the Hardwood classes also agree. Note, this example exemplifies differences in aspect.
Figure II-15	Anderson Valley Focal Area showing DOQQ and streams.
Figure II-16	Anderson Valley Focal Area showing CALVEG Cover Types. A DOQQ is the backdrop.
Figure II-17	Anderson Valley Focal Area showing the AVIRIS Riparian Vegetation classes within the Riparian Extent. Note, Agriculture class is shown in pink.
Figure II-18	Anderson Valley Focal Area showing Confinement

	Cluster stream segments restricted to Riparian Extent.
Figure II-19	Anderson Valley Focal Area showing two Insets (C - F) that are used for detailed visual comaparisons.
Figure II-20	Inset C of Anderson Valley Focal Area showing DOQQ.
Figure II-21	Inset C of Anderson Valley Focal Area showing CALVEG.
Figure II-22	Inset C of Anderson Valley Focal Area showing AVIRIS Riparian Vegetation classes.
Figure II-23	Inset C of Anderson Valley Focal Area showing both data overlaid. Target points indicate mutual agreement. In this example, CALVEG correctly identifies the water storage pond and the surrounding viticultural areas. Areas of agreement include the viticulture on the margins of the streams segments and a small patch of Hardwoods.
Figure II-24	Inset D of Anderson Valley Focal Area showing DOQQ.
Figure II-25	Inset D of Anderson Valley Focal Area showing CALVEG.
Figure II-26	Inset D of Anderson Valley Focal Area showing AVIRIS Riparian Vegetation classes.
Figure II-27	Inset D of Anderson Valley Focal Area showing both data overlaid. Target points indicate mutual agreement. In this example, CALVEG and AVIRIS agree for the Hardwoods class. CALVEG does, however, miss the ribbon stands of AVIRIS true riparian by coding them as annual grasslands. CALVEG does pick up the small stands of Shrubs on the margin of the Riparian Extent.
Figure II-28	Inset E of Anderson Valley Focal Area showing DOQQ.
Figure II-29	Inset E of Anderson Valley Focal Area showing CALVEG.
Figure II-30	Inset E of Anderson Valley Focal Area showing AVIRIS Riparian Vegetation classes.
Figure II-31	Inset E of Anderson Valley Focal Area showing both data overlaid. Target points indicate mutual agreement. In this example, CALVEG and AVIRIS agree for the agricultural areas on the margins of the Riparian Extent. CALVEG misses the true riparian along the stream segments.
Figure II-32	Inset F of Anderson Valley Focal Area showing DOQQ.
Figure II-33	Inset F of Anderson Valley Focal Area showing CALVEG.
Figure II-34	Inset F of Anderson Valley Focal Area showing AVIRIS Riparian Vegetation classes.
Figure II-35	Inset F of Anderson Valley Focal Area showing both data overlaid. Target points indicate mutual

	agreement. In this example, CALVEG and AVIRIS agree for Conifer (in this case the boundary of Hendy Woods State Park). The Herbaceous class of CALVEG encompassed within this Inset is errant; based on field observations, this classified area is predominately viticulture and alluvial gravels. Although CALVEG picks up some gravels, coded as Barren, it misses much of the true riparian class found in the AVIRIS.
Figure II-36	Gut Creek Focal Area showing DOQQ and streams.
Figure II-37	Gut Creek Focal Area showing CALVEG Cover Types. A DOQQ is the backdrop.
Figure II-38	Gut Creek Focal Area showing the AVIRIS Riparian Vegetation classes within the Riparian Extent.
Figure II-39	Gut Creek Focal Area showing Confinement Cluster stream segments restricted to Riparian Extent.
Figure II-40	Inset G of Gut Creek Focal Area showing DOQQ.
Figure II-41	Inset G of Gut Creek Focal Area showing CALVEG.
Figure II-42	Inset G of Gut Creek Focal Area showing AVIRIS Riparian Vegetation classes.
Figure II-43	Inset G of Gut Creek Focal Area showing both data overlaid. Target points indicate mutual agreement. In this example, CALVEG and AVIRIS agree for selected areas of the Hardwood class. The AVIRIS data are classified as predominately Hardwood, with only intermittent patches of Conifer. CALVEG shows large blocks of either Harwood or Conifer, thus there is only marginal agreement.

Part 4. Data Production Analysis

Part 4.1. Data Production Analysis Rationale

The production of large research projects is not without monetary costs. The use of hyperspectral data in resource inventories is no exception. The benefits of high-resolution data are many, but the costs, when applied over large geographical areas, can be prohibitive. To this end, a brief analysis is provided to summarize some of the costs, in terms of employee hours and infrastructure investment, involved in the acquisition, processing, classifying, analyzing, and verifying the AVIRIS data collected for the Navarro River watershed. It is not exhaustive, and many additional facets of the research are not summarized in this report; therefore, it should serve only as a guide to what similar projects may incur in terms of costs. Also, other data sources and other sensor options are provided with notes as to their resolution and availability.

Part 4.2. Data Production Analysis Methods

An estimate of time spent, in total, by several researchers was calculated through the use of time accounting software developed by ICE. Because this project was funded by many state and federal agencies, this estimate does not partition among those entities; rather, it is a block estimate of actual task time adjusted to full time employee equivalents. The synopsis of different data product attributes and availability is an augmentation of information held by the Center for Spatial Technologies and Remote Sensing (CSTARS) at UC Davis.

Part 4.3. Data Production Analysis Results

A sum of over 5000 hours has been spent on the myriad of tasks and activities required in this research project, equivalent to 2.5 person years or 2.5 FTE for one year. These tasks and activities have included all phases of the project from initial scoping to report writing. A detailed breakdown of activities by percent of total allocation is as follows: Data Acquisition & Processing represented 35.6% of total time; Data Analysis represented 45.2% of the total time; and the remainder, 19.2%, was Data Development/Dissemination, Publications and Report Writing, and Client Communications, among other types of activities.

Major infrastructure investments included hardware, software, training, and data acquisition. NASA-JPL uses a recharge amount of approximately $45,000 per day of AVIRIS acquisition; the Navarro River over-flight took the better part of four days. Because images are several Gigabytes each, and each modification or transformation compounds these figures, total data storage is estimated to be in the 400Gb range and requires storage on several, separate storage devices. The use of ATCOR4 and PARGE software for data correction required a substantial investment for both software licensure and in-house training. The software also required upgrades to Interactive Data Language and MODTRAN, which was unanticipated. Other unanticipated events included the receipt of data on 8mm tape; this data storage format is cumbersome, far from failsafe, and considerably slow in data transmission. Data were also received partially corrected for terrain effects. The use of ATCOR4 required unaltered imagery for its correction algorithms to work properly,

prompting an additional round of data transmission. Lastly, hyperspectral data analysis is best handled by ENVI, developed expressly for hyperspectral feature extraction and modeling, and, as such, required additional training for staff, both in-house and externally.

Other hyperspectral sensors are available for contract use and, coupled with multi-data-type options such as multi-spectral or radio sensing, these other options might provide other researchers with a more cost-effective means of pursuing similar lines of work. Although the AVIRIS sensor was airborne and implemented at low-altitudes, other, newer platforms are often space-borne. A partial listing of sensors and their characteristics are presented in Appendix III.

Part 4.4. Data Production Analysis Discussion

In summary, data production for research into the uses of hyperspectral data and watershed analysis methodologies was prodigious. It required focused effort on behalf of the researchers, a substantial monetary investment by collaborators, and flexibility to follow important discoveries as they arose. Although these data are well positioned for further analyses, and the production of a complete riparian representation for the watershed is foreseeable, it is the initial bulk processing of the AVIRIS data that can be prohibitive to initiating projects of this scope. It is this reason that many hyperspectral data analysis research projects focus on constrained areas; however, it is difficult to pursue research within a watershed context if the breadth of the analysis is restricted to small geographical area.

Acknowledgements

We would like to thank the North Coast Regional Water Quality Control Board for the funding to pursue hyperspectral data analysis in the Navarro River watershed; we would like to acknowledge Bruce Gwynne, David Leland, and Bryan McFadin for providing insight and support throughout the process. We would also like to thank the California Department of Forestry and Fire Protection and the United States Department of Agriculture — Forest Service for their financial support, specific to this report, and their project leads Chris Keithley and Lisa Levien, for procedural recommendations and oversight. We would like to thank the University of California, Davis, the Department of Environmental Science and Policy, the John Muir Institute of the Environment, the Center for Image Processing and Integrated Computing, the Center for Spatial Technologies and Remote Sensing, for all supporting our efforts at the Information Center for the Environment. Lastly, we would like to acknowledge the following individuals for the their contributions: Professor James F. Quinn, Michael C. McCoy, Paul Fulton, Eric Lehmer, Bob Brewer, George Scheer, and Zhi-Wei Lu.

Appendix I **Field Plot Samples**

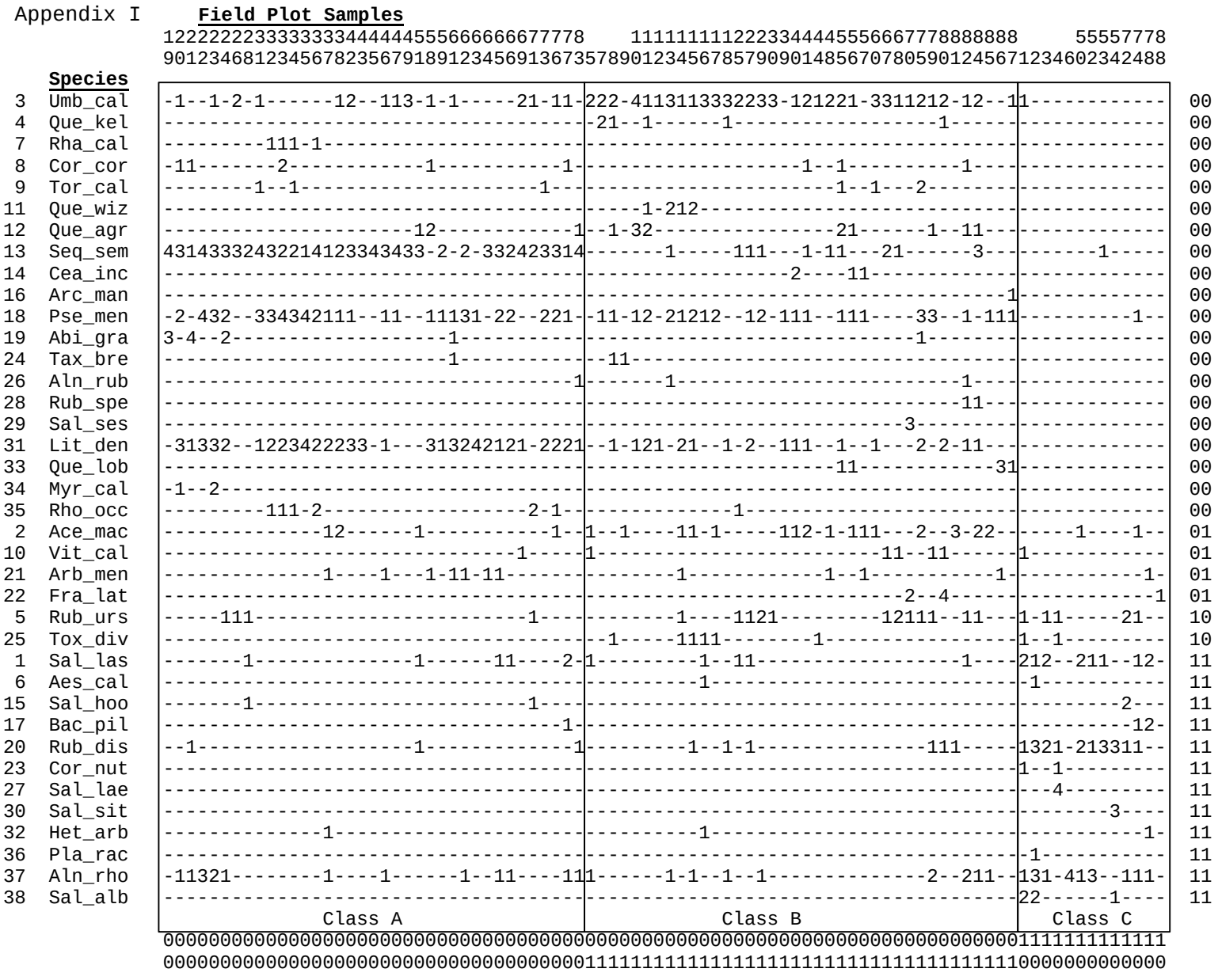

Appendix II

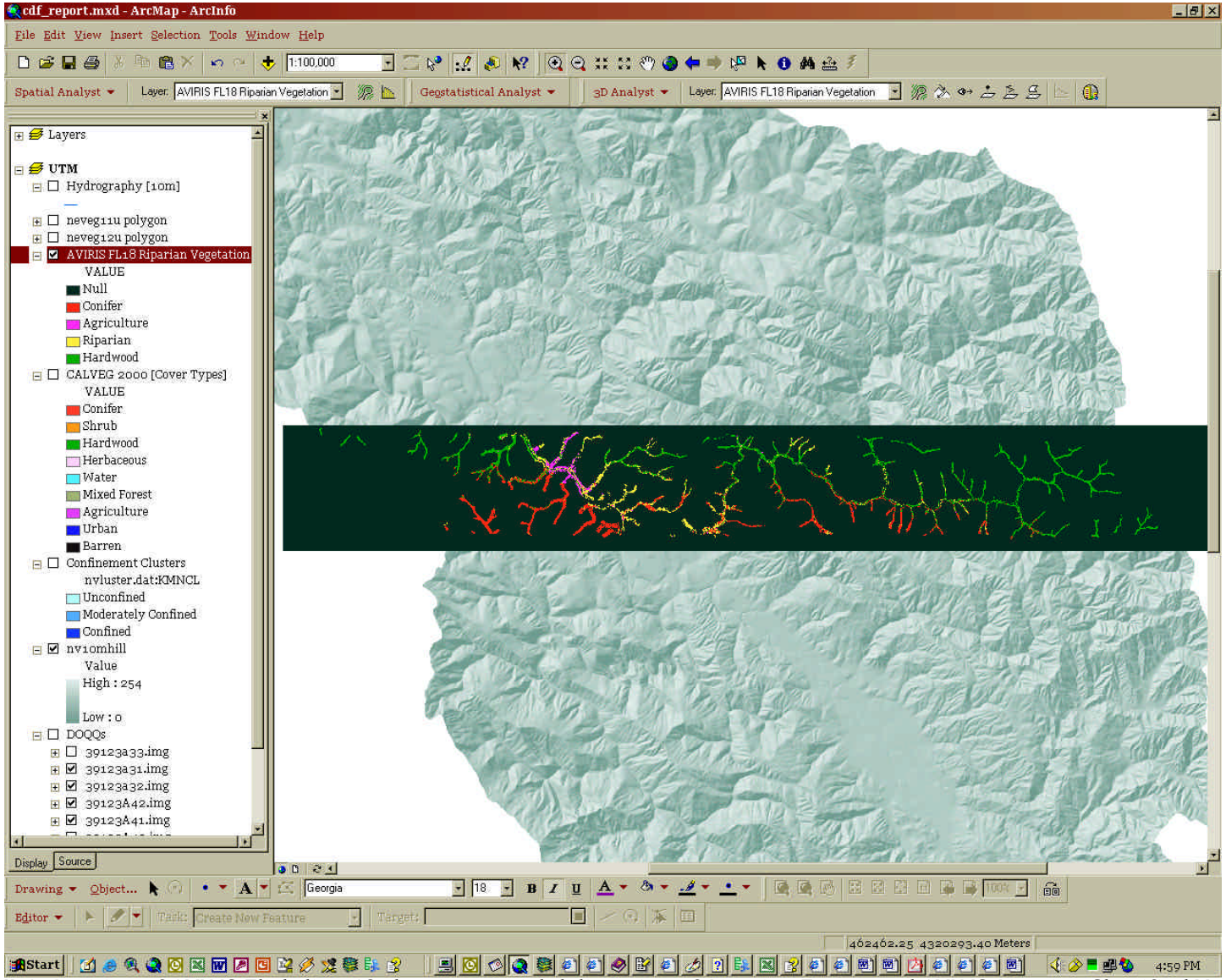

Figure II-1. Position of AVIRIS Flightline 18 showing spatial delineation of Riparian Extent and AVIRIS Riparian Classified Vegetation. Legend is embedded in image; scale is 1:100000.

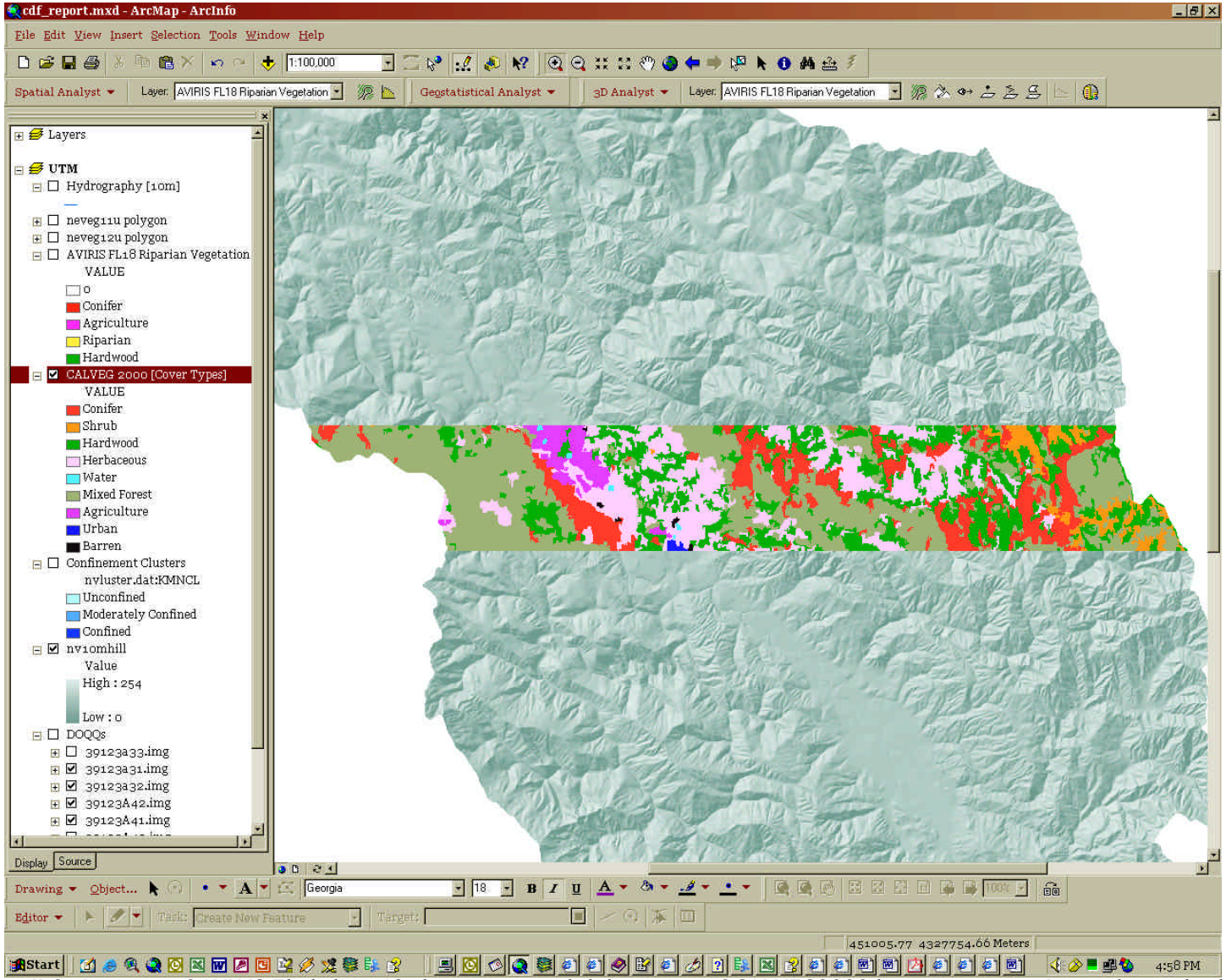

Figure II-2. Position of AVIRIS Flightline 18 showing spatial delineation of CALVEG2000 by cover types. Legend is embedded in image; scale is 1:100000.

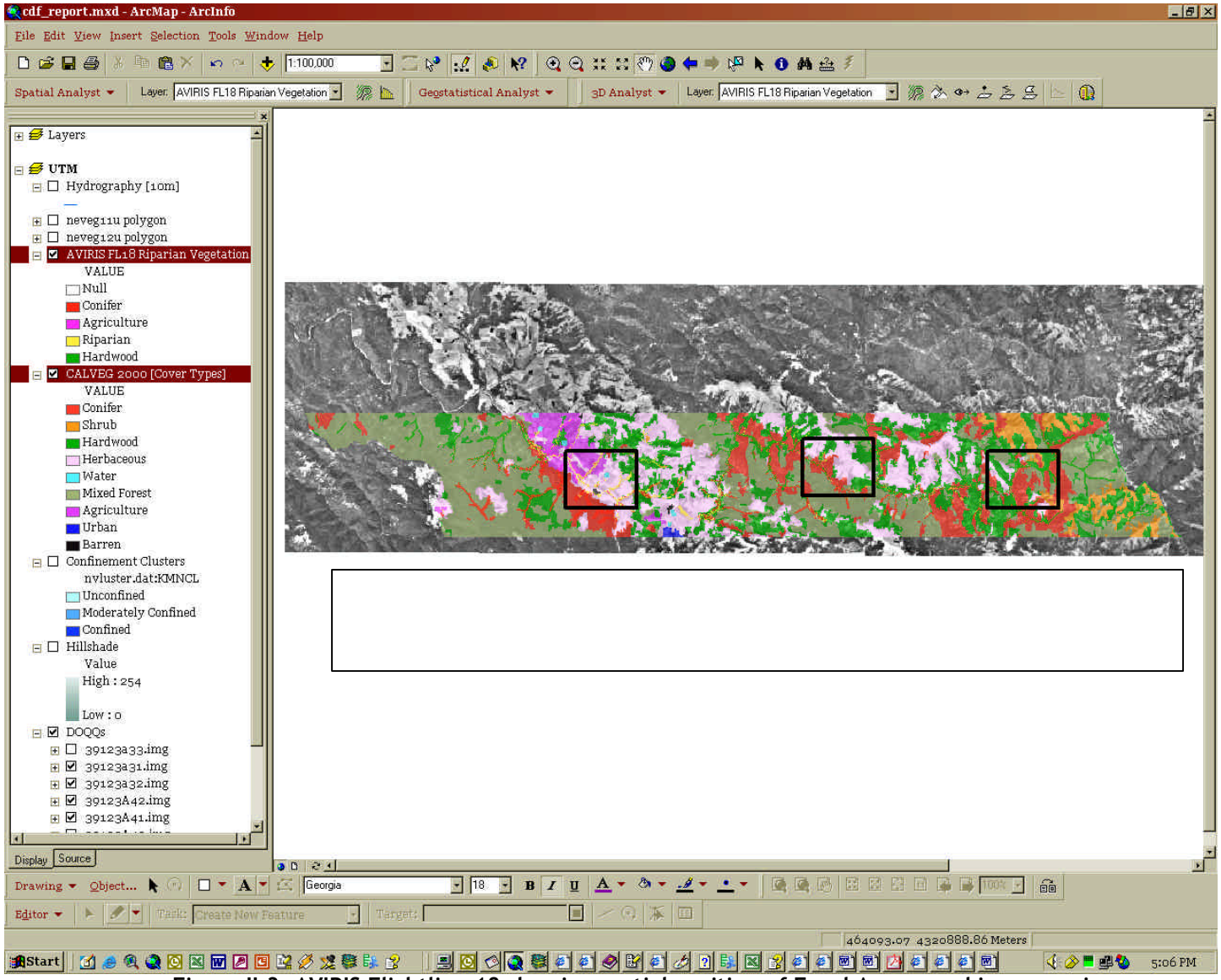

Figure II-3. AVIRIS Flightline 18 showing spatial position of Focal Areas used in comparison.

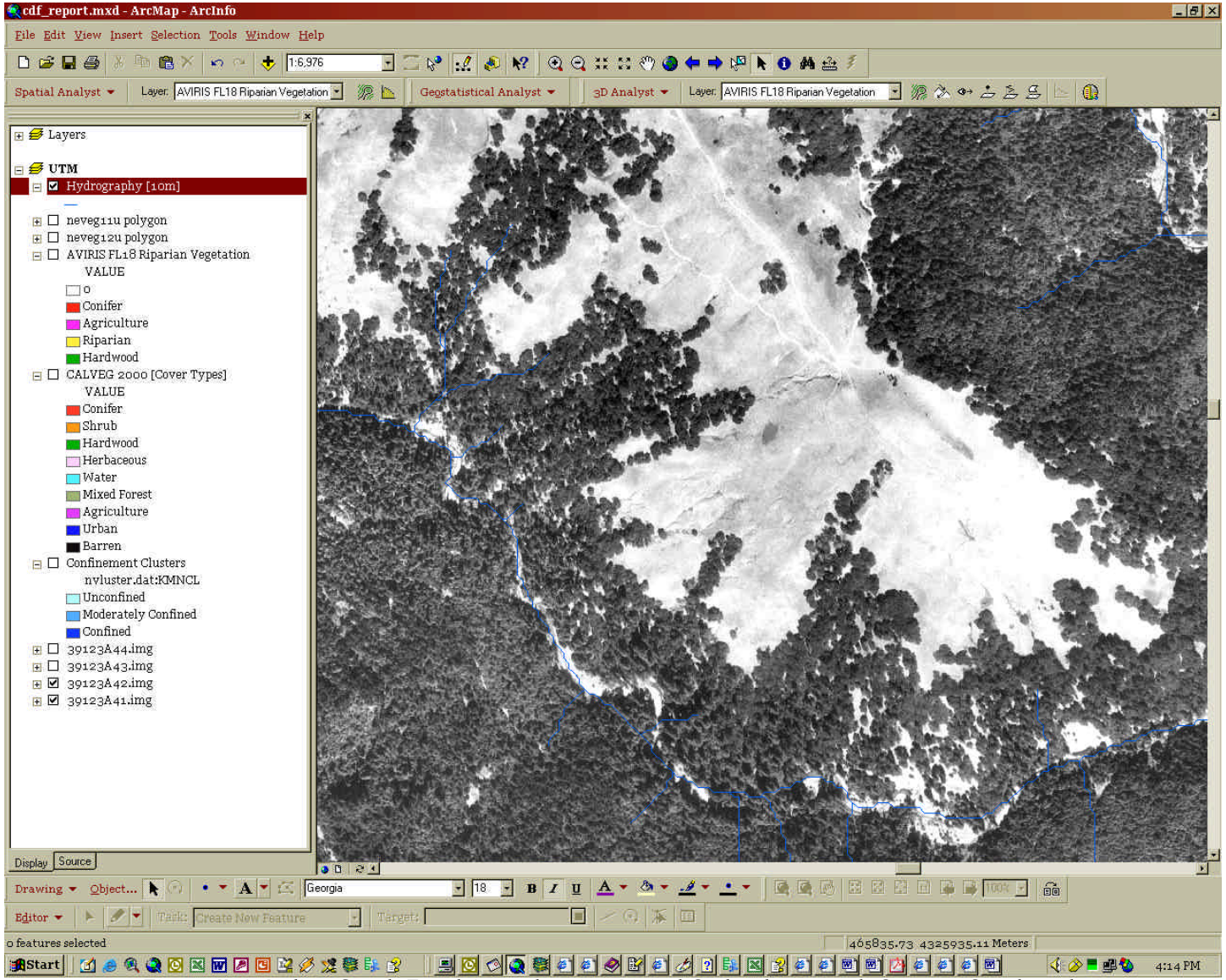

Figure II-4. Indian Creek Focal Area showing Digital Orthophotograph Quarter Quadrangle image.

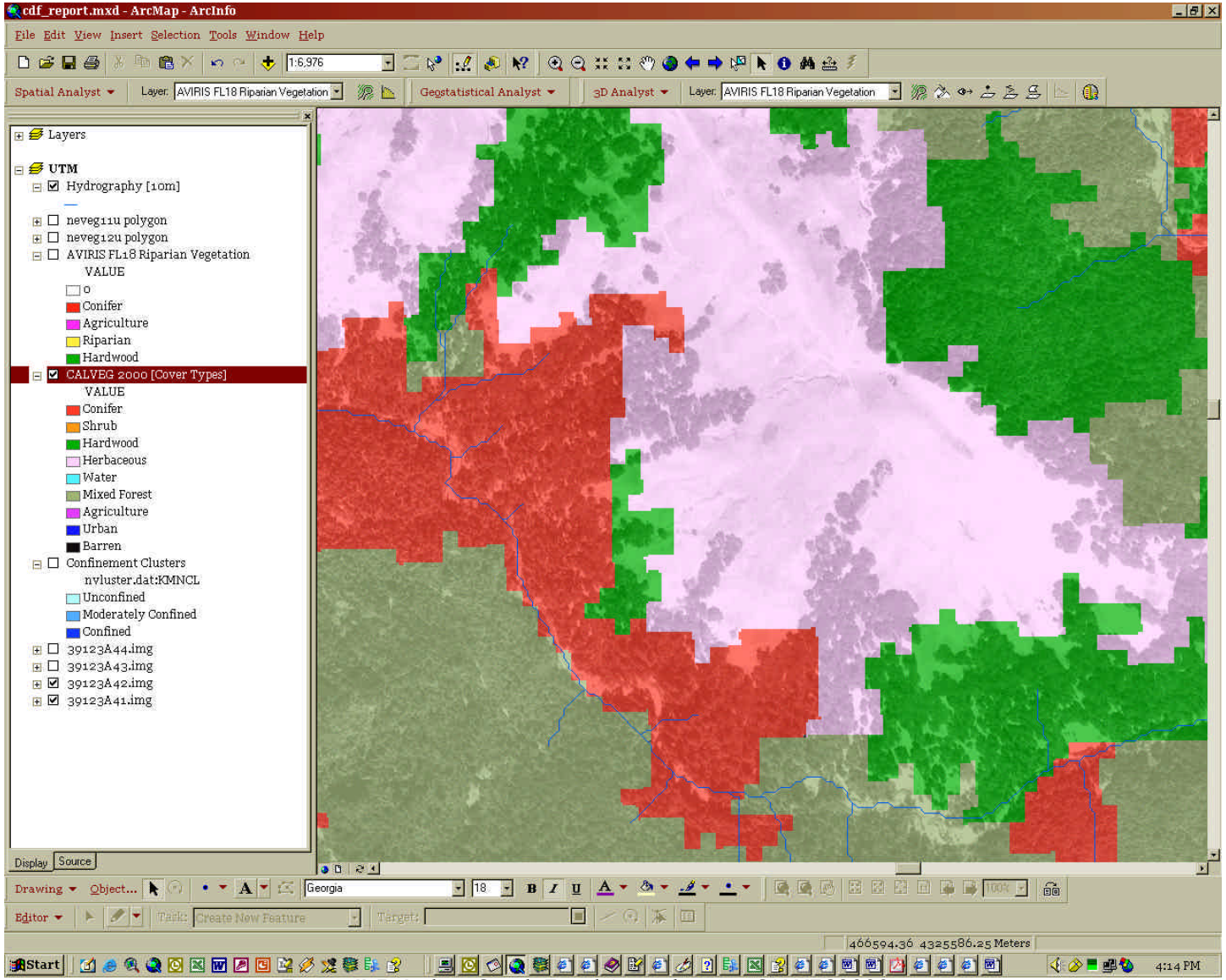

Figure II-5. Indian Creek Focal Area showing CALVEG2000 cover types.

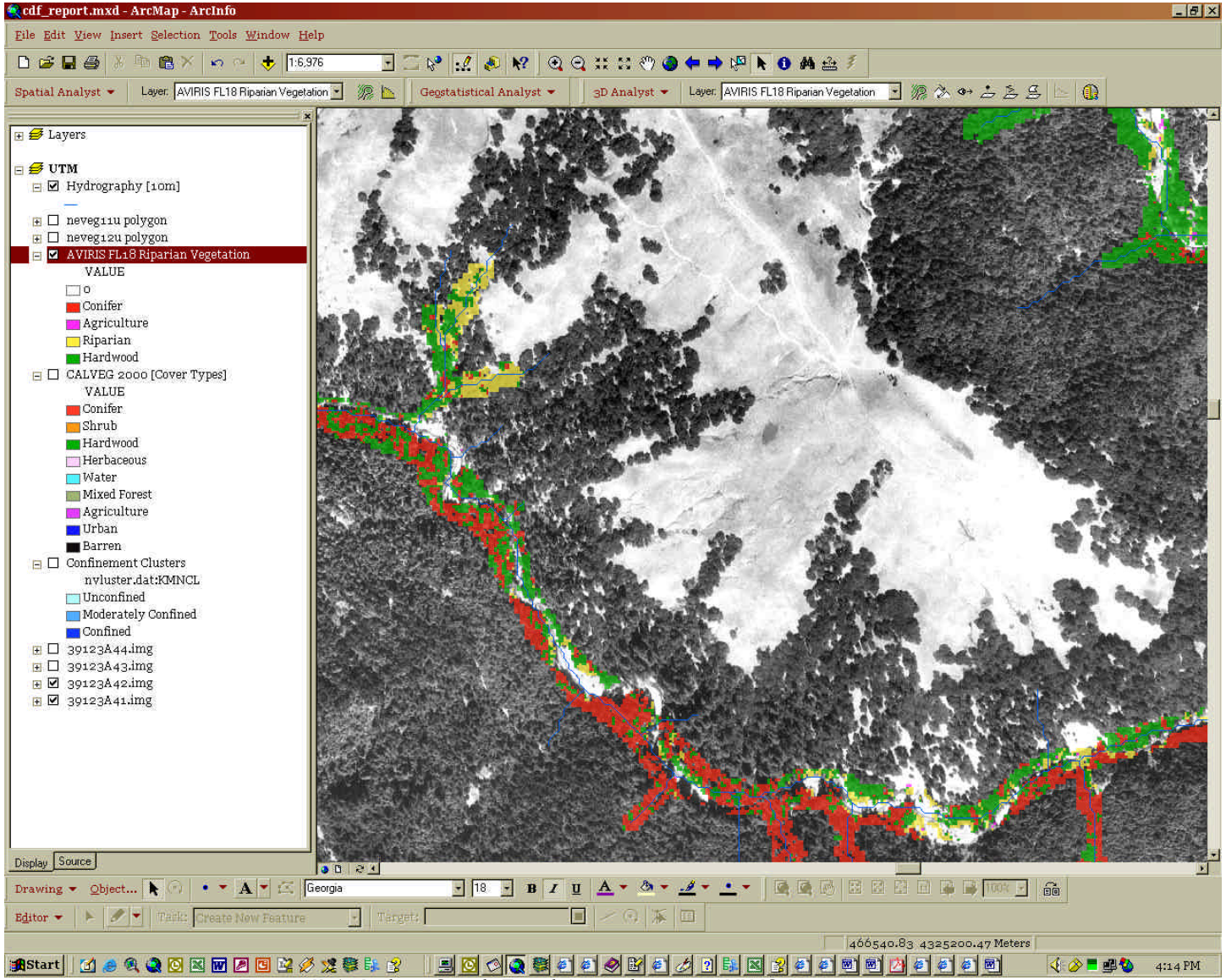

Figure II-6. Indian Creek Focal Area showing AVIRIS Riparian cover types.

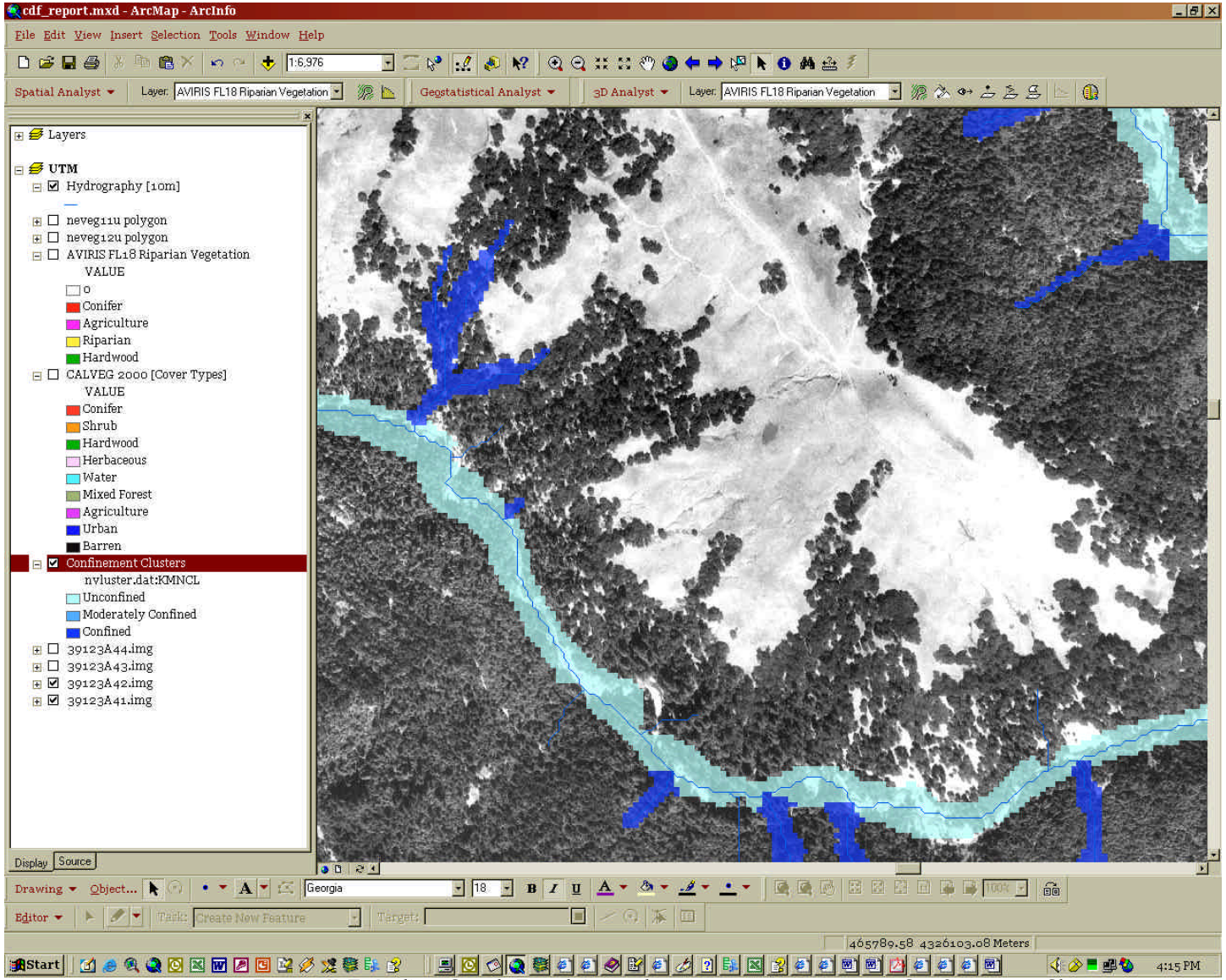

Figure II-7. Indian Creek Focal Area showing stream segment Confinement Clusters.

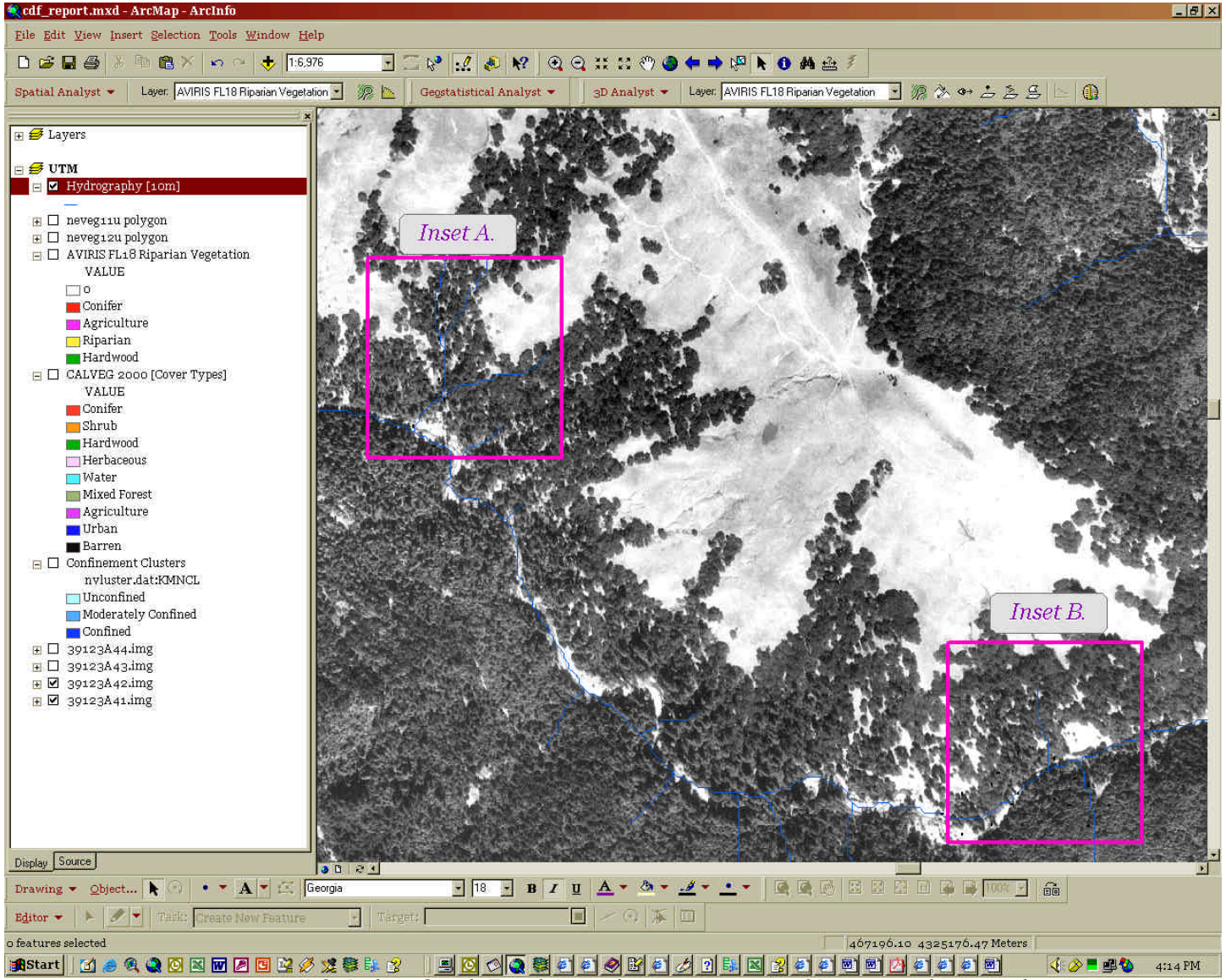

Figure II-8. Indian Creek Focal Area showing position of Insets used in visual comparison.

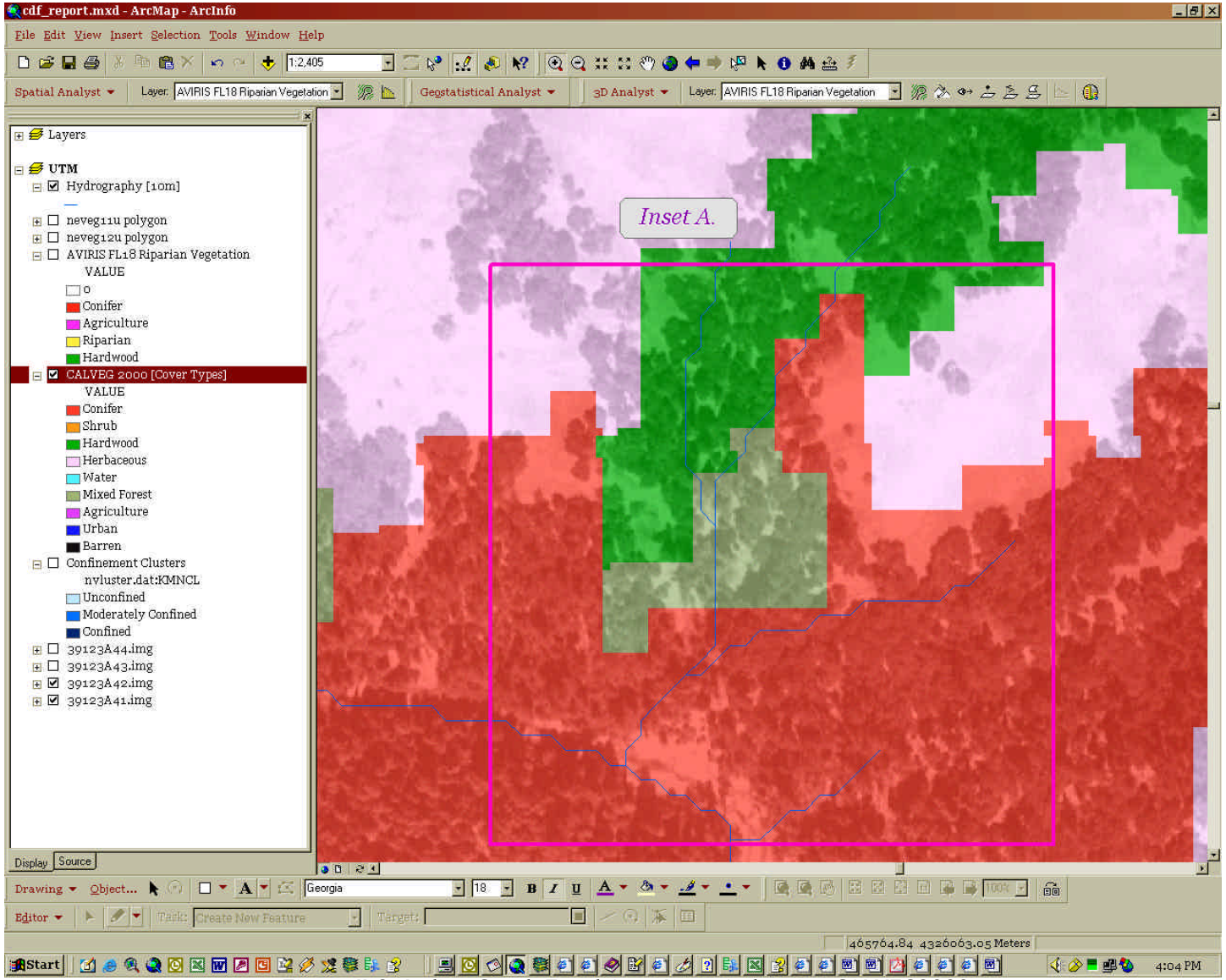

Figure II-9. Indian Creek Focal Area Inset A showing CALVEG2000 cover types.

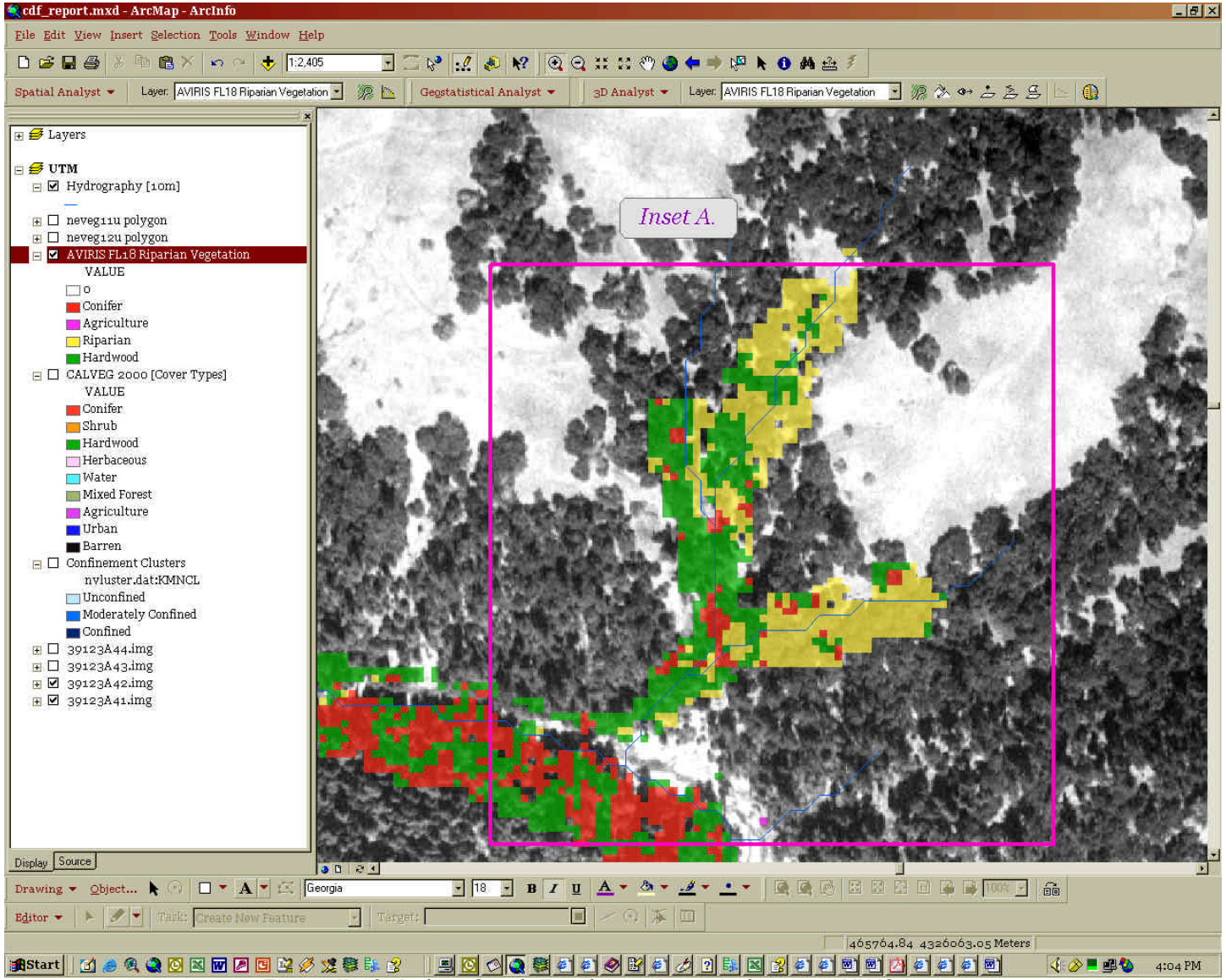

Figure II-10. Indian Creek Focal Area Inset A showing AVIRIS Riparian cover types.

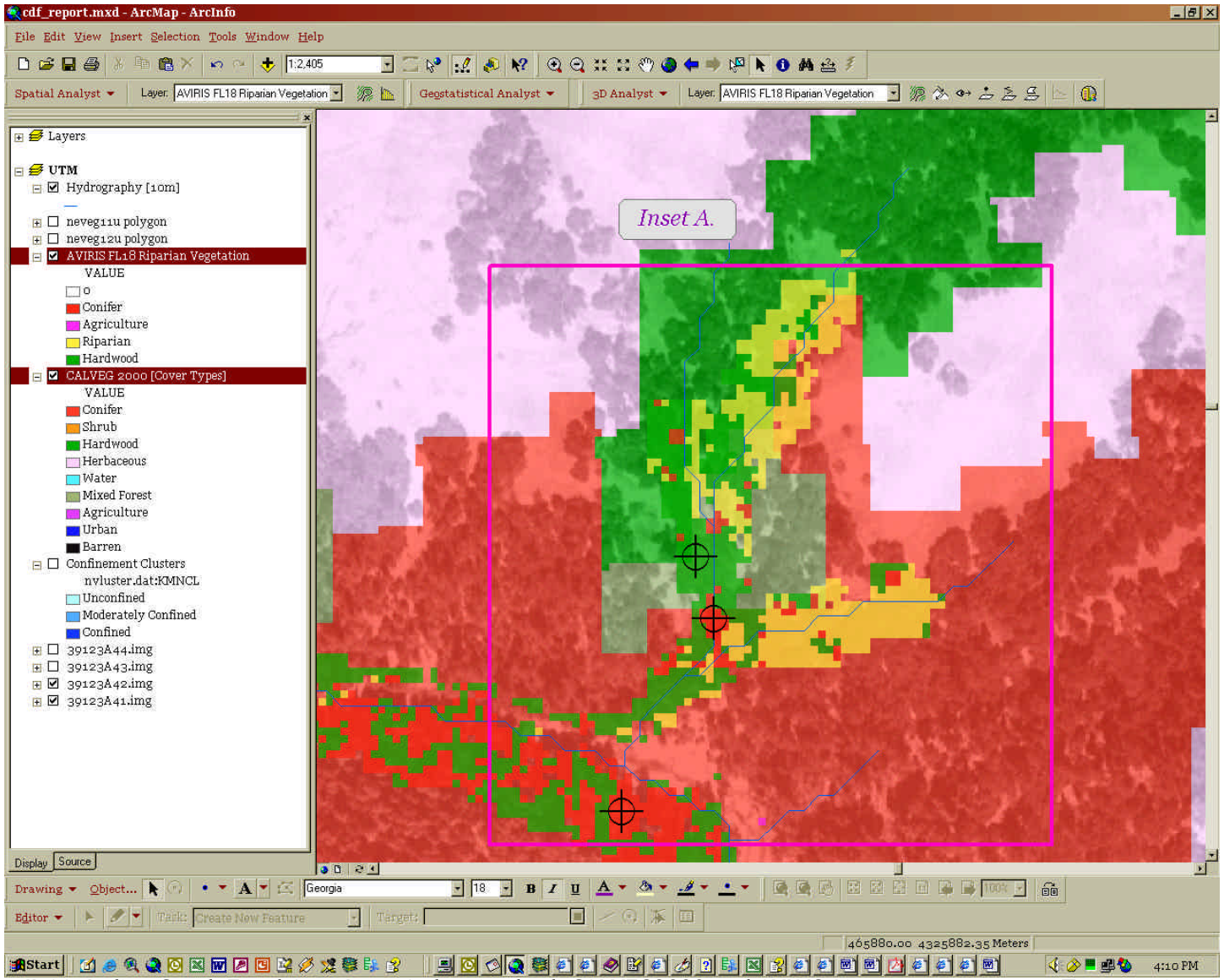

Figure II-11. Indian Creek Focal Area Inset A showing both CALVEG2000 and AVIRIS Riparian cover types. Target points indicate mutual agreement between data.

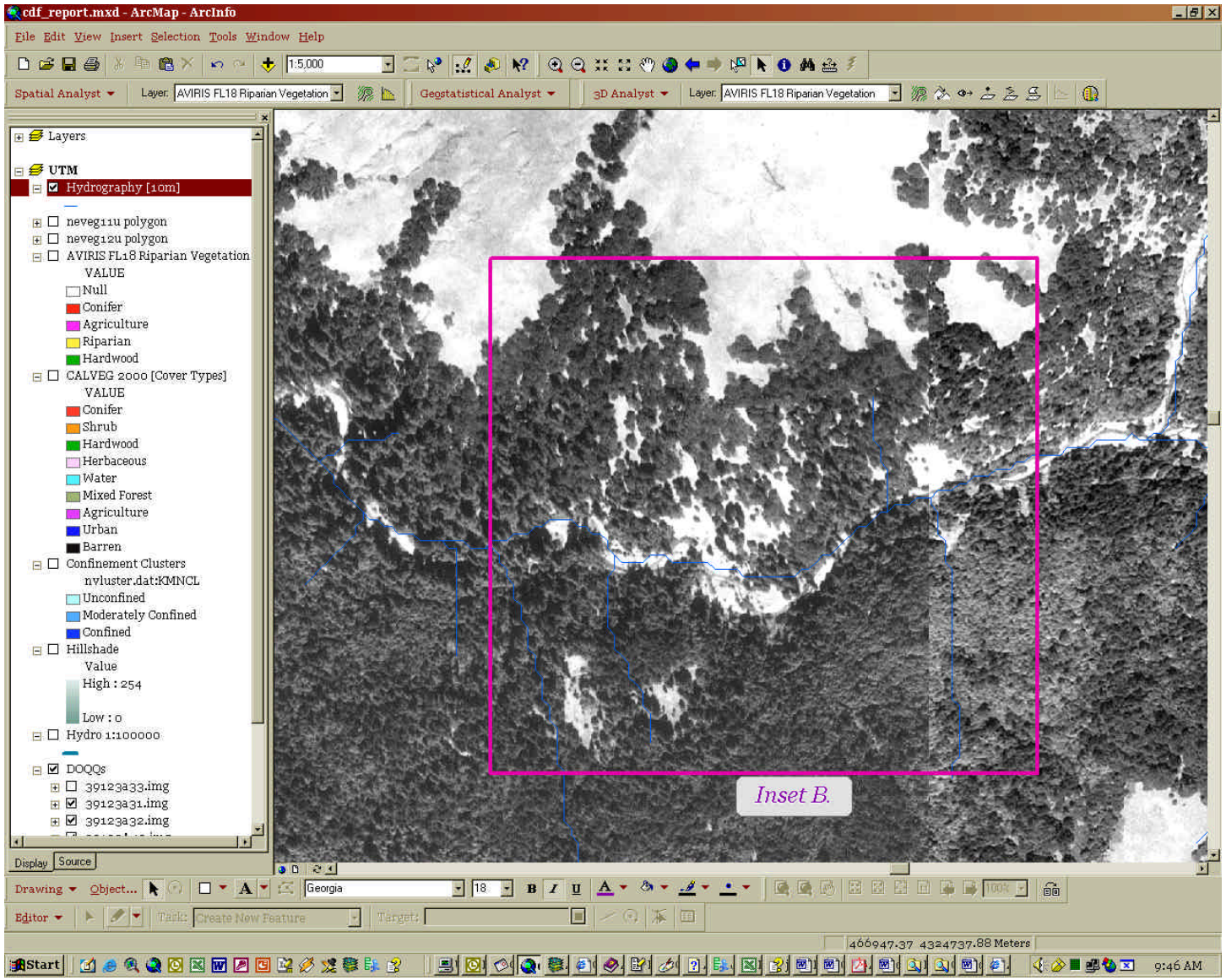

Figure II-12. Indian Creek Focal Area showing Digital Orthophotograph Quarter Quadrangle image for Inset B.

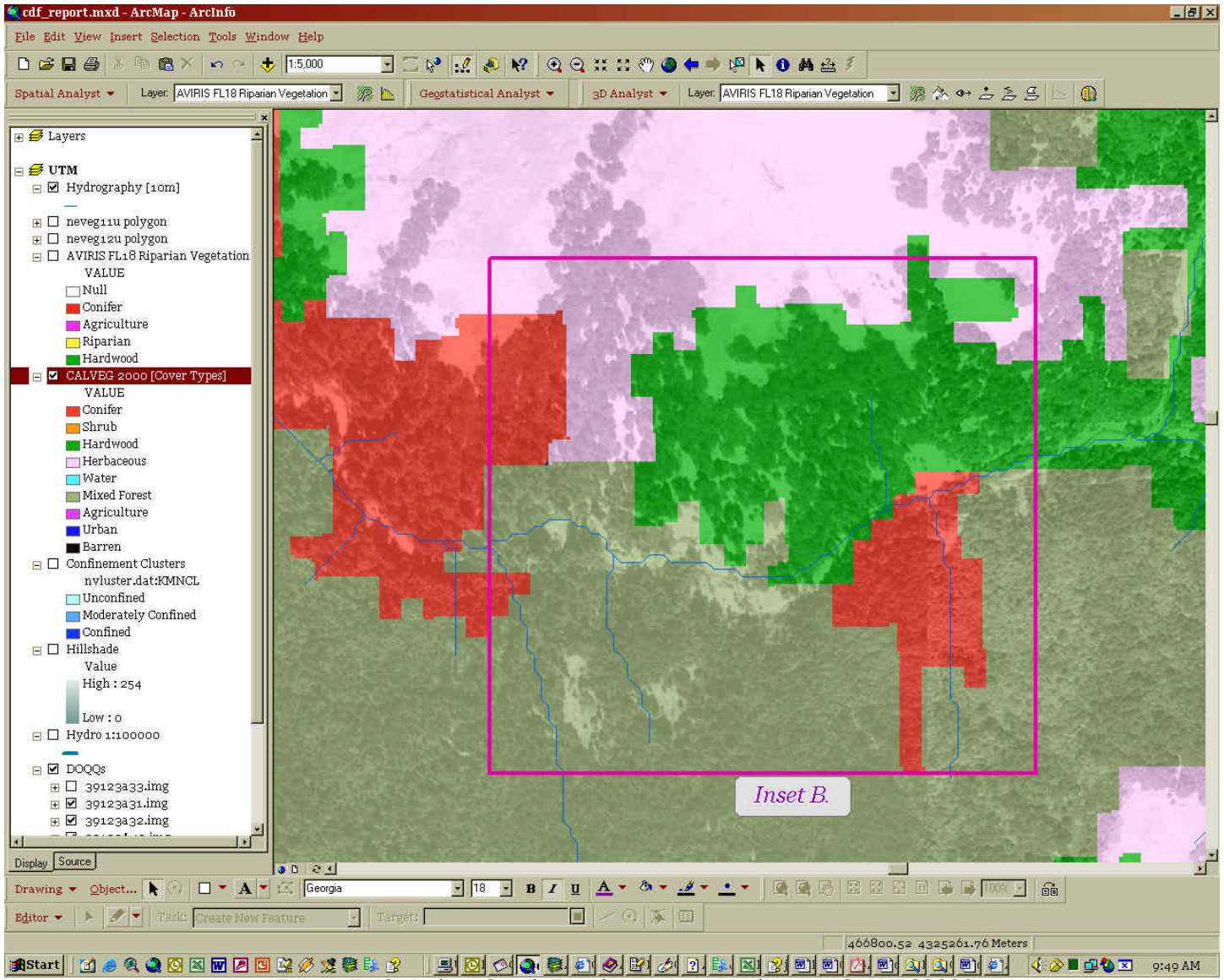

Figure II-13. Indian Creek Focal Area Inset B showing CALVEG2000 cover types.

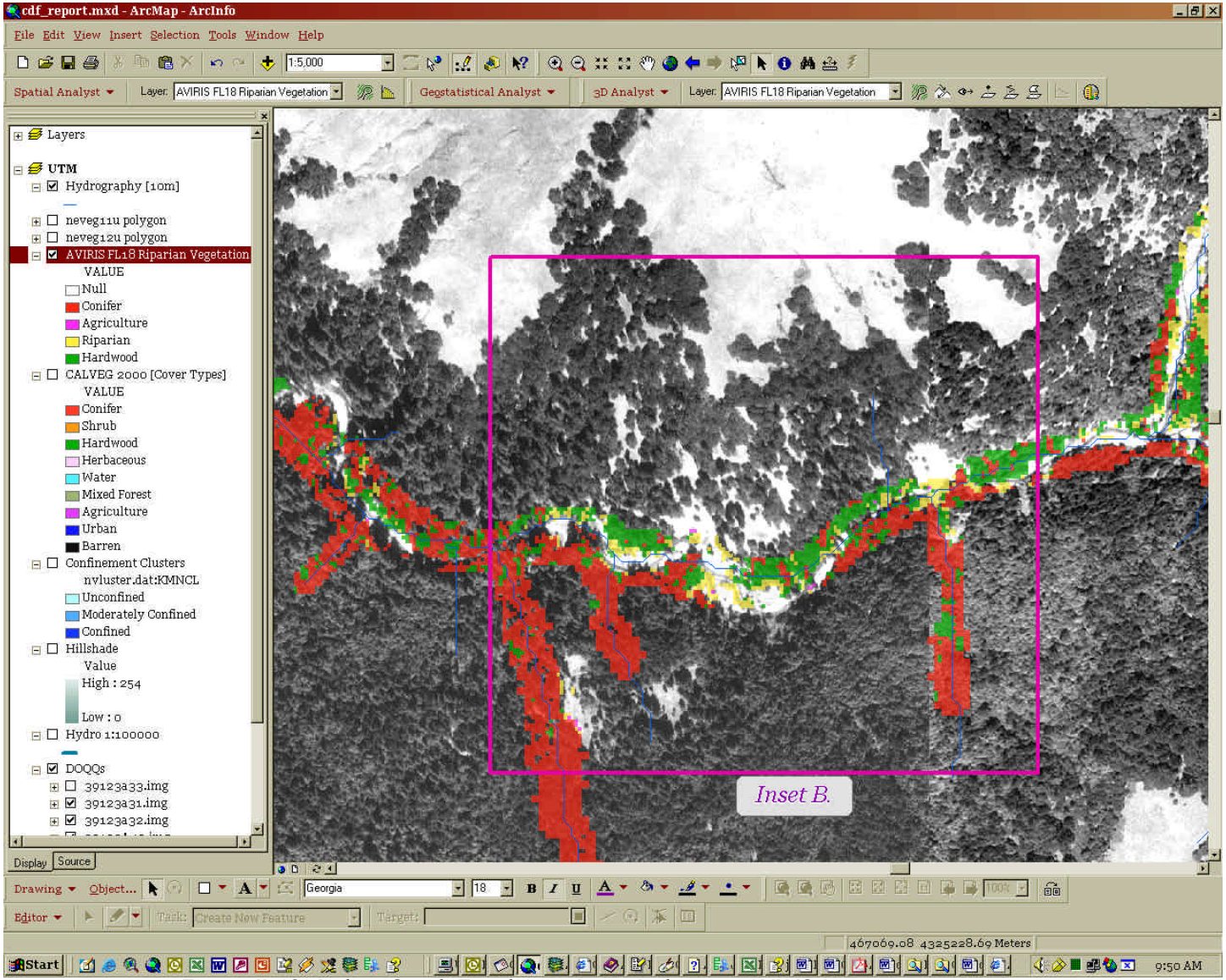

Figure II-13. Indian Creek Focal Area Inset B showing AVIRIS Riparian cover types.

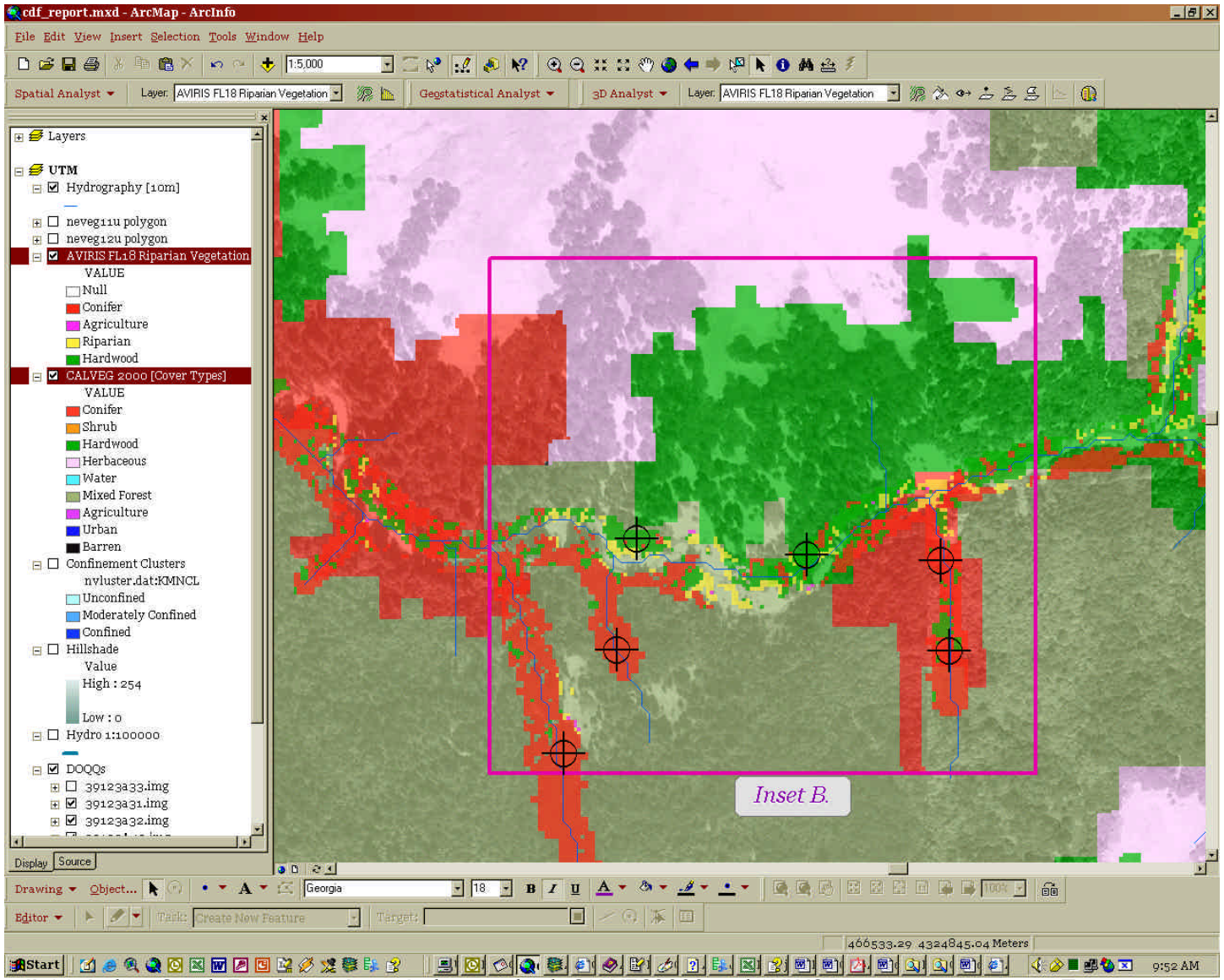

Figure II-14. Indian Creek Focal Area Inset B showing both CALVEG2000 and AVIRIS Riparian cover types. Target points indicate mutual agreement between data.

.

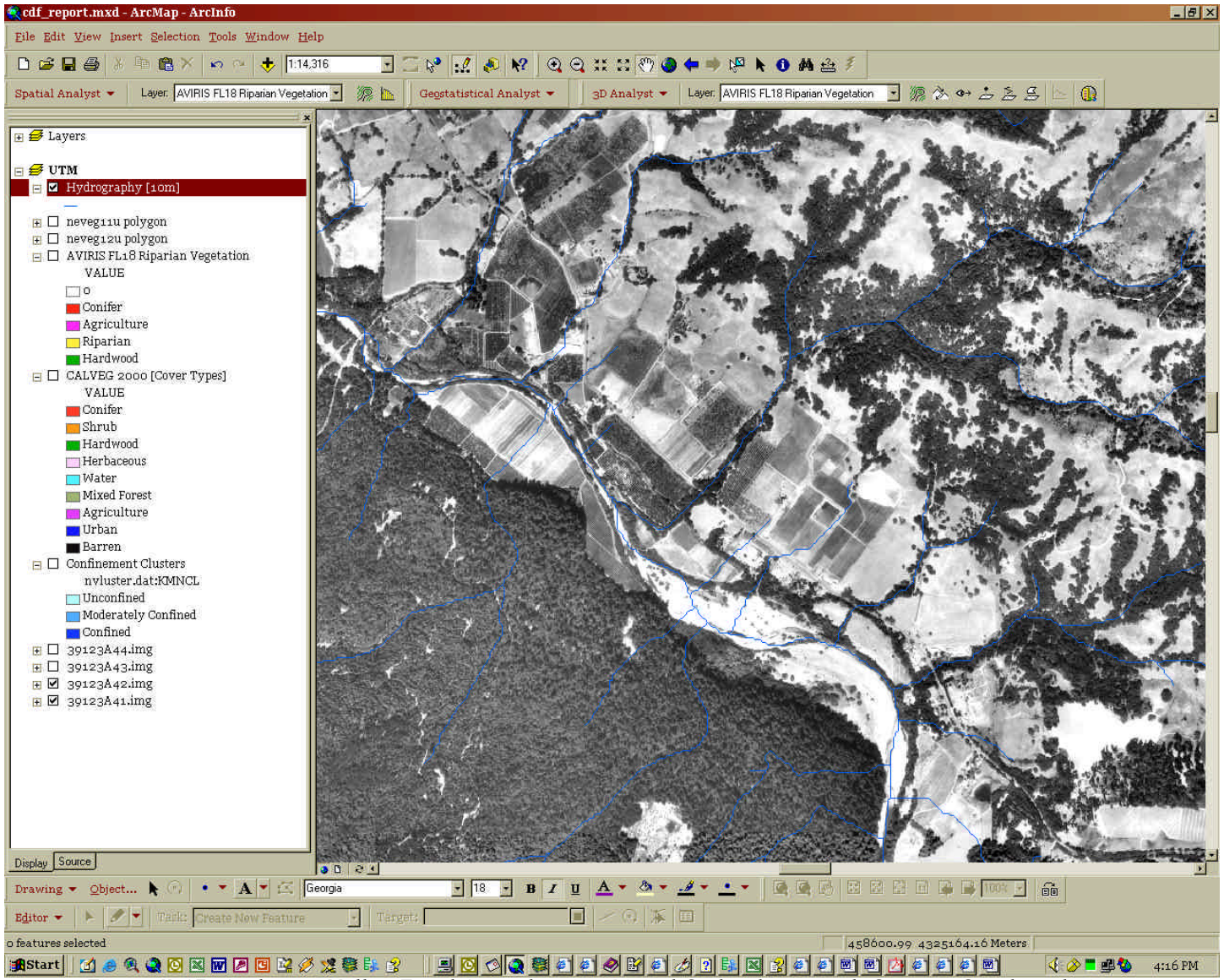

Figure II-15. Anderson Valley Focal Area showing Digital Orthophotograph Quarter Quadrangle image.

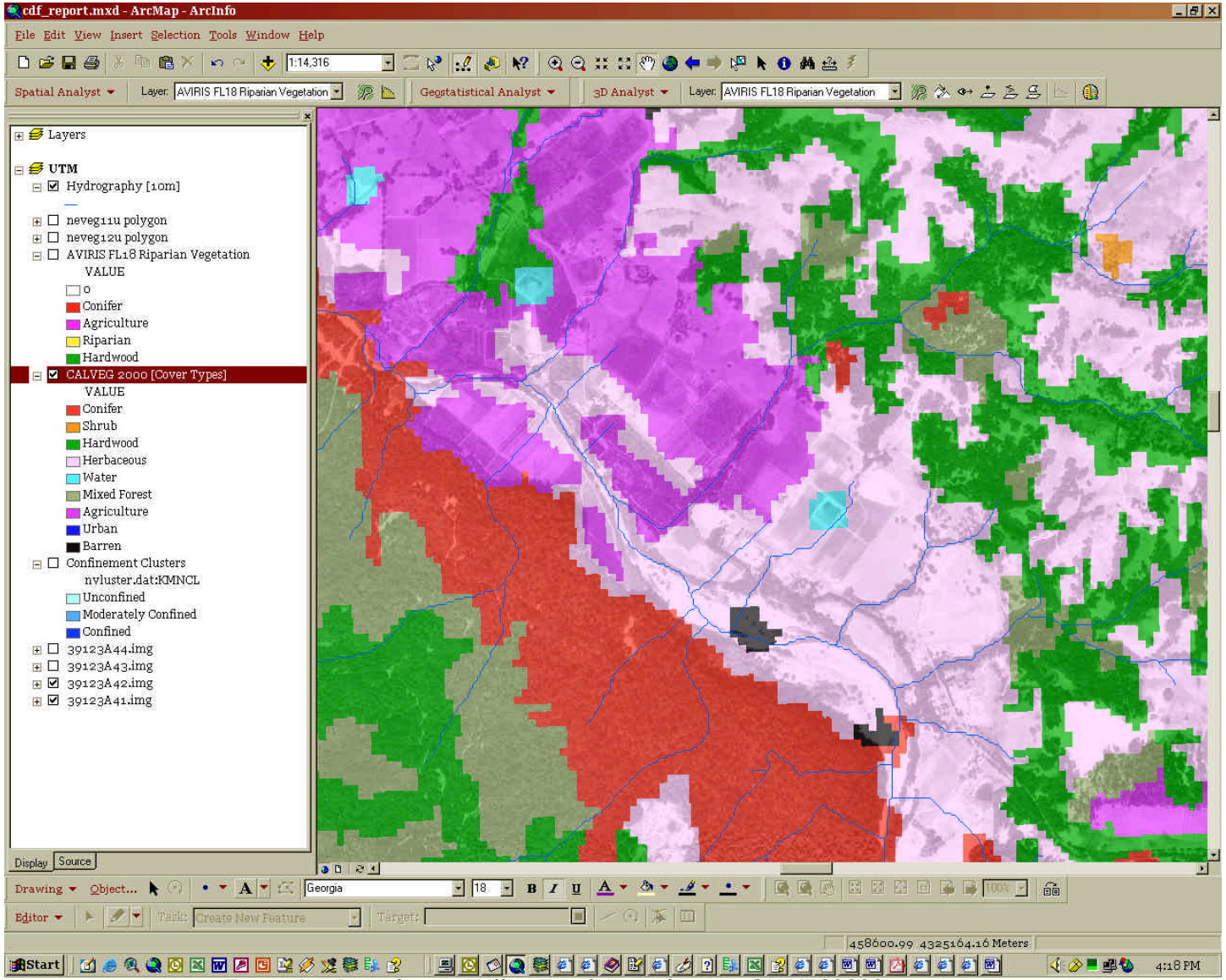

Figure II-16. Anderson Valley Focal Area showing CALVEG2000 cover types.

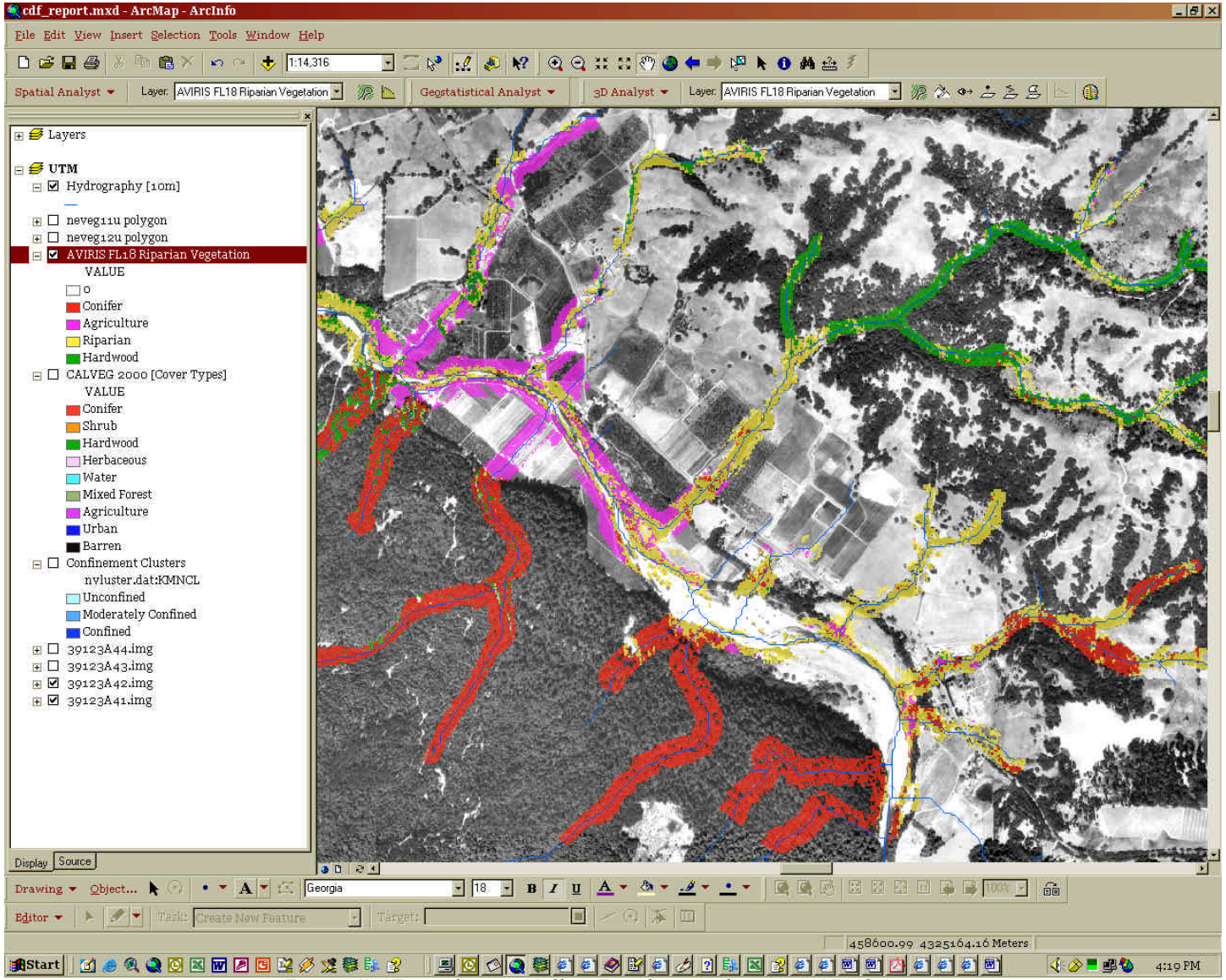

Figure II-17. Anderson Valley Focal Area showing AVIRIS Riparian cover types.

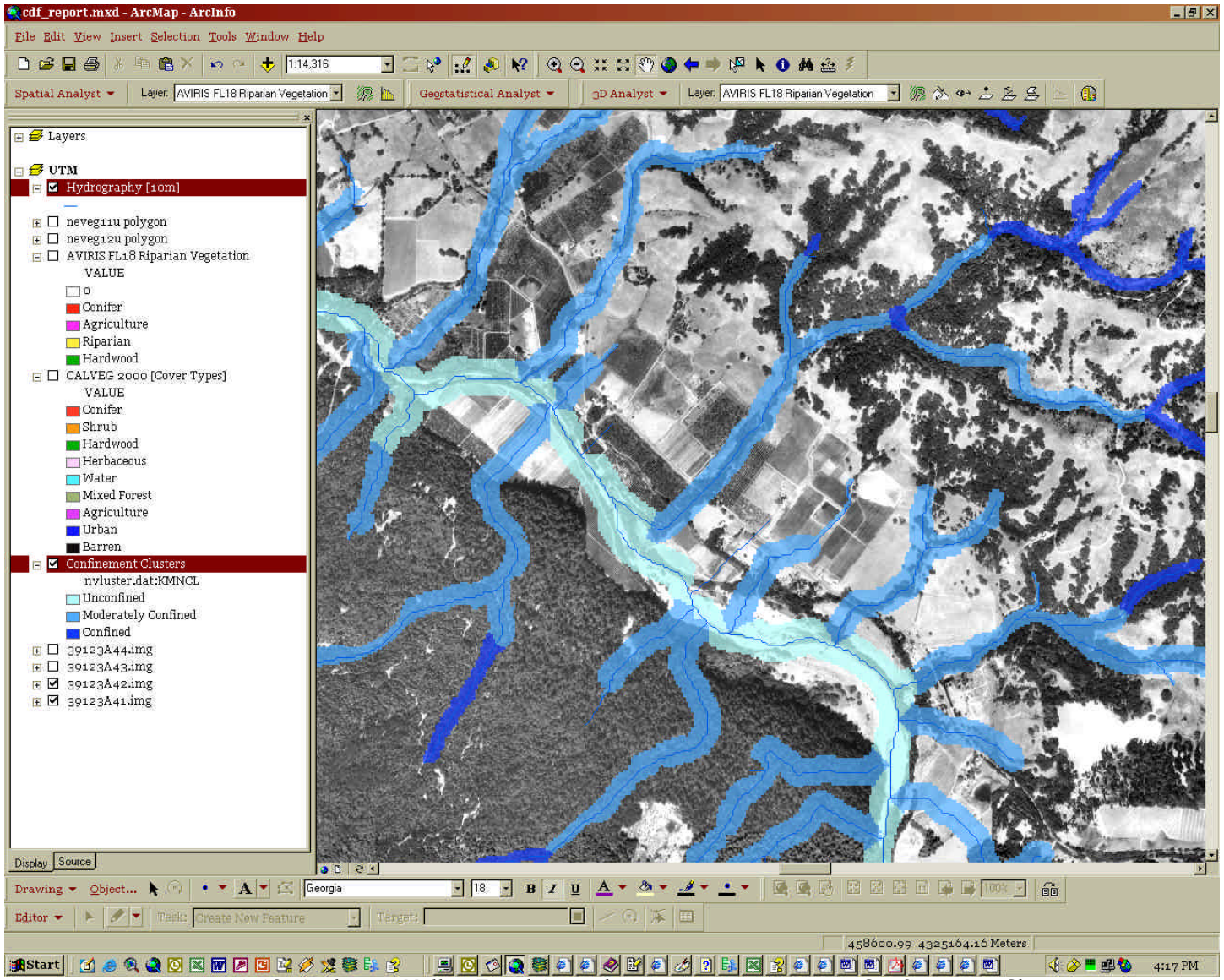

Figure 11-18. Anderson Valley Focal Area showing stream segment Confinement Clusters.

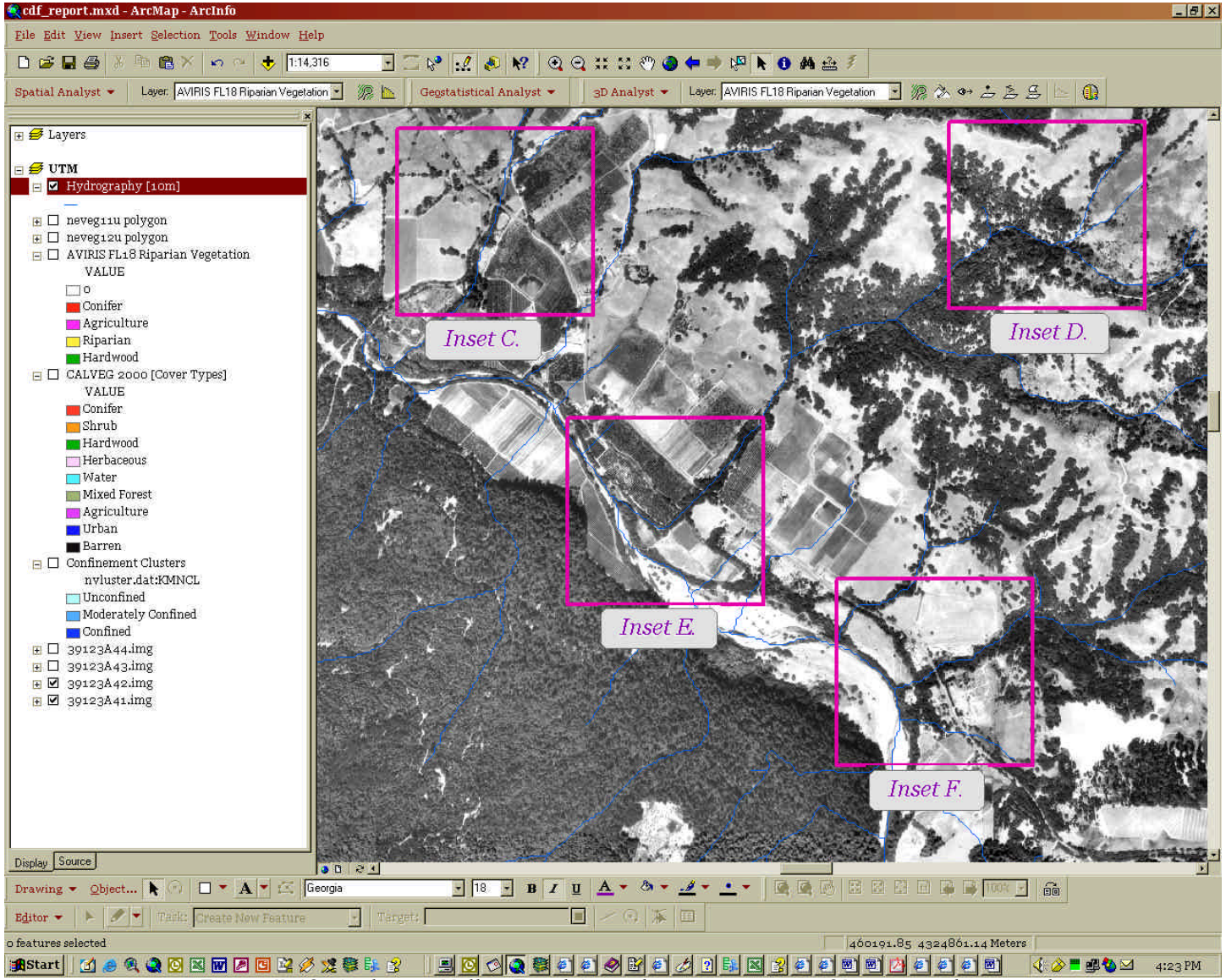

Figure II-19. Anderson Valley Focal Area showing position of Insets used in visual comparison.

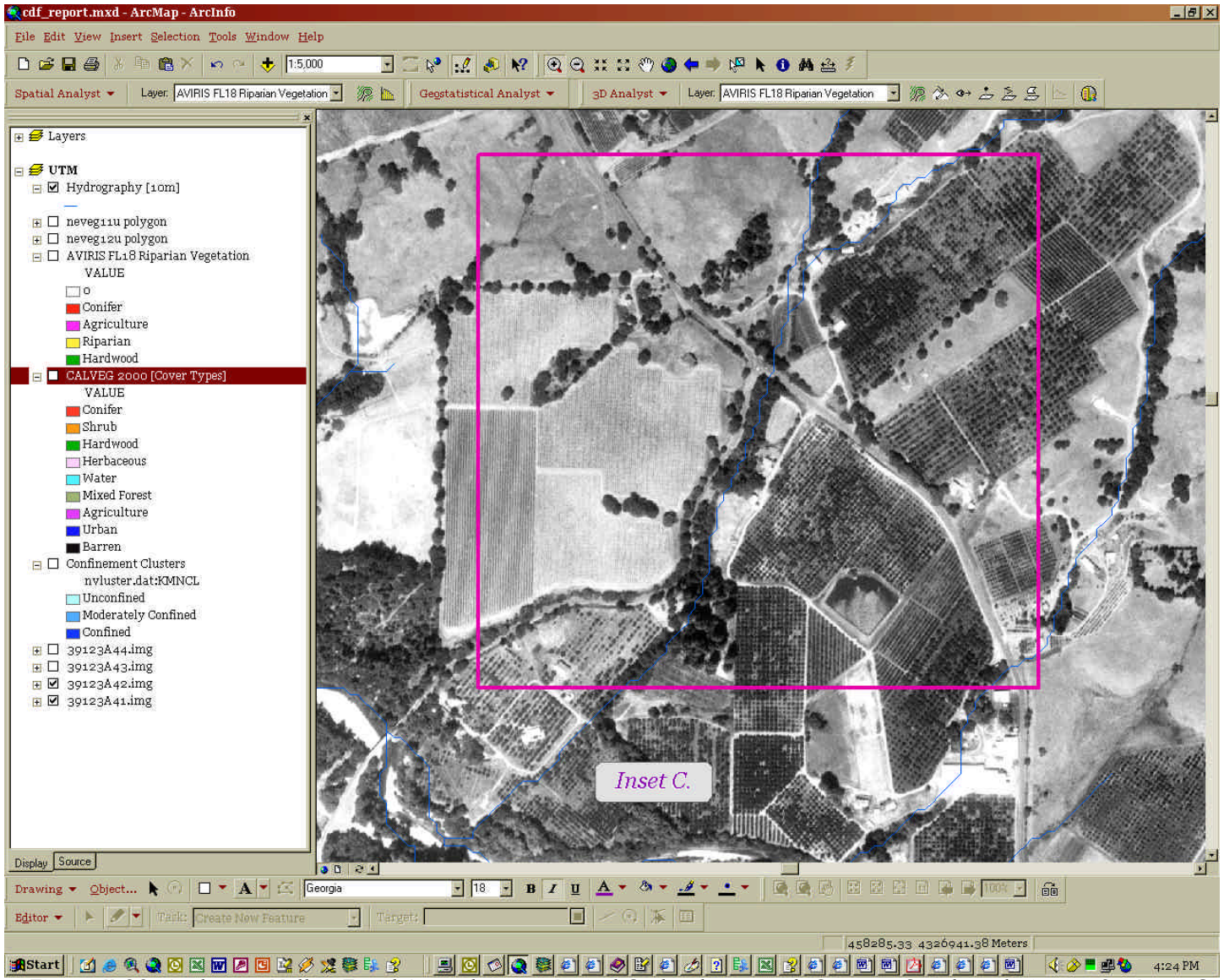

Figure II-20. Anderson Valley Focal Area showing Digital Orthophotograph Quarter Quadrangle image for Inset C.

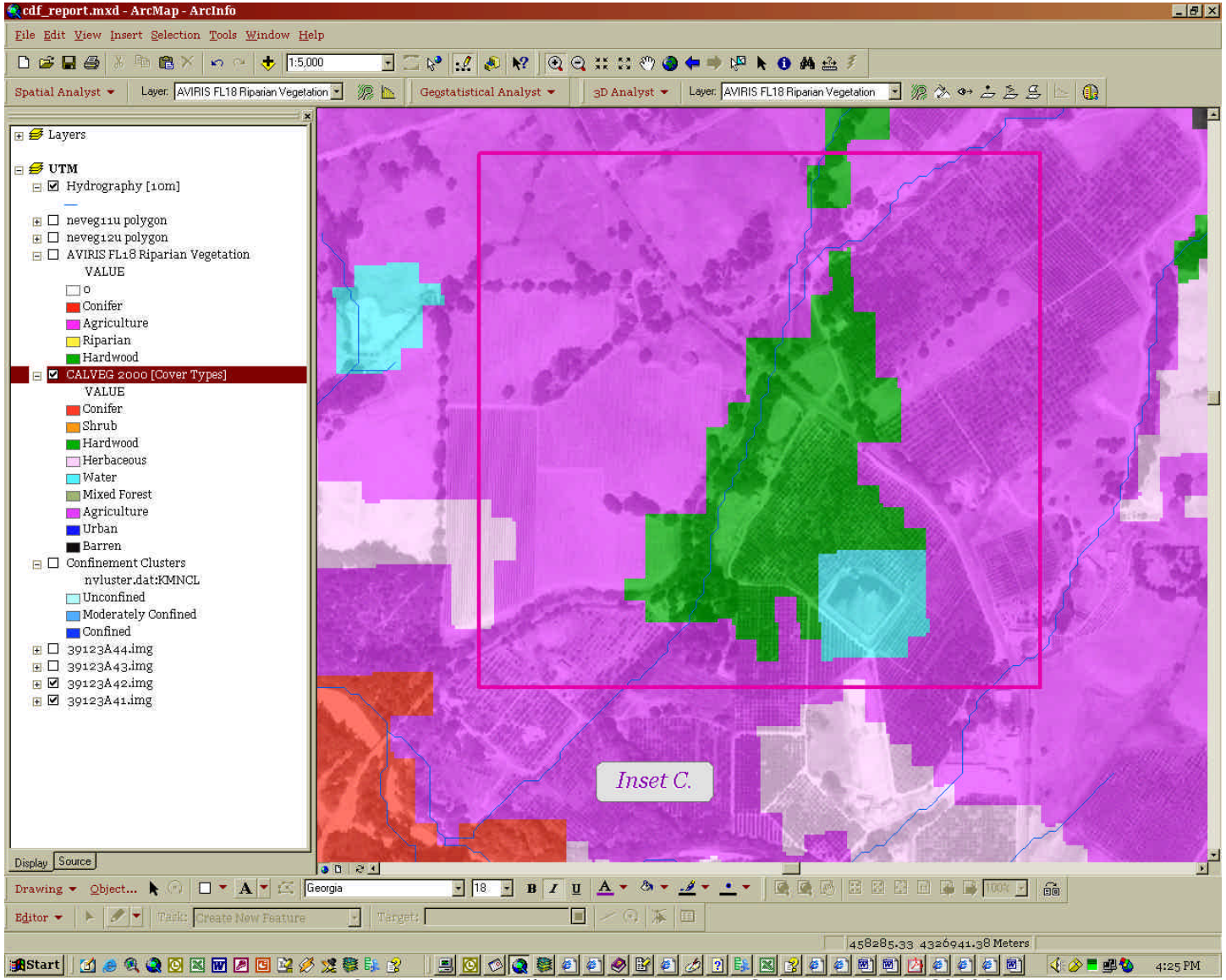

Figure II-21. Anderson Valley Focal Area Inset C showing CALVEG2000 cover types.

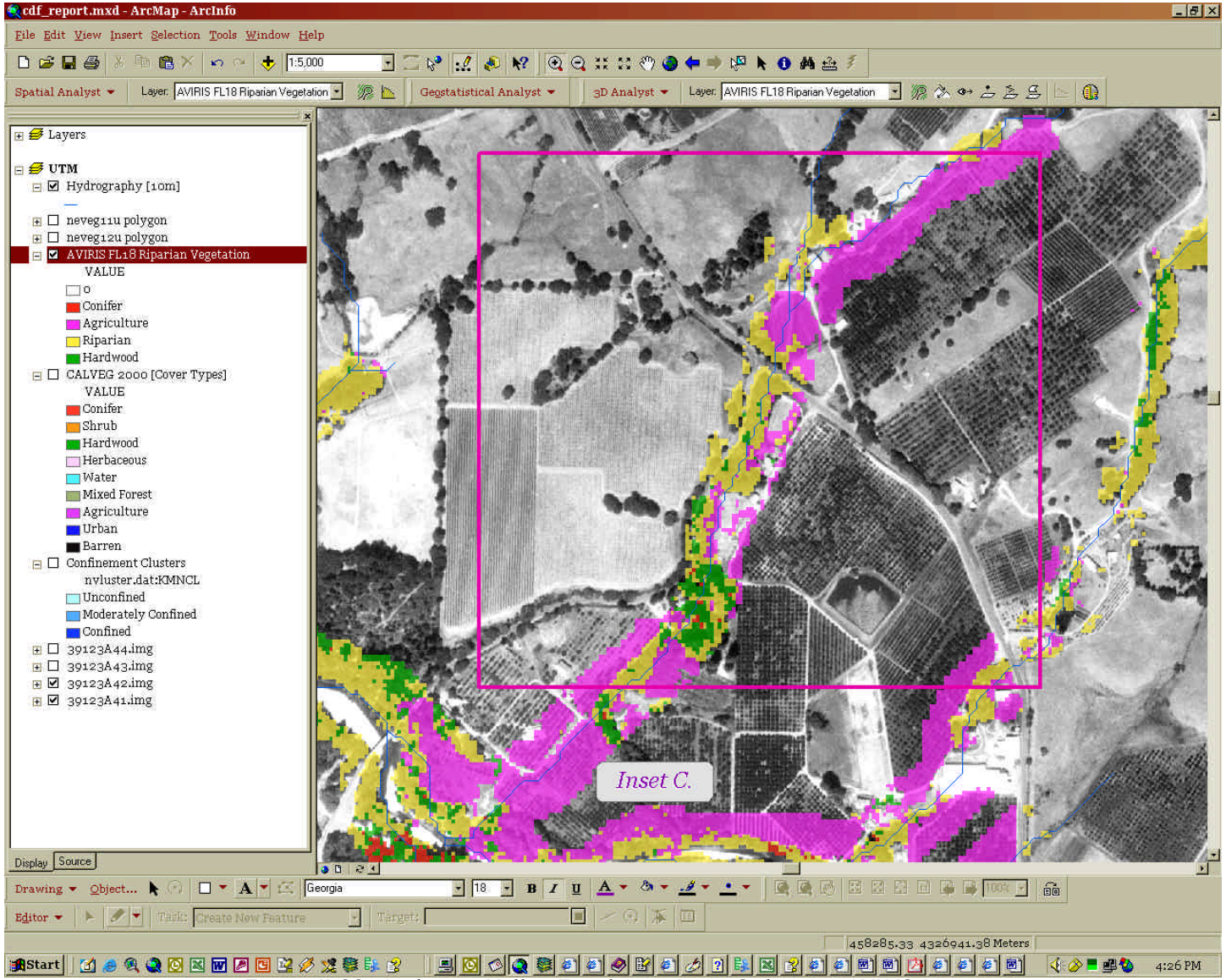

Figure II-22. Anderson Valley Focal Area Inset C showing AVIRIS Riparian cover types.

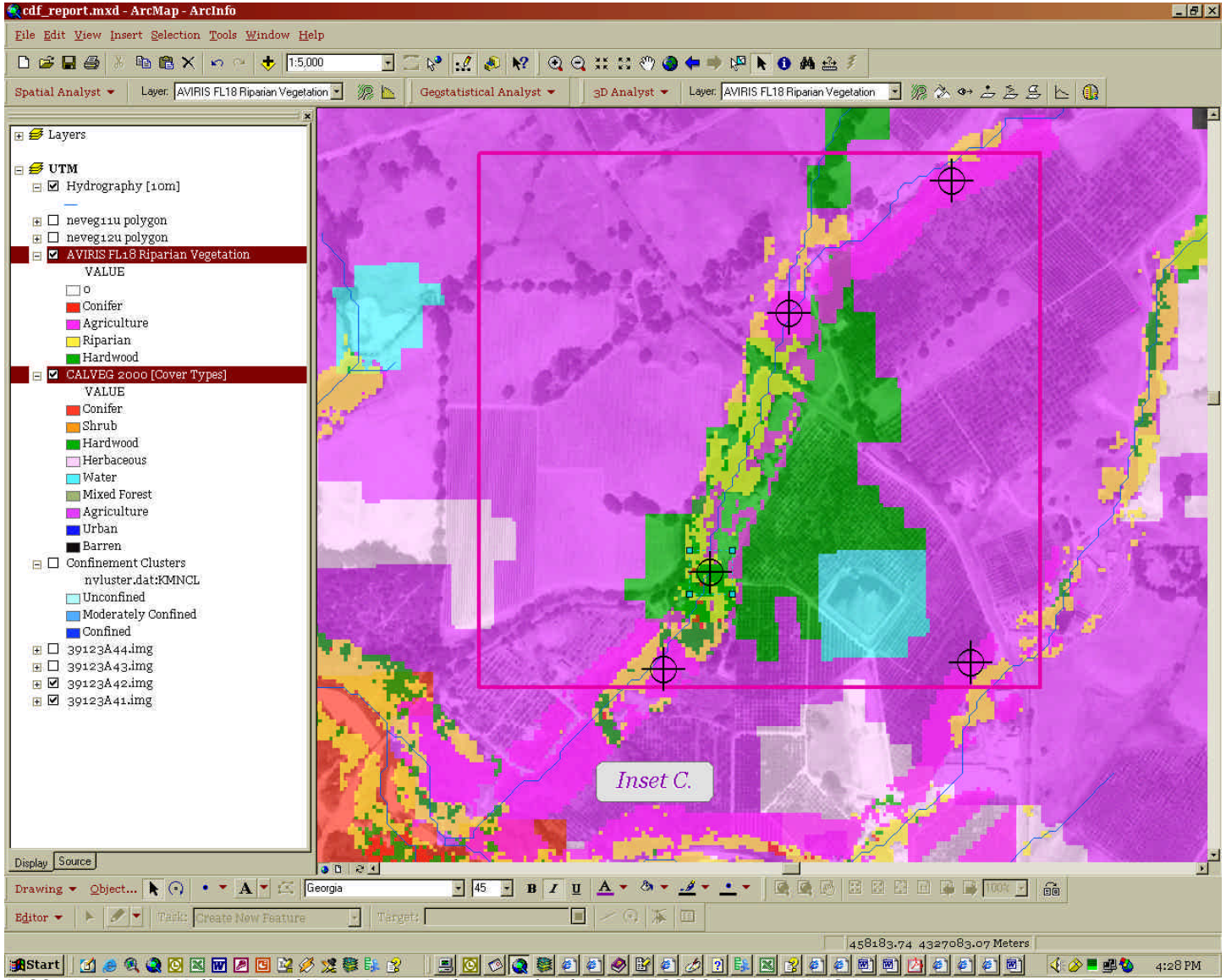

Figure II-23. Anderson Valley Focal Area Inset C showing both CALVEG2000 and AVIRIS Riparian cover types. Target points indicate mutual agreement between data.

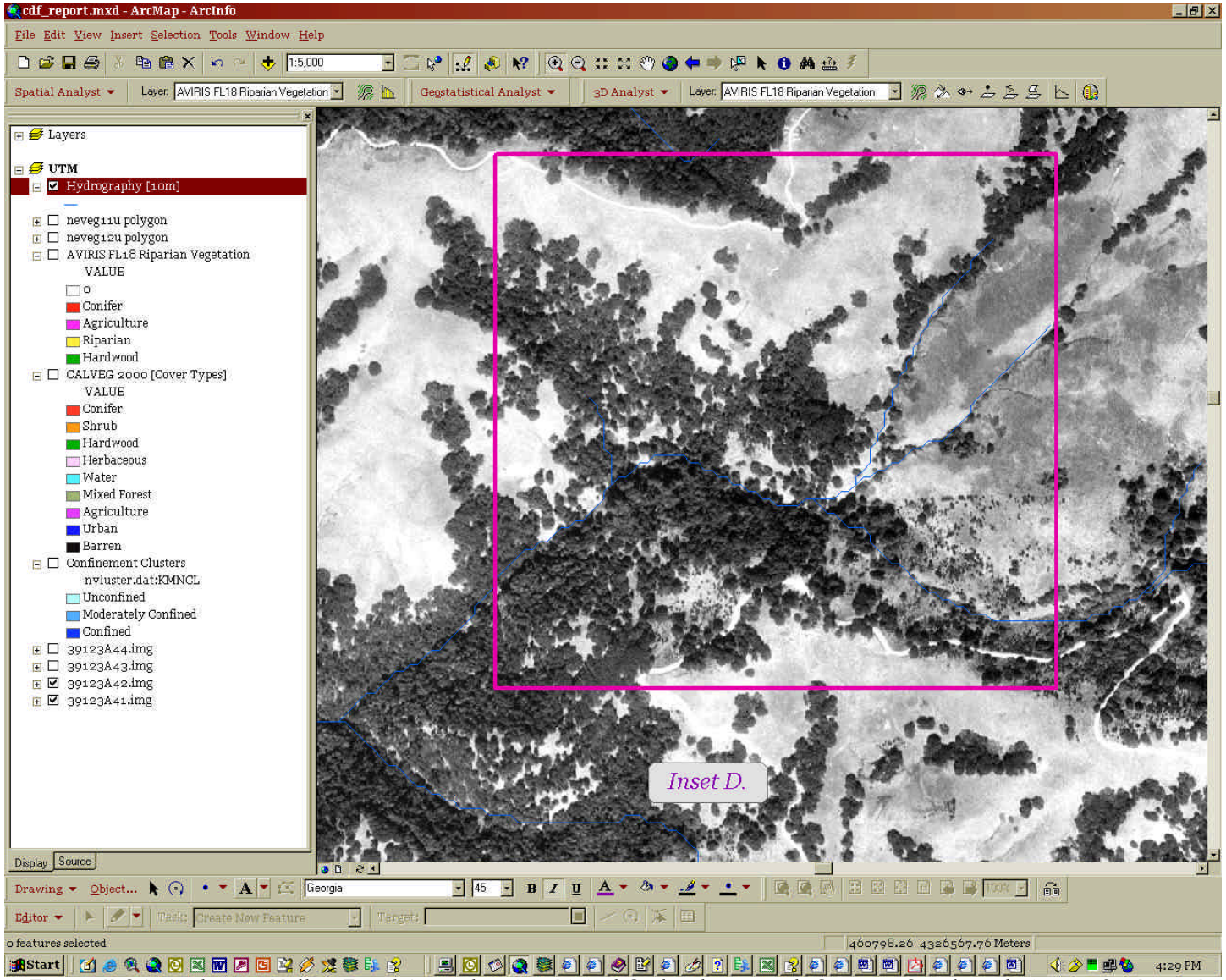

Figure II-24. Anderson Valley Focal Area showing Digital Orthophotograph Quarter Quadrangle image for Inset D.

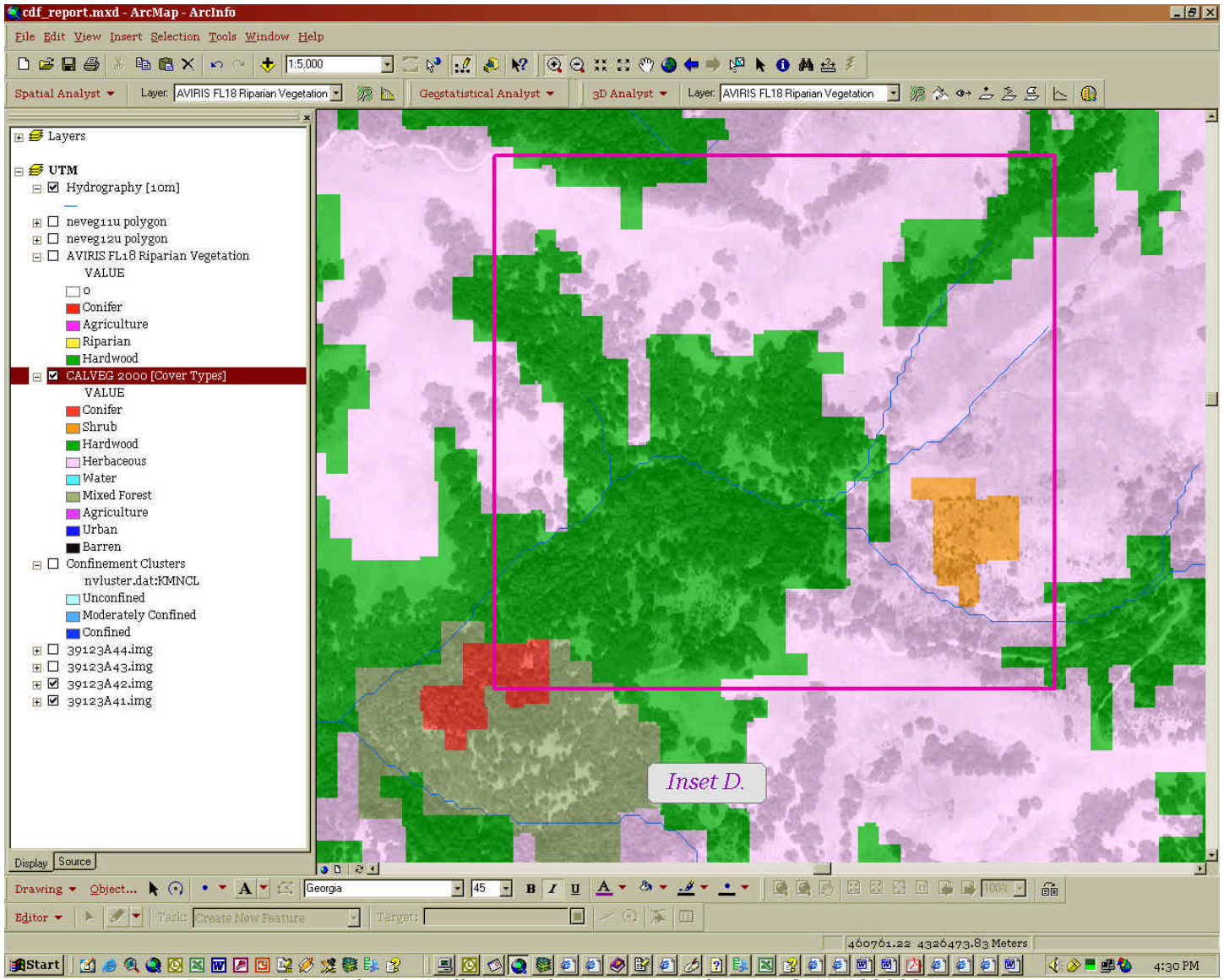

Figure II-25. Anderson Valley Focal Area Inset D showing CALVEG2000 cover types.

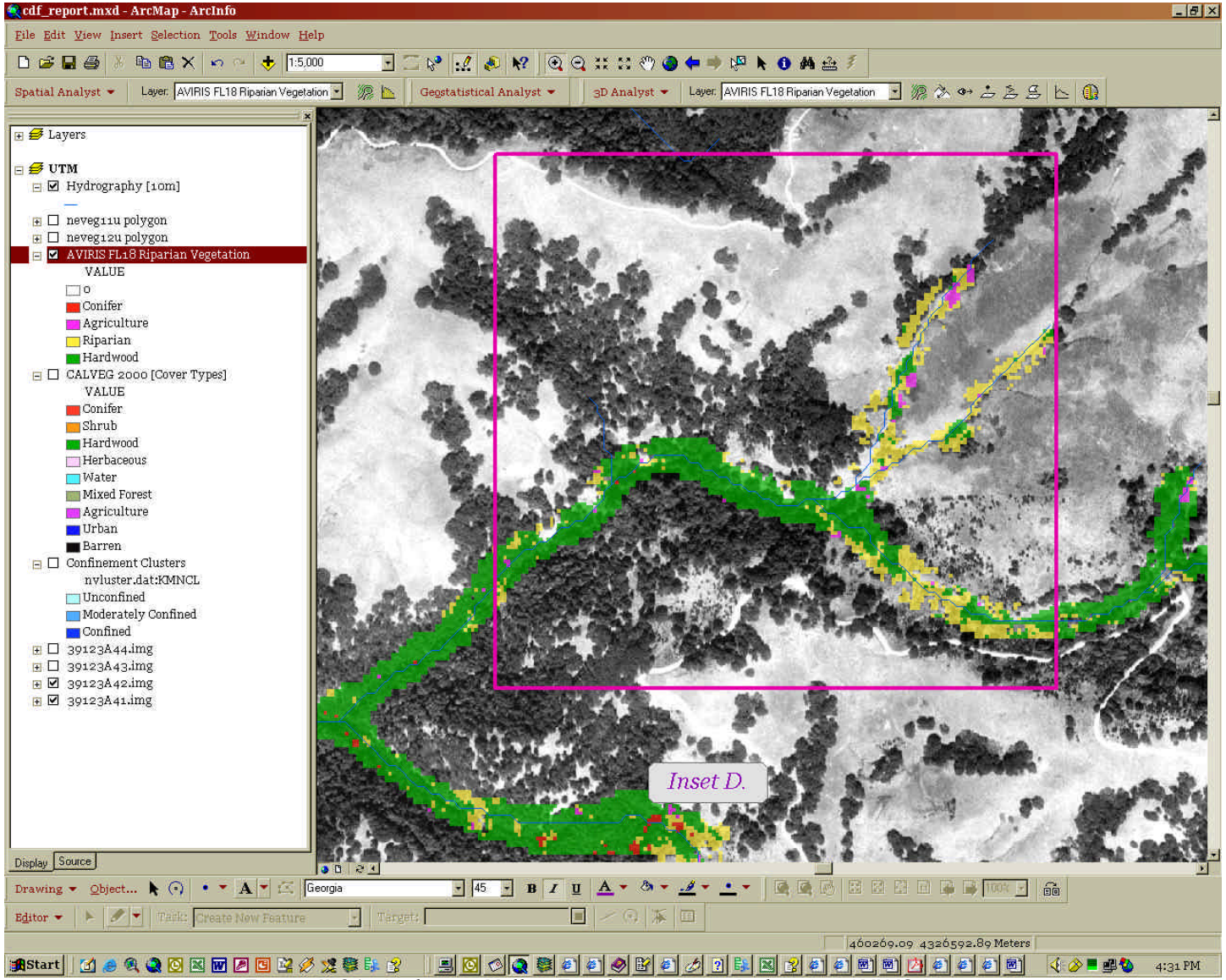

Figure II-26. Anderson Valley Focal Area Inset D showing AVIRIS Riparian cover types.

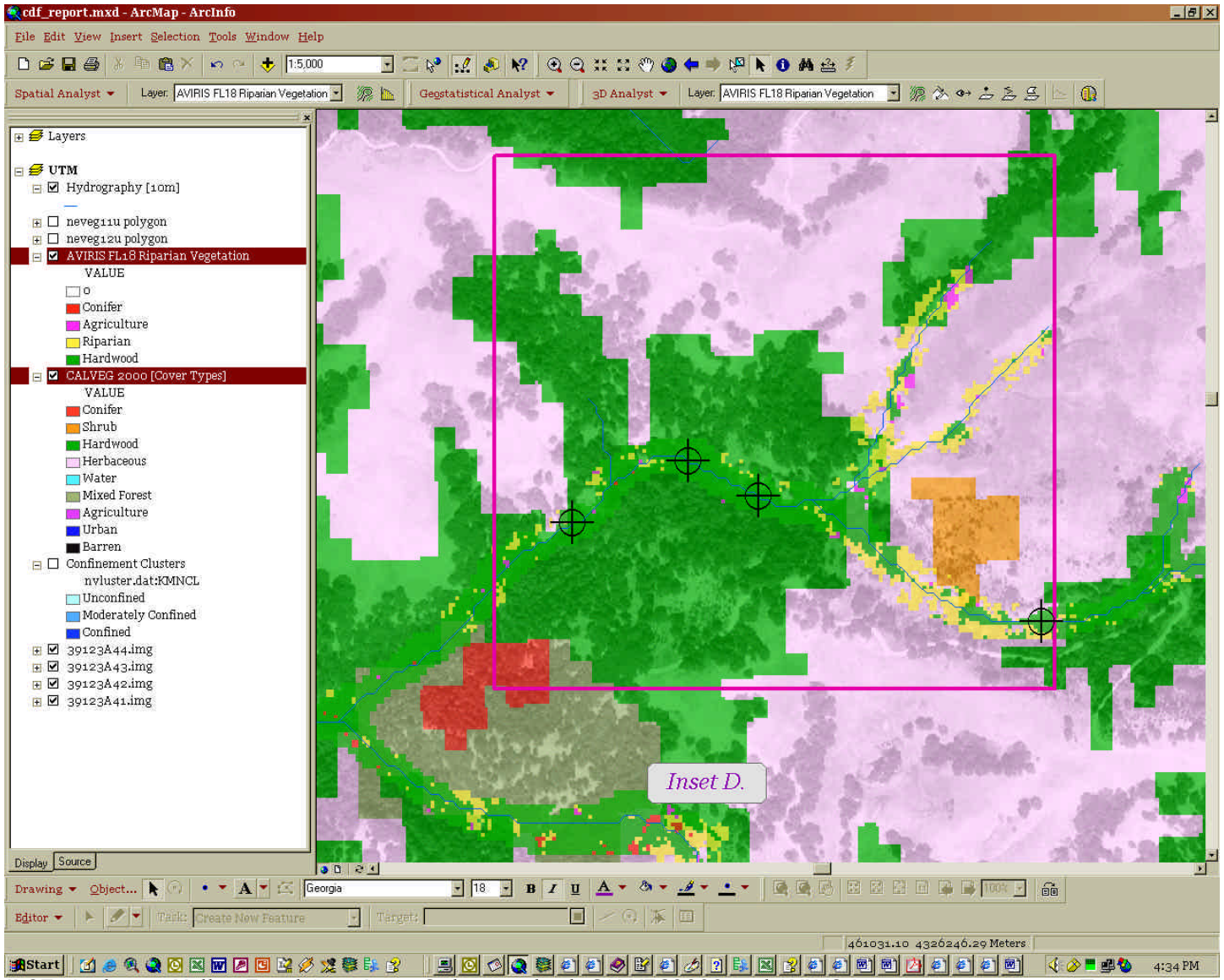

Figure II-27. Anderson Valley Focal Area Inset C showing both CALVEG2000 and AVIRIS Riparian cover types. Target points indicate mutual agreement between data.

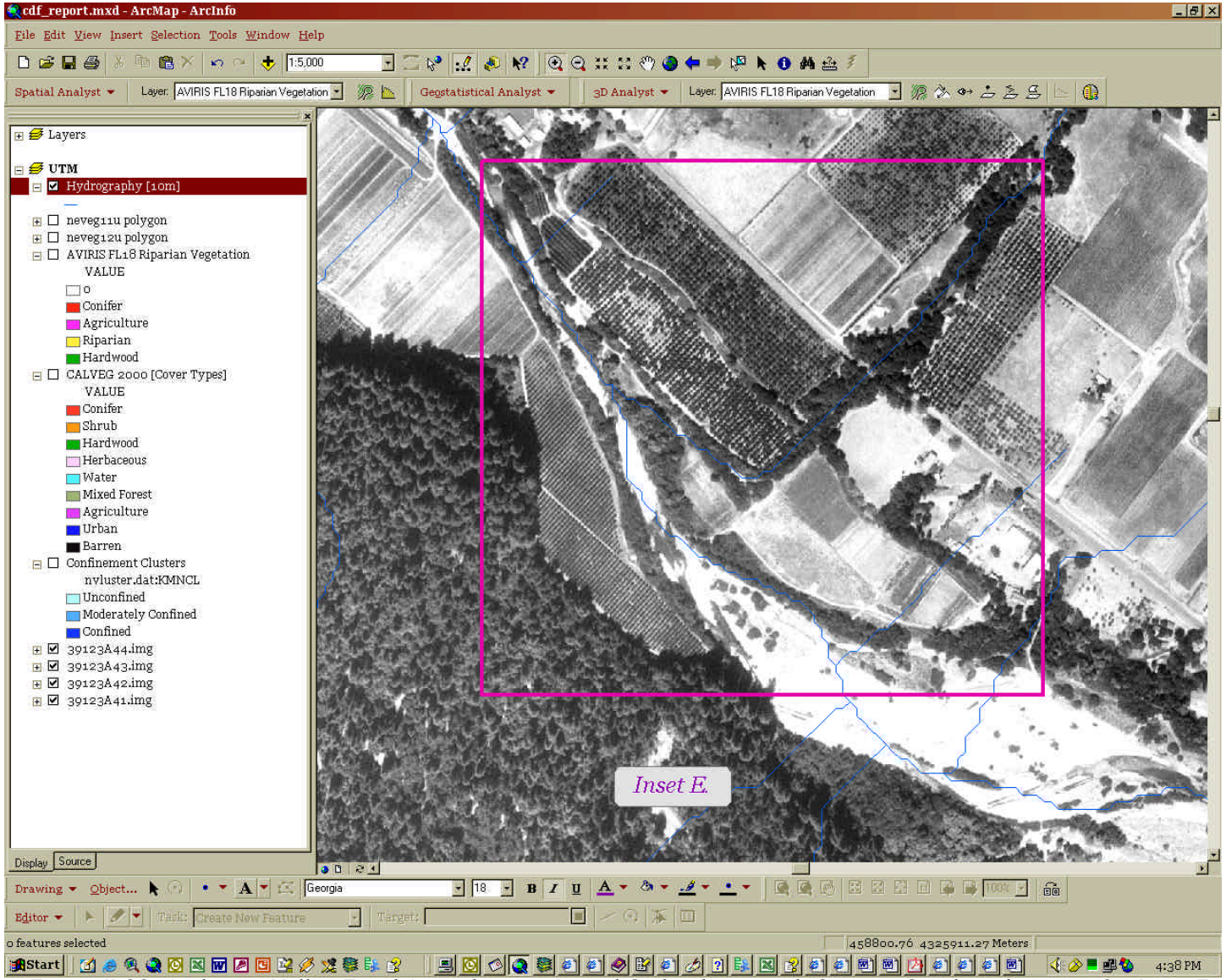

Figure II-28. Anderson Valley Focal Area showing Digital Orthophotograph Quarter Quadrangle image for Inset E.

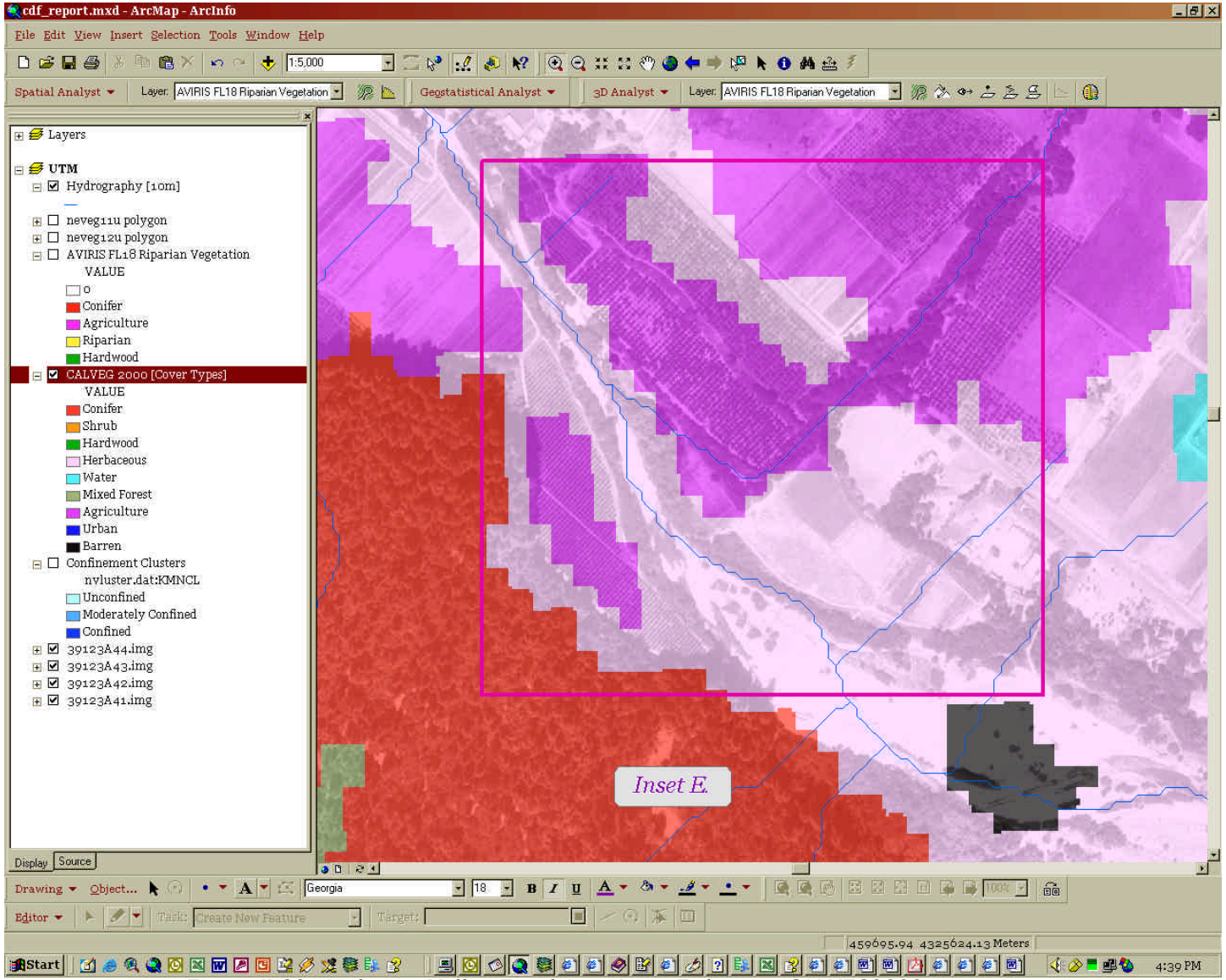

Figure II-29. Anderson Valley Focal Area Inset E showing CALVEG2000 cover types.

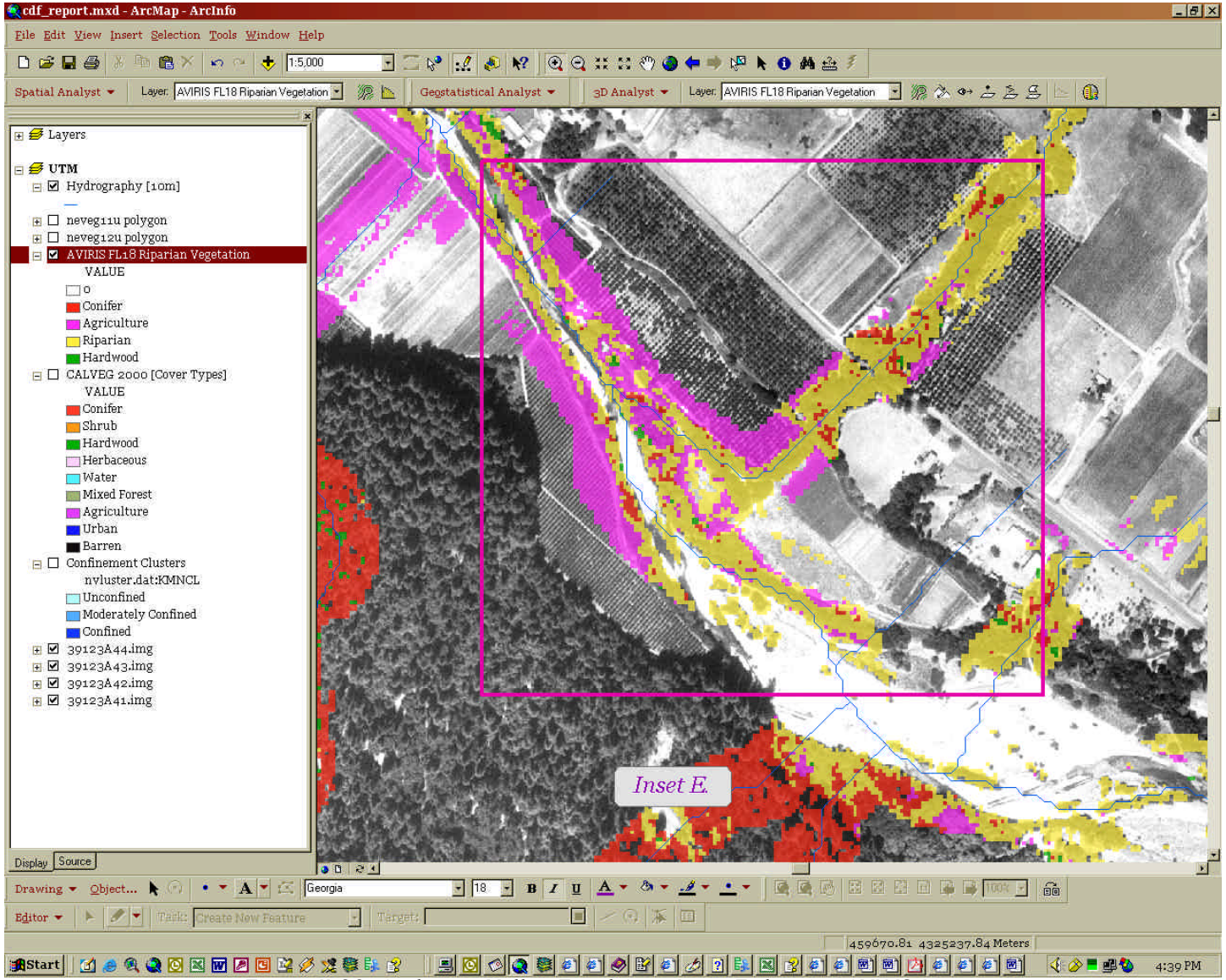

Figure II-30. Anderson Valley Focal Area Inset E showing AVIRIS Riparian cover types.

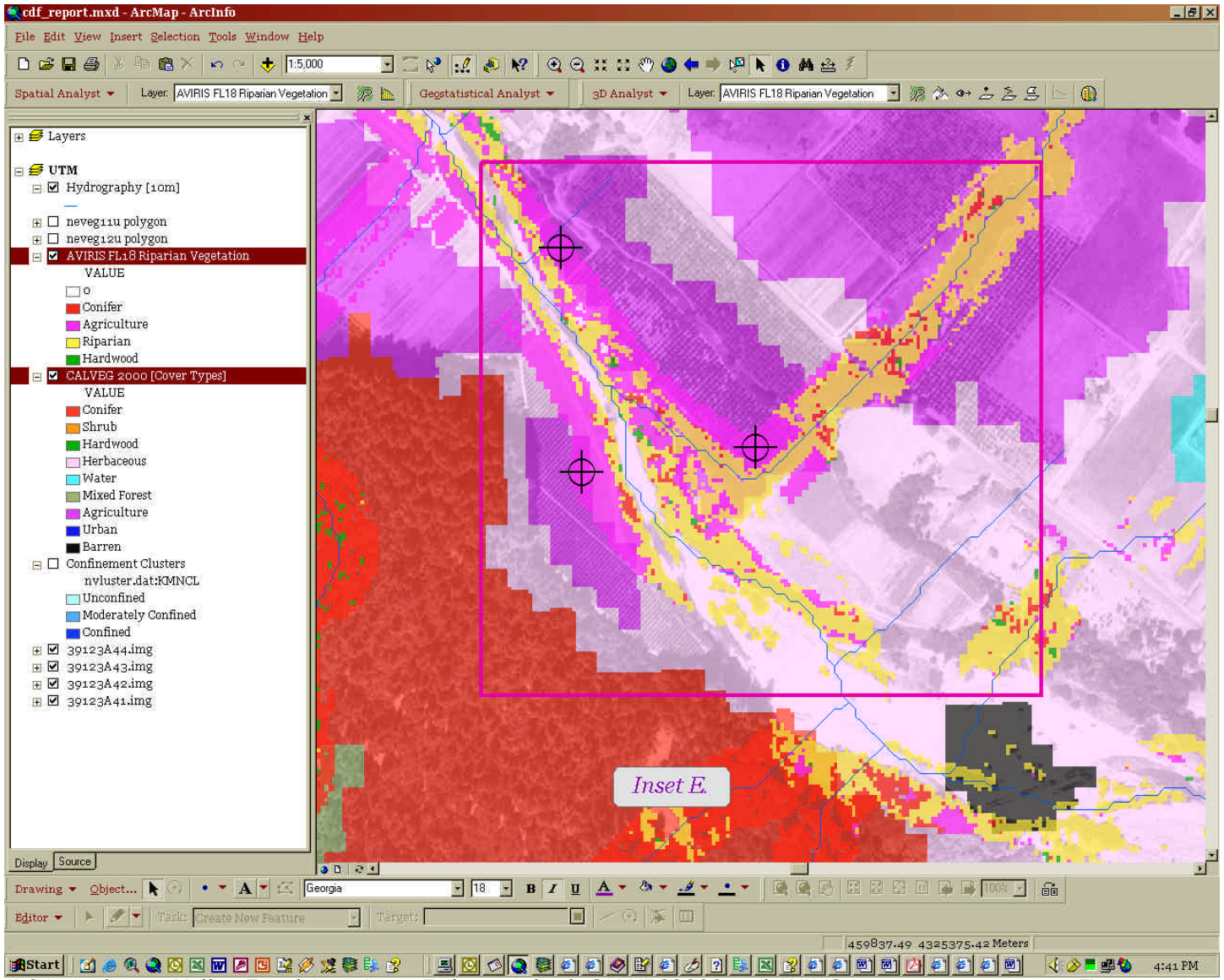

Figure II-31. Anderson Valley Focal Area Inset E showing both CALVEG2000 and AVIRIS Riparian cover types. Target points indicate mutual agreement between data.

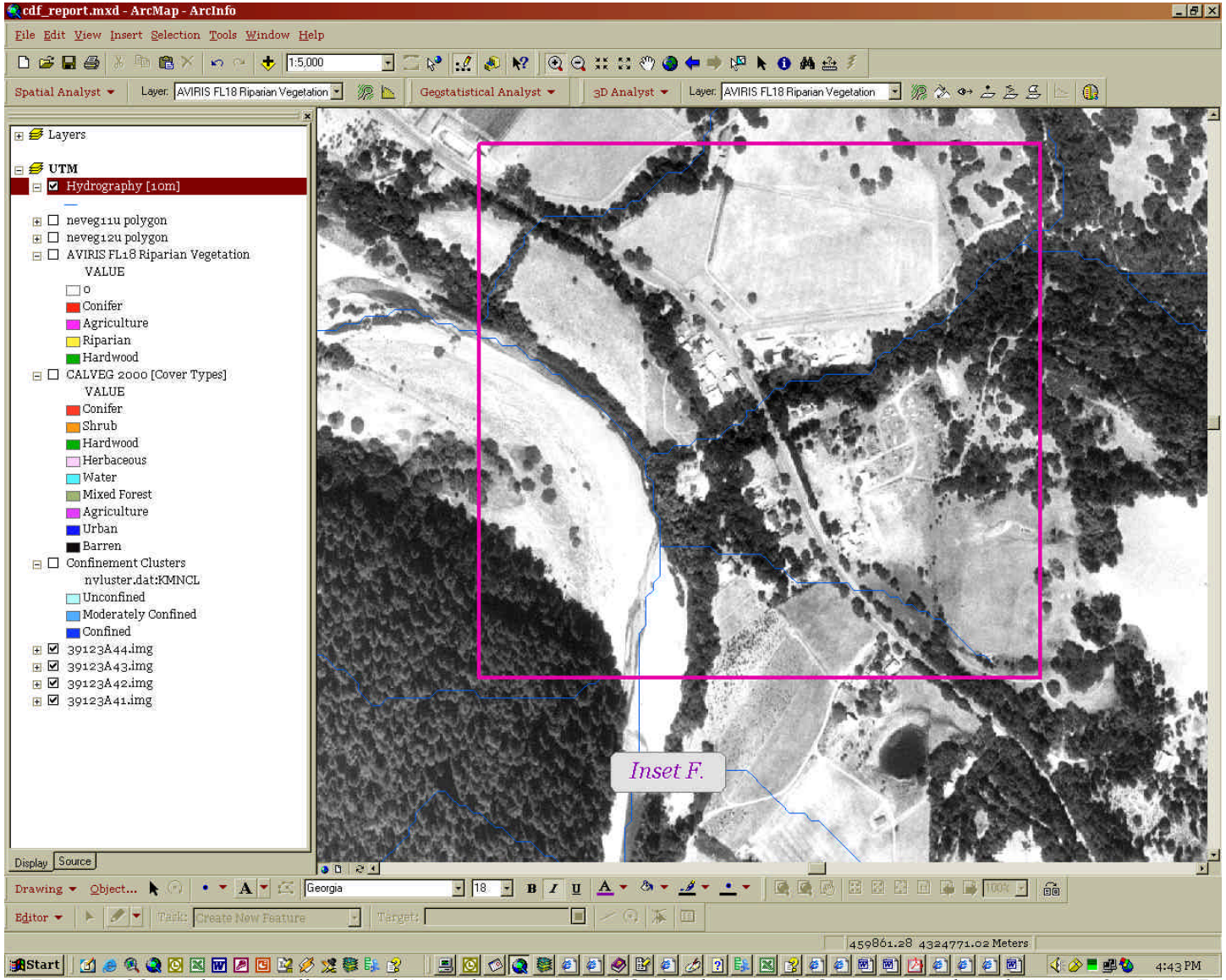

Figure II-32. Anderson Valley Focal Area showing Digital Orthophotograph Quarter Quadrangle image for Inset F.

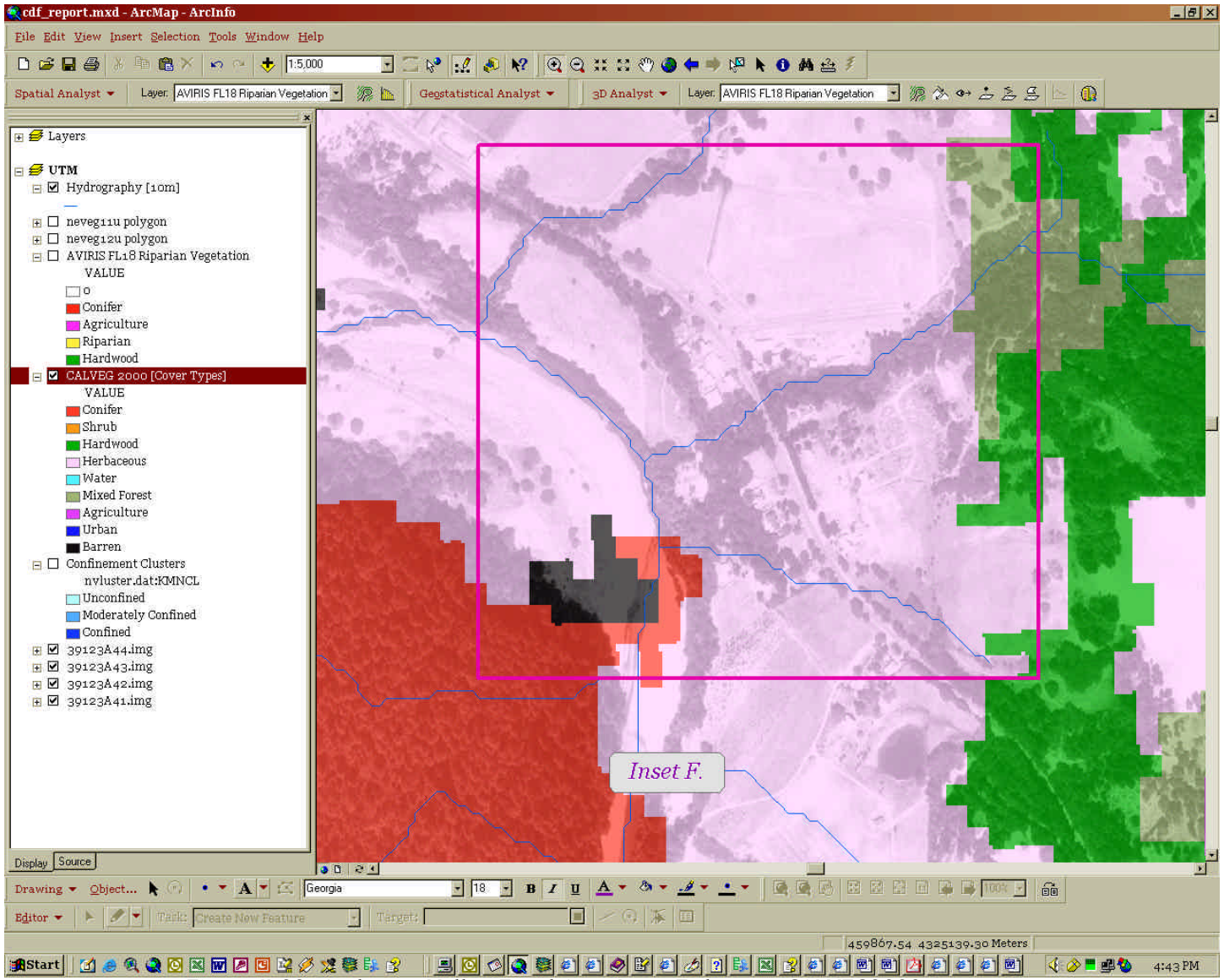

Figure II-33. Anderson Valley Focal Area Inset F showing CALVEG2000 cover types.

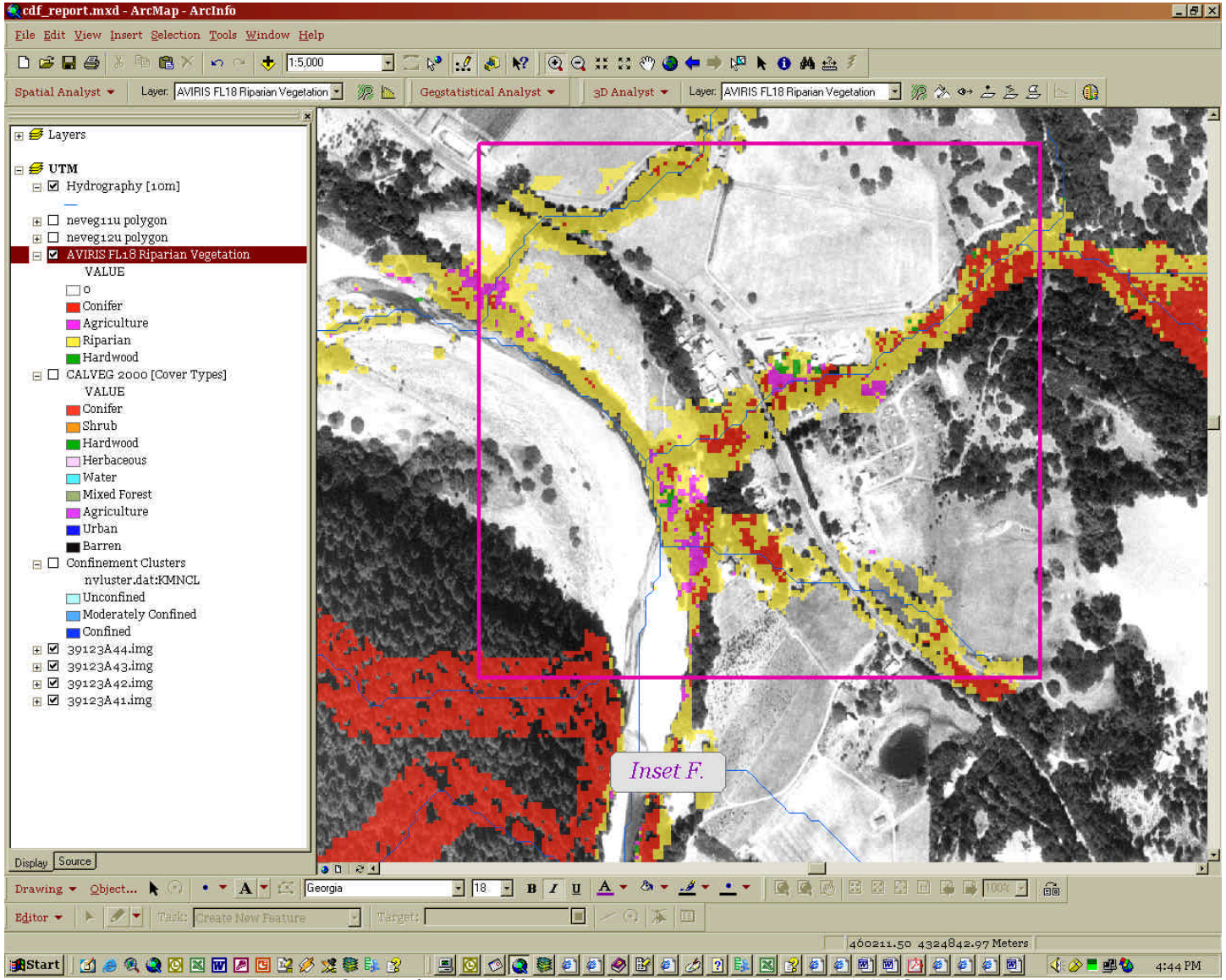

Figure II-34. Anderson Valley Focal Area Inset F showing AVIRIS Riparian cover types.

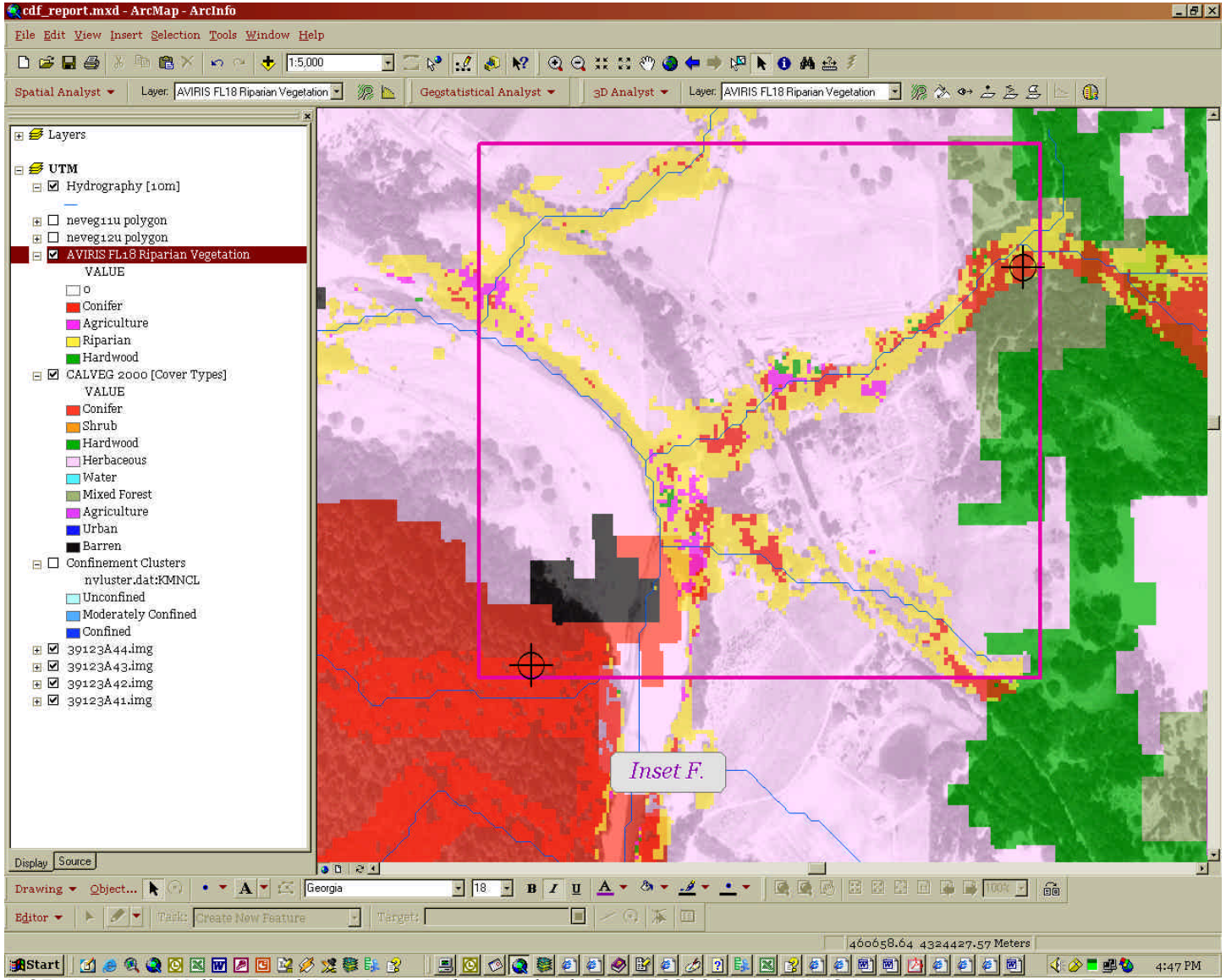

Figure II-35. Anderson Valley Focal Area Inset F showing both CALVEG2000 and AVIRIS Riparian cover types. Target points indicate mutual agreement between data.

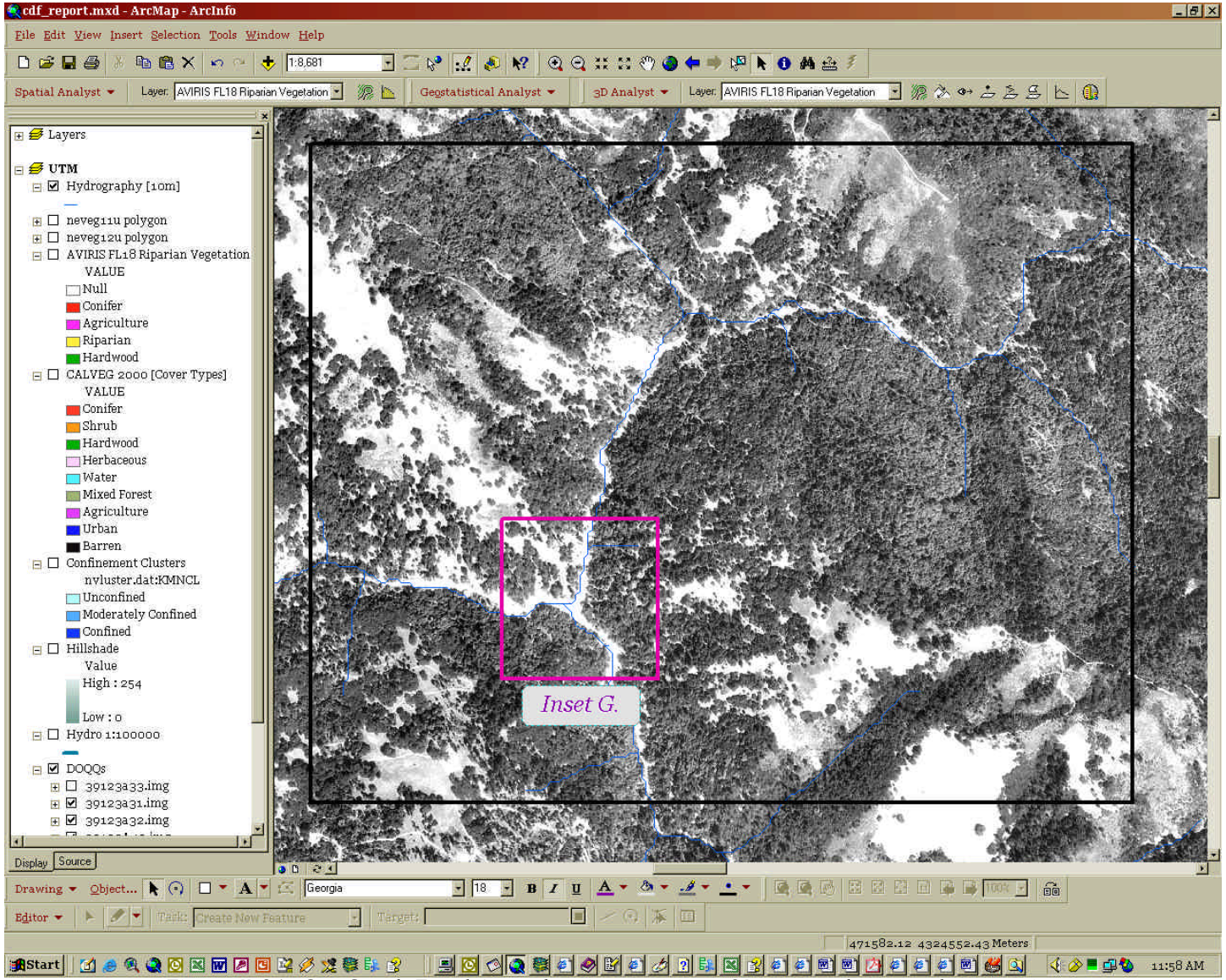

Figure II-36. Gut Creek Focal Area showing position of Inset used in visual comparison.

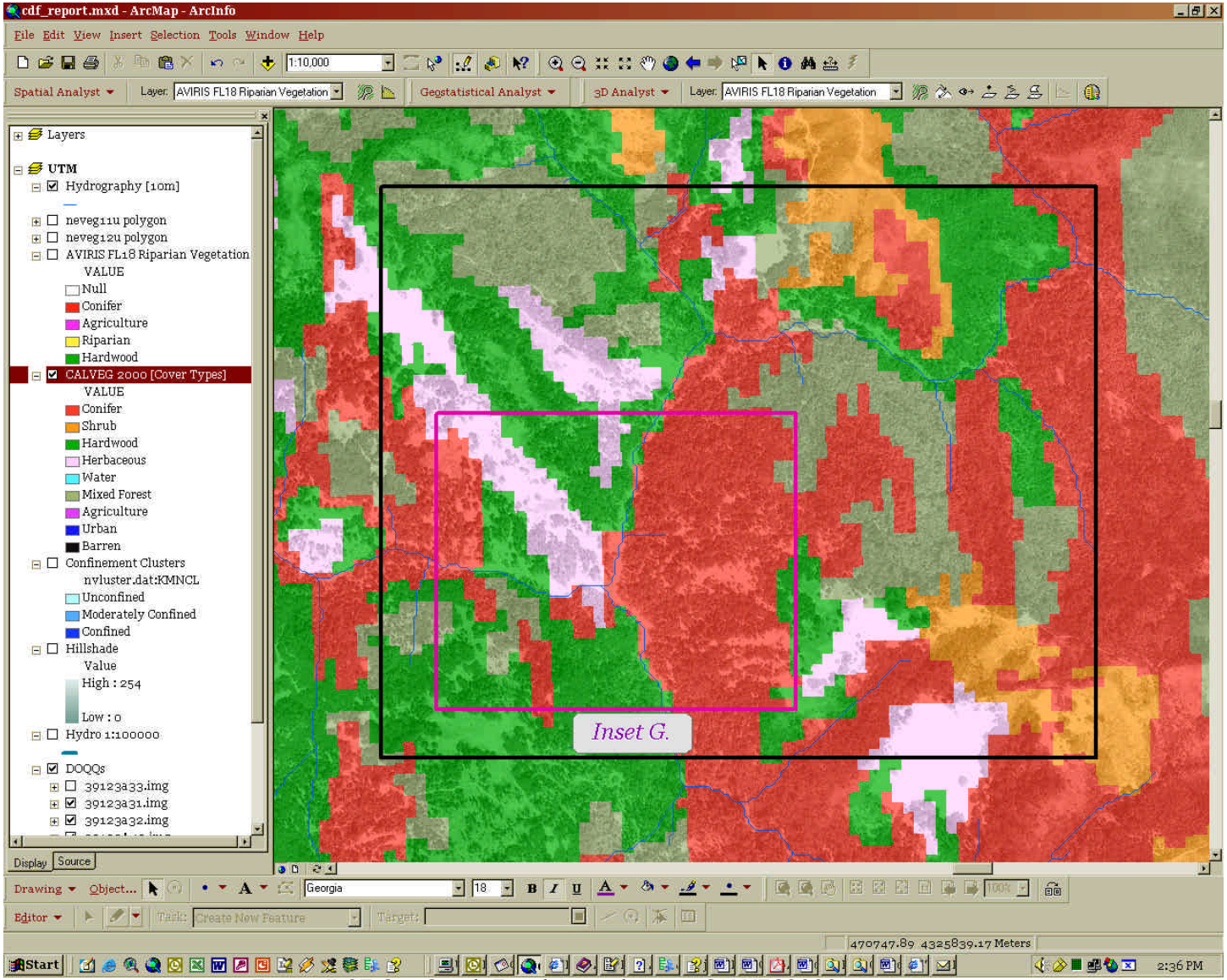

Figure II-37 Gut Creek Focal Area showing CALVEG2000 cover types.

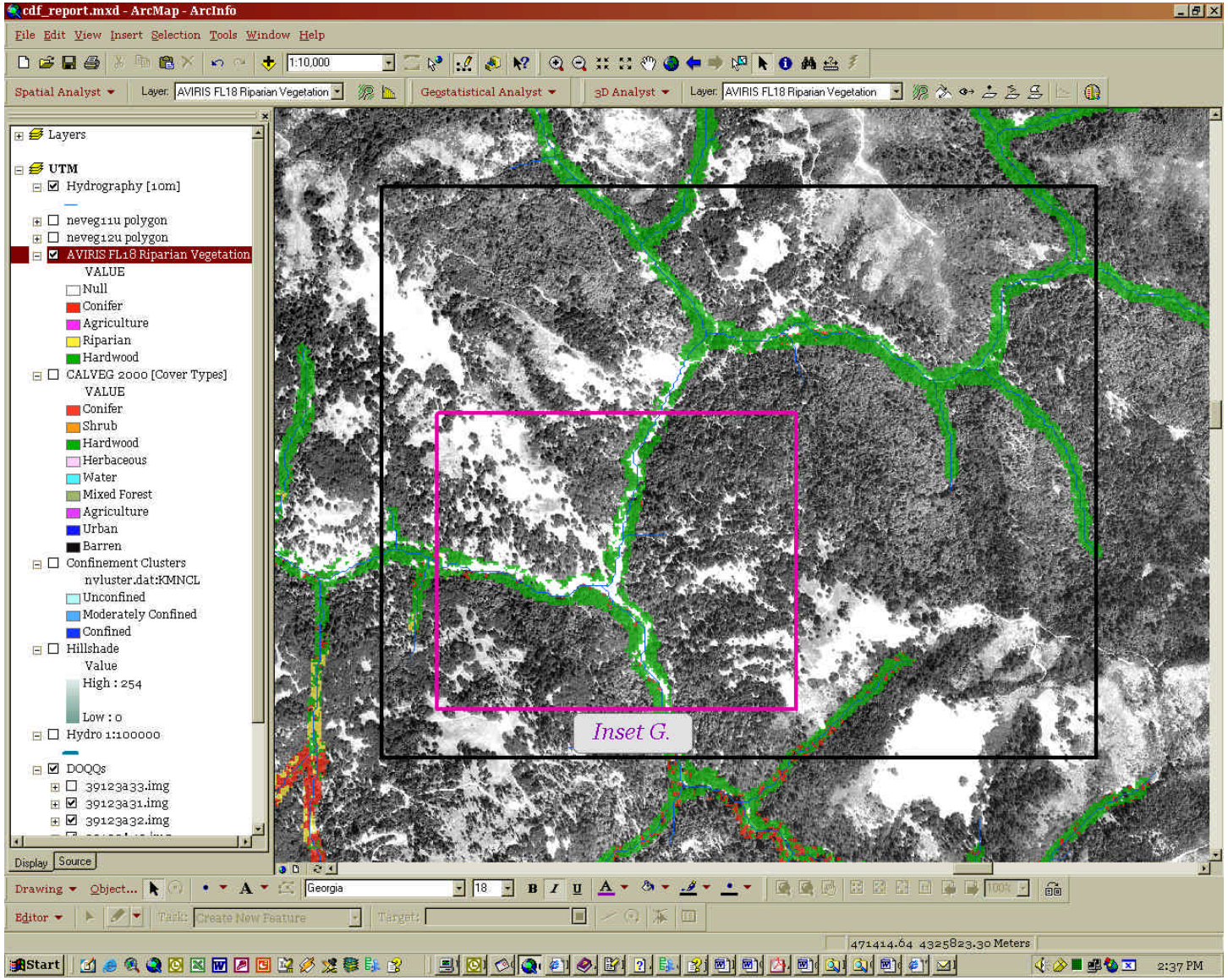

Figure II-38. Gut Creek Focal Area showing AVIRIS Riparian Vegetation.

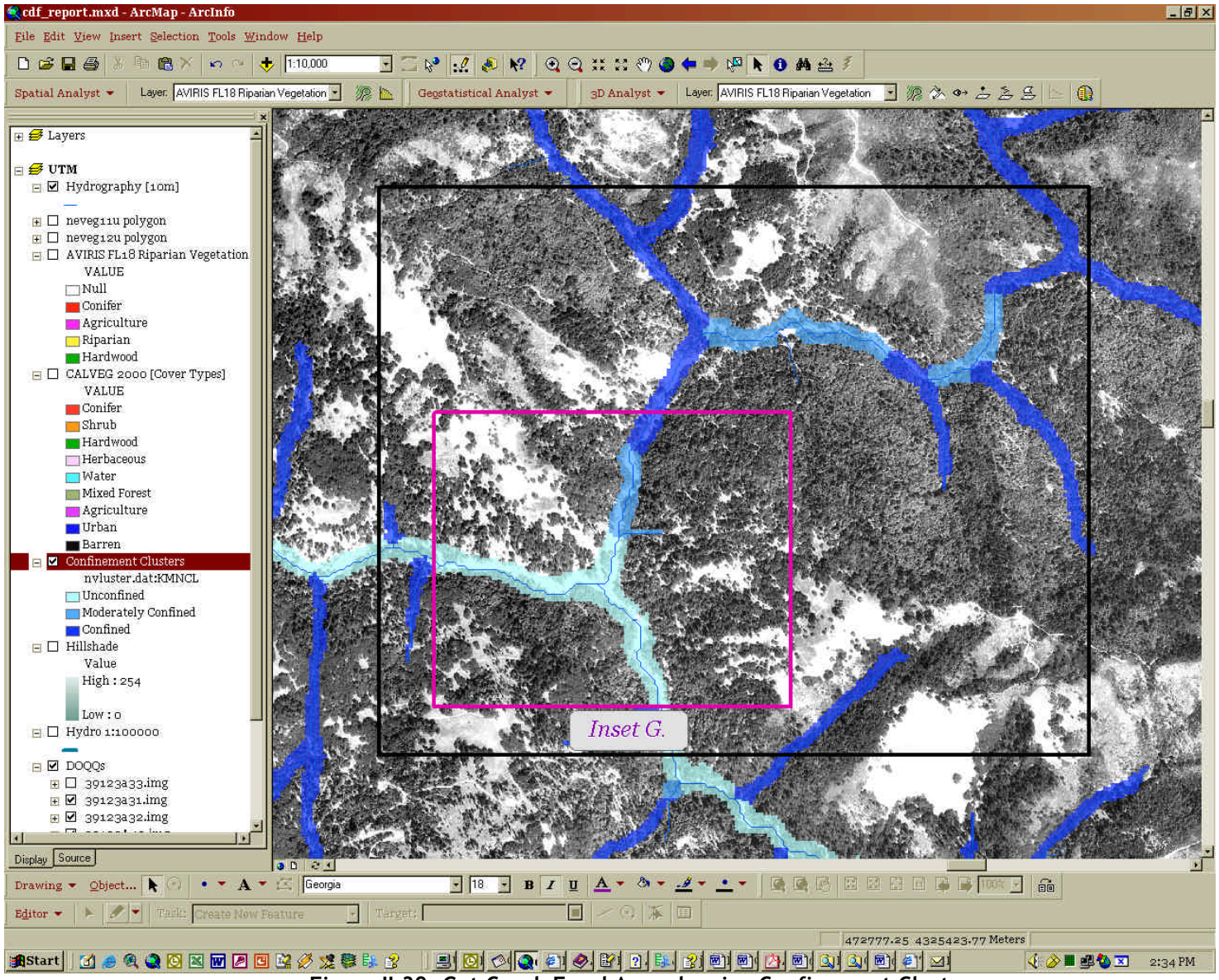

Figure II-39. Gut Creek Focal Area showing Confinement Clusters.

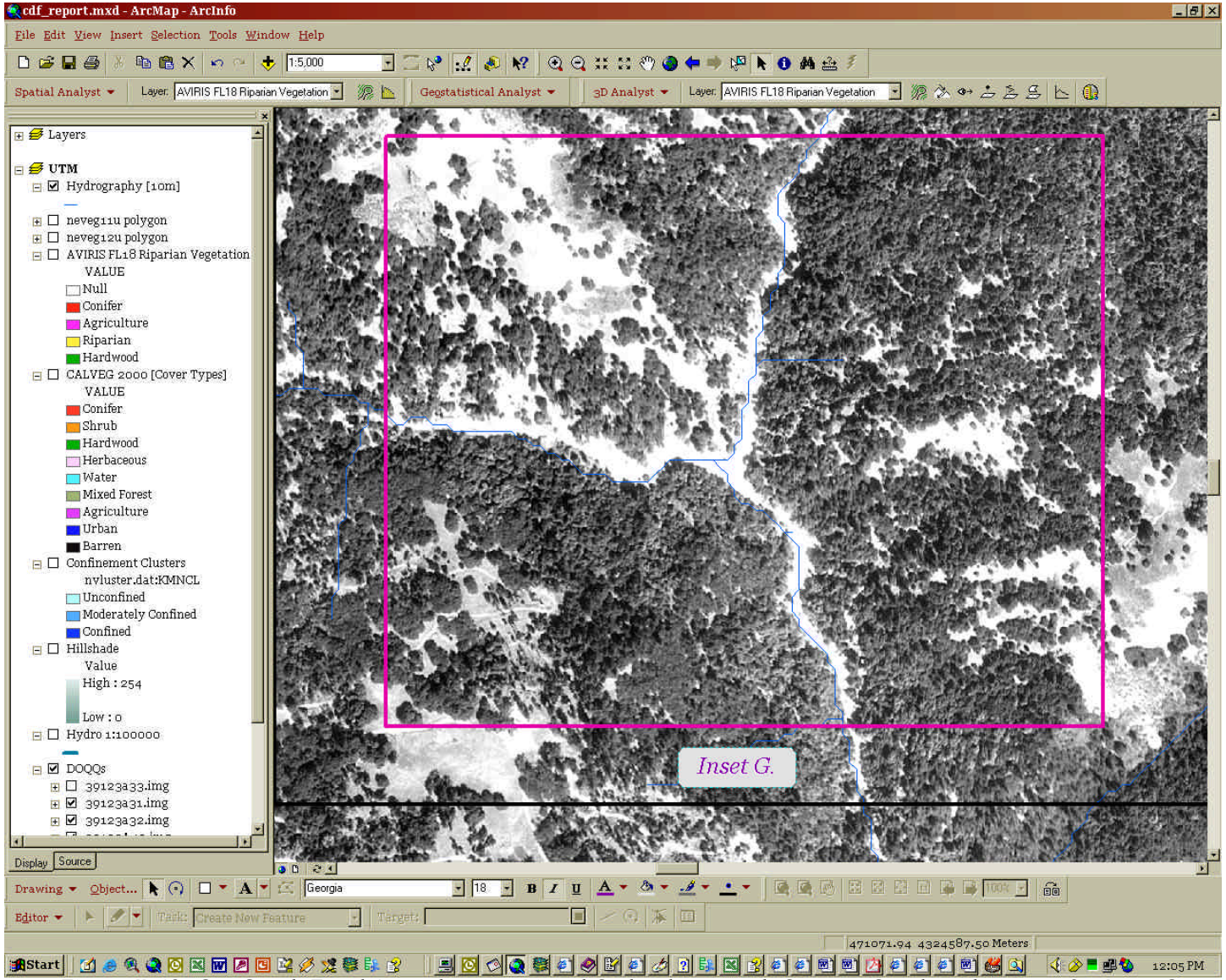

Figure II-40. Gut Creek Focal Area showing Digital Orthophotograph Quarter Quadrangle image for Inset G.

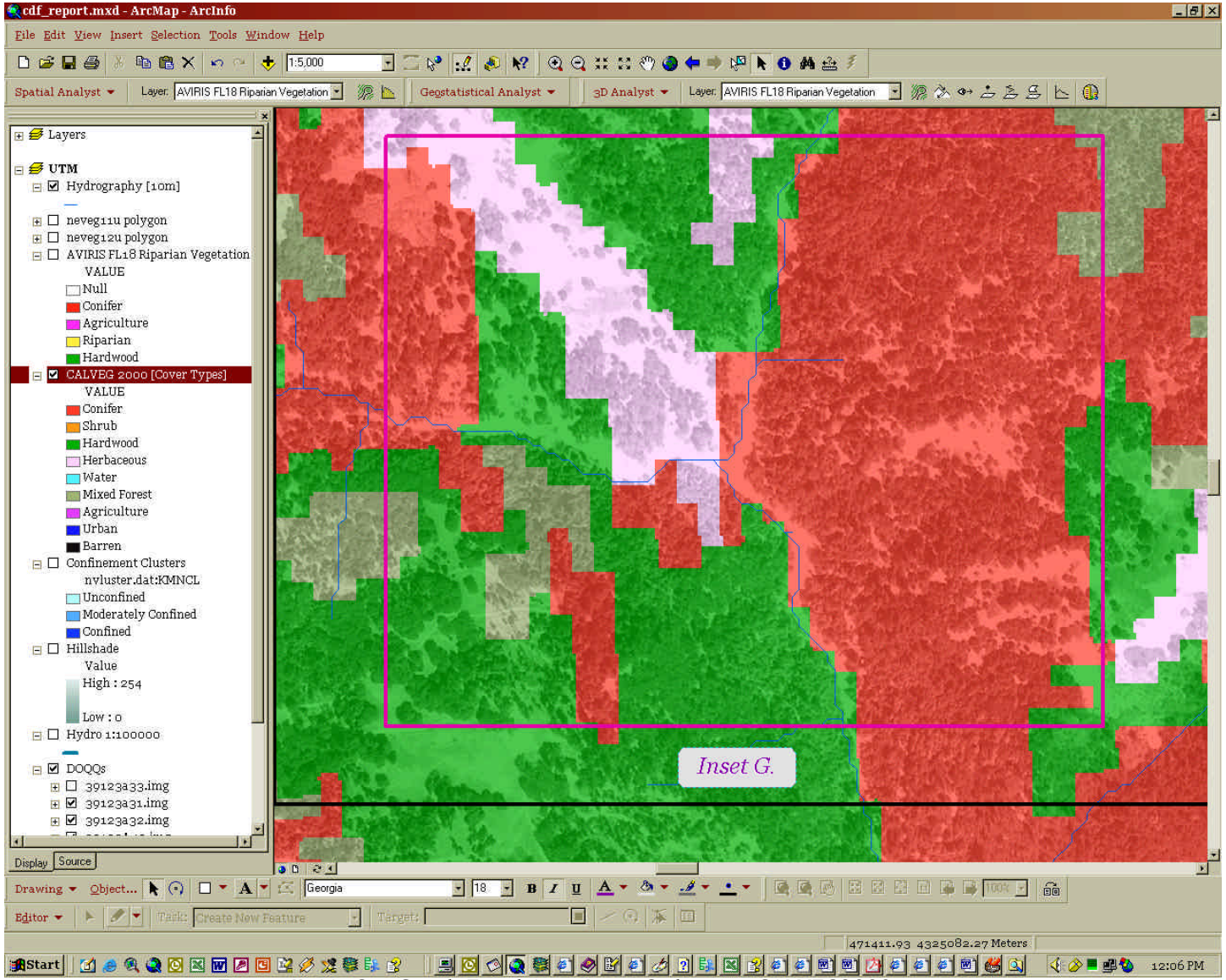

Figure II-41. Gut Creek Focal Area Inset G showing CALVEG2000 cover types.

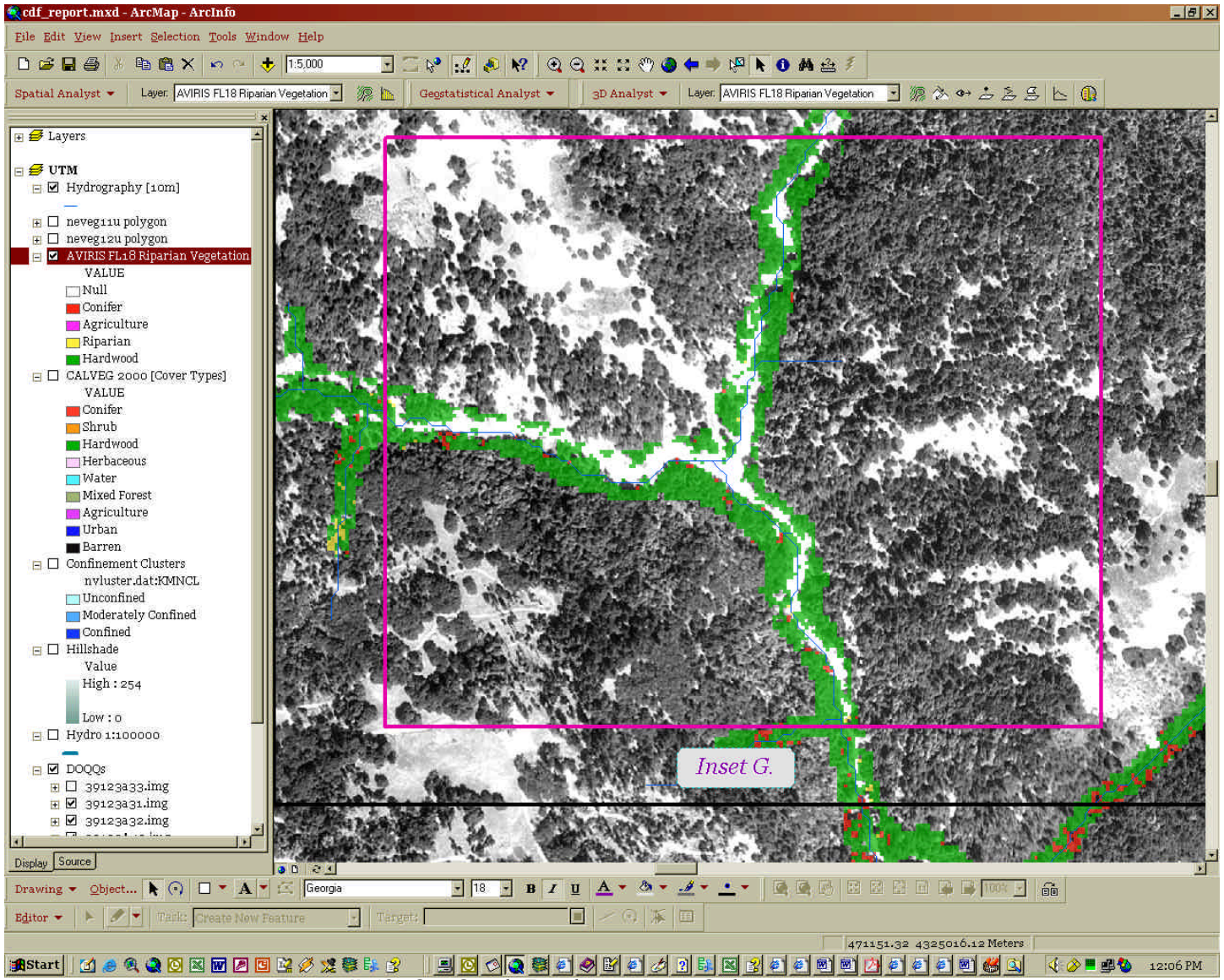

Figure II-42. Gut Creek Focal Area Inset G showing AVIRIS Riparian cover types.

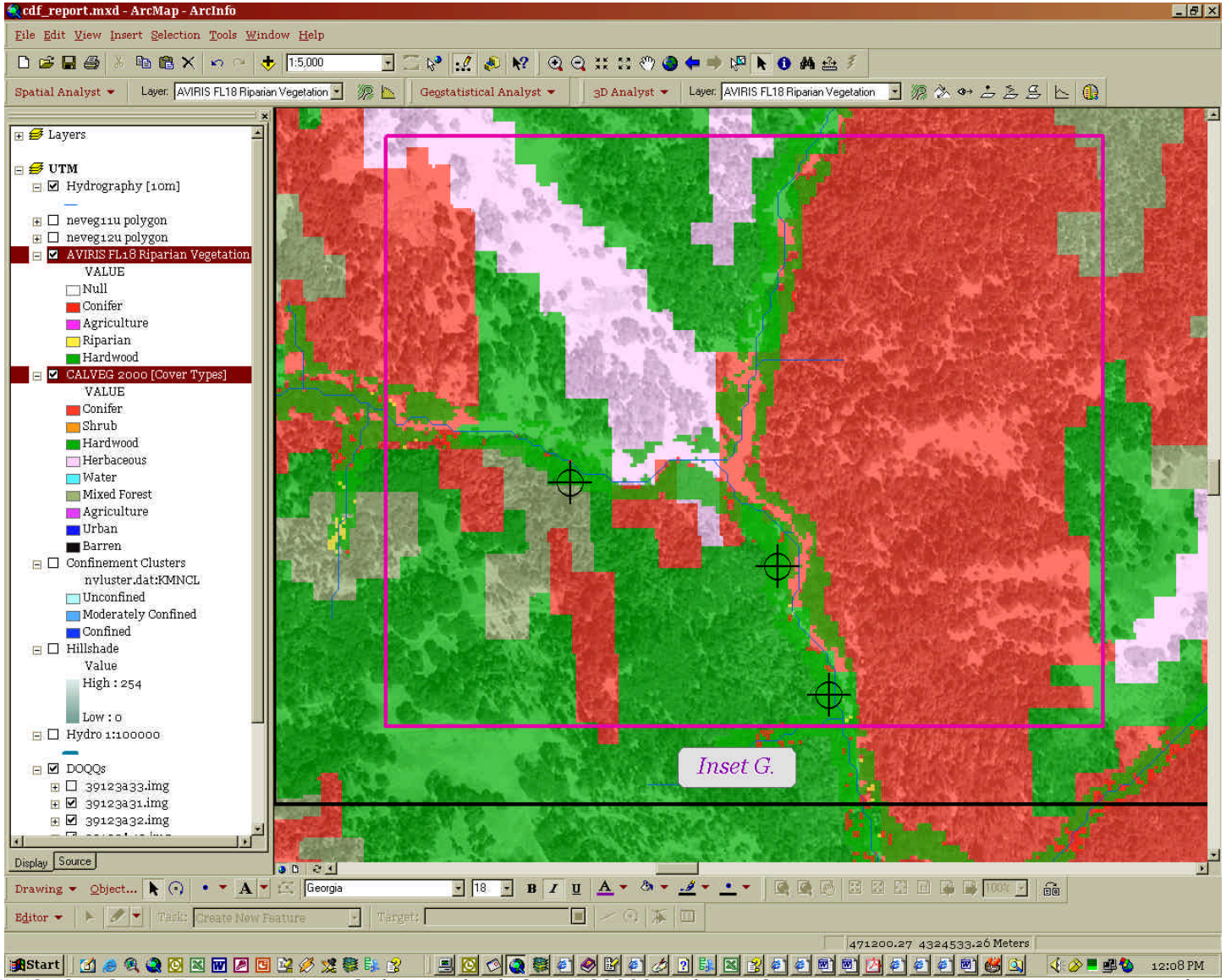

Figure II-43. Gut Creek Focal Area Inset G showing both CALVEG2000 and AVIRIS Riparian cover types. Target points indicate mutual agreement between data.

Appendix III. Current Sensors and their Characteristics

COUNTRY	SENSOR OWNER	PROGRAM	INSTRUMENT(S)	LAUNCH Date	SENSOR TYPES	RESOLUTION IN METERS									STEREO Type	SW KM	GLOBAL COVER REPEAT days	COST OF ACQUISITION
						THEMATIC MAPPER BANDS												
						PAN	VNIR				SWIR		TIR	RADAR				
							1	2	3	4	5	7	6	res,band				
FREQUENT GLOBAL COVERAGE, LANDSAT LIKE CLASSIFICATION CAPABILITY																		
INDIA	Gov.	IRS-1 C,D	LISS-3, PAN, (WIFS)	'95	M&P	6		23	23	23	70				C/T	148	22	
JAPAN	Gov.	ADEOS-2	AVNIR	01	M&P	8	16	16	16	16					C/T	80	41	
CHINA-BRAZIL	Gov.	CBERS	CCD, IRMSS	'97	M&P	20, 80	20	20	20	20	80	80	160		C/T	120	26	
FRANCE		Spot 4	HRVIR, (VEGETATION)	'97	M&P	10		20	20	20	20				C/T	120*	26	2.5 m Pan $6500 / scene; 5.0 m Pan $3250 / scene; 10 m multi-spectral $3250 / scene
INDIA	Gov.	IRS-P5	LISS 4, LISS-3'	'98	M			<10	<10	<10	70				C/T	148	22	
U.S.	Com.	OSC	SeaWIFS (OrbView3)	97	M		3bands	2b	1b	2 b	3					2801	1	
U.S.	Gov.	Landsat 7	ETM+	'99	M&P	15	30	30	30	30	30	30	60			185	16	$600 / Scene (Radiometrically Corrected)
INDIA	Gov.	IRS-2A	LISS 4', LISS-3', (WIFS)	'00	M			5	5	5	70				F/A	148	22	
HIGH RESOLUTION, SMALL AREA COVERAGE (PAN & VNIR ONLY)																		
RUSSIA	Gov.	SPIN-2	KVR-1000, TK-350	'96	P(f)	2,10									F/A	40,300		
U.S.	Com.	EarthWatch	EarlyBird	--	M&P	3		15	15	15					F/A	36	120	
U.S.	Com.	SpaceImaging	Ikonos	'98	M&P	1	4	4	4	4					F/A	12	247	Precision-1m & 4m @ $55/sq km; 1m color @ $60.50/sq km; bundled $82.50 sq km
U.S.	Com.	EarthWatch	QuickBird	?	M&P	1	4	4	4	4					F/A	20	148	Pan $6120 / scene; Multi $6800 / scence; bundle $8160
U.S.	Com	Orbimage	OrbView	'98	M&P	1&2	8	8	8	8					F/A	4&8	740,370	
RUSSIA	Gov.	Almaz 1B	1 SLR, 3 SARs, 4 SCANNERS***	'98	M&P&R	2.5		4,10	4,10	4,10				5,40 S	F/A	20,170		
U.S.	Com.	GDE	XXX	'99	P	1									F/A			
INDIA	Gov.	IRS-P6	PAN	'99	P	2.5									F/A	10	296	
France		SPOT 5	PAN	02	M&P	2.5		10	10	10	20				C/T			2.5 m Pan $6500 / scene; 5.0 m Pan $3250 / scene; 10 m multi-spectral $3250 / scene
MULTISPECTRAL, HYPERSPECTRAL APPLICATION TESTS																		
U.S.	Gov.	TRW Lewis	HSI	'96	H&P	5	128 bands @ 30				256 bands @ 30					8	370	
U.S./JAPAN	Gov.	EOS	ASTER	98	M		15	15	15	15	6 bands @ 30		5@90		1@A/CT	60	49	
U.S.	Gov.	EOS	MODIS	98	M				250	250						2330	1 or 2	
			MODIS	98	M		500	500		500	2bands @500							
			MODIS	98	M		7		5bands			1km	16bands					
U.S.	Gov.	EO-1	Hyperion	00	H		220 bands @ 30m				0.4-2.5um					7.5	16	~$500 / archived scene; ~$2000 / requested scene
U.S.	Gov.	Warfighter 1	Mil/Commercial (OrbView4)	01	H		128 bands @ 30				256 bands @ 30					24	16	
U.S.	Gov.	Warfighter 1	Mil/Commercial (OrbView4)	01	H		Minimum of 60 bands from 0.4 to 5 µm @ <10								TBD	5 to >25	TBD	
U.S.	Gov.	NEMO	Mil/Commercial (ESSI)	02	H													
Australia	Gov.	AIRES	Gov/Commercial	02	H&P													
RUSSIA	Gov.	Resurs F1	KFA-1000, KATE-200	'94	M(f)										F/A	80		
RUSSIA	Gov.	Resurs F2	MK-4 Frame MS	'94	M(f)										F/A	150		
RUSSIA	Gov.	Resurs FT	KFA-3000	'94	P(f)	3									F/A	30	N/A	
RUSSIA	Gov.	Resours-02	MCY-2, (MCY-CK)	'95	M											90*		
U.S.	Gov.	MTI (DOE)	MTI	'96	M										C/T	12	247	
AIRBORNE MULTI- AND HYPERSPECTRAL																		
U.S.	Gov.		AVIRIS	87	H		224 bands, 374 to 2500 nm @ ~1.5 to 20 m, bandwidths ~10 nm											~$45,000 / day
Canada	ITRES		CASI 2		H		288 bands @ sub-meter to 10 m											
Australia	Integrated Spectronics		HYMAP		H		100 - 200 bands @ 2-10 m, bandwidths of 10 - 20 nm											
U.S.	Space Imaging		DAIS		M		B 450-530 nm, G 520-610 nm, R 640-720 nm, Near IR 770-880 nm @ 0.5, 1 or 2 meters											
Germany	DLR-German Aerospace Center		DAIS 7915		H		79 bands, 400-12600 nm @ 5-20 m											
U.S.	Earth Search Sciences, Inc.		Probe-1		H		128 bands, 440 to 2500 nm @ 5 to 10 m, bandwidths ~ 15 nm											

Multispectral		M
Hyperspectral		H
Panchromatic		P
Radar		R
Film		(f)
IR	Infrared	
VNIR	Visible and near IR	
SWIR	Short wave IR	
TIR	Thermal IR	

All satellites in polar sun synchronous orbits except SPIN-2 (65 Deg), ALMAZ 1B (73 Deg), QuickBird (> 52 Deg) and TBD Warfighter 1 (>45 Deg)
F/A = fore/aft stereo, C/T = side to side stereo. All stereo satellites have 2 to 3 day site repeat capabilities
(XXX) = Wide swath, lower resolution inst. used for near daily, large area vegetation mapping
* = Swath is achieved by two side by side instruments
** = 4 satellites are planned to provide 3.5 to 4 day global repeat coverage.
*** = SLR-3, SAR-3, SAR-10, SAR-70, OES, MSU-E, (MSU-SK, SROSM)

Part 5. Citations

Boardman, J. W., Kruse, F. A. and Green, R. O. (1995). "Mapping target signatures via partial unmixing of AVIRIS data." Fifth JPL Airborne Earth Science Workshop, California Institute of Technology, Pasadena, California, National Aeronautics and Space Administration; Jet Propulsion Laboratory.

Boardman, J. W. and Kruse, F. A. (1994). "Automated Spectral Analysis: A Geological Example Using AVIRIS Data, North Grapevine Mountain, Nevada." ERIM Tenth Thematic Conference on Geologic Remote Sensing, Ann Arbor, MI, Research Institute of Michigan.

Brown, L. R. and Moyle, P. B. (1994). "Distribution, Ecology, and Status of the Fishes of the San Joaquin River Drainage, California." California Fish & Game **79**(3): 96-114.

Dufrene, M. and Legendre, P. (1997). "Species Assemblages and Indicator Species - the Need for a Flexible Asymmetrical Approach." Ecological Monographs **67**(3): 345-366.

ESRI, E. S. R. I. (2002). ArcGIS 8.1. Redlands, CA, Environmental Systems Research Institute, Inc -- ESRI.

Hill, M. O. (1979). TWINSPAN--A FORTRAN program for arranging multivariate data in an ordered two-way table by classification of the individuals and attributes. Ithaca, NY, Ecology and Systematics, Cornell University.

Jackson, R. D. (1983). "Spectral Indices in n-Space." Remote Sensing of Environment. **13**: 409-421.

Kruse, F. A., Lefkoff, A. B. Boardman, J.B., Heidebrecht, K.B., Shapiro, A.T., Barloon, P.J., and Goetz, A.F.H.. (1993). "The Spectral Image Processing System (SIPS) - Interactive Visualization and Analysis of Imaging Spectrometer Data." Remote Sensing of the Environment, Special Issue on AVIRIS **44**: 145-163.

Leica Geosystems. (2001). ERDAS Imagine. Atlanta, GA, Leica Geosystems.
Research Systems Incorporated ENVI v. 3.5 (Boulder, CO); Research Systems Incorporated

Ligon, F., Rich, A., Rynearson, G., Thornburgh, D. Trush, W. (1999). Report of the scientific review panel on California Forest Practice Rules and salmonid habitat. Sacramento, California, Resources Agency of California and the National Marine Fisheries Service. (Naiman et al. 1992, Murphy 1995).

McCune, B. and Mefford, M. J. (1999). Multivariate Analysis of Ecological Data. Gleneden Beach, Oregon, USA, MjM Software.

Montgomery, D. R. and Buffington, J. M. (1997). "Channel-Reach Morphology In Mountain Drainage Basins." Geological Society of America Bulletin **109**(5): 596-611.

Montgomery, D. R. (1994). "Road Surface Drainage, Channel Initiation, and Slope Instability." Water Resources Research **30**(6): 1925-1932.

Moyle, P. B. and Williams, J. E. 1990. Biodiversity loss in the temperature zone: decline of the native fish fauna of California. Cons. Biol. **4**(3): 275-284.

Naiman, R. J., Beechie, T., Benda, L. E., Berg, D. R., Bisson, P. A., MacDonald, L. H., O'Conner, M. D., Olson, P. L., and Steel, E. A.. (1992). Fundamental elements of ecologically healthy watersheds in the Pacific Northwest coastal ecoregion. Watershed Management: Balancing Sustainability and Environmental Change. R. Naiman. New York, NY, Springer-Verlag**:** 127 -188.

Nehlsen, W., Williams, J. E., and Lichatowich, J. A. (1991). "Pacific Salmon at the Crossroads - Stocks at Risk from California, Oregon, Idaho, and Washington." Fisheries **16**(2): 4-21.

PC ORD v 4.14 (MjM Software Design – Gleneden Beach, OR).

Research Systems, Inc. (2002). Environment for Visualizing Images. Boulder, CO, Research Systems, Inc.

Research Systems, Inc. (2002). Interactive Data Language (IDL). Boulder, CO, Research Systems, Inc.

Richter, R. (2000). ATCOR4: Atmospheric / Topographic Correction for Wide FOV Airborne Imagery. Wessling, Germany, DLR-German Aerospace Center.

Richards, J. A. and X. Jia (1999). Remote Sensing Digital Image Analysis: An Introduction. Berlin, Germany, Springer-Verlag.

Roberts, D. A., Gardner, M., Church, R., Ustin, S., Scheer, G., and Green, R. O. (1998). "Mapping Chaparral in the Santa Monica Mountains Using Multiple Endmember Spectral Mixture Models." Remote Sensing of Environment **65**(3): 267-279.

Rosgen, D. L. (1994). "A Classification of Natural Rivers." Catena **22**: 169-199

SAS (2002). JMP Version 5 Statistics and Graphics Guide. Cary, NC, SAS.

Schläpfer, D. (2000). Parametric Geocoding. Zurich, Switzerland, Remote Sensing Laboratories, University of Zurich.

Tarboton, D. G., Bras, R. L., and Rodrigueziturbe, I. (1991). "On the Extraction of Channel Networks from Digital Elevation Data." Hydrological Processes **5**(1): 81-100.

van Tongeren, O. F. R. (1995). Cluster analysis. Data Analysis in Community and Landscape Ecology. R. H. Jongman, C. J. F. ter Braak and O. F. R. van Tongeren. Pudoc, Wageningen, Netherlands: 174-212.

Viers, J. H., Sailer, C. T., Ramirez, C. M., Quinn, J. F., and Johnson, M. L.. (2002). "An Integrated Approach to the Discrimination of Riparian Vegetation in the Navarro River Watershed." Eleventh JPL Airborne Earth Science Workshop, California Institute of Technology, Pasadena, California, National Aeronautics and Space Administration; Jet Propulsion Laboratory.

Viers, J. H., McCoy, M. C., Viers, J. H., McCoy, M. C., Quinn, J. F., and Johnson, M. L. (1999). "Nonpoint Source Pollution Modeling in the North Coast of California Within a GIS: A Predictive Screening Tool for Watershed Management." ESRI International User Conference, San Diego, CA, Environmental Systems Research Institute, Inc.

Yoshiyama, R. M., Fisher, F. W. and Moyle, P. B. (1998). "Historical Abundance and Decline of Chinook Salmon in the Central Valley Region of California." North American Journal of Fisheries Management **18**(3): 487 (35 pages).

Zar, J. H. (1999). Biostatistical Analysis. Upper Saddle River, New Jersey, Prentice Hall.